CORROSION OF ALUMINUM ALLOYS – POLYMER MATRIX COMPOSITE INTERFACES IN DIVERSE NATURAL ATMOSPHERIC ENVIRONMENTS

A THESIS SUBMITTED TO THE GRADUATE DIVISION OF THE
UNIVERSITY OF HAWAIʻI AT MĀNOA IN PARTIAL FULFILLMENT OF
THE REQUIREMENTS FOR THE DEGREE OF

MASTER OF SCIENCE

IN

MECHANICAL ENGINEERING

May 2017

By

Brent Ernest Howard

Thesis Committee:

Lloyd H. Hihara, Chairperson
Reza Ghorbani
Scott Miller

Acknowledgments

First and foremost, I would like to thank Dr. Lloyd Hihara for his support and expertise in shaping this thesis and all of the research that went with it. His knowledge, patience, and kindness were the pillars on which this research stands.

I would like to thank my committee members, Dr. Reza Ghorbani and Dr. Scott Miller for agreeing to serve on my thesis committee and for their input in the writing of this thesis.

Also, I would like to thank the Office of the Under Secretary of Defense for the project entitled, "Corrosion and Corrosion Control Studies of Aluminum Alloys that are Mechanically-Coupled or Adhesively-Bonded to PMCs in Diverse Micro-Climates," [United States Air Force Academy (USAFA), Grant Number F47000-12-2]. This includes Mr. Daniel Dunmire, Director, Corrosion Policy and Oversight, Office of the Under Secretary of Defense (OUSD); Dr. Gregory Shoales, USAFA Program Manager; Dr. Christopher Scurlock, LMI, and Mr. Richard Hays with the Technical Corrosion Collaboration sponsored by the OUSD. Thank you, too, Mrs. Denise A. Aylor and Dr. Elissa Bumiller of the Naval Surface Warfare Center, Carderock Division; and Farrel Martin, Center for Corrosion Science and Engineering, U.S. Naval Research Laboratory for initial discussions.

I would like to extend a thank you to the current and former members of the Hawai'i Corrosion Laboratory that provided support and guidance (and to make sure I didn't kill myself in some of the

experiments) to the creation of this thesis: Mr. Khoa Huynh, Mr. Dan Jensen, Mrs. Jan Kealoha, Mr. Jeff Nelson, Ms. Kathleen Quiambao, Ms. Melissa Sanders, and Ms. Natalie Wohner.

A special thanks to Dr. Raghu Srinivasan for his assistance and patience in teaching me to use multiple pieces of very expensive lab equipment without breaking anything.

I would like to extend a very special thanks to Mr. Ryan Sugamoto for his knowledge, unending kindness, and ability to successfully herd a seemingly endless number of cats to keep the lab running like a well-oiled machine.

Lastly I am extremely grateful for the support my family and my wife, Sarah, that allowed me to quit my job, move to Hawai'i, and go back to school full time, all without ending up living in a cardboard box. To them I dedicate this thesis.

Abstract

The environmental corrosion of carbon-fiber/epoxy and E-glass/epoxy composite laminated aluminum alloys [e.g., Al 1100-H14, Al 5456-H116 (non-sensitized), Al 5456-H116 (sensitized), and Al 7075-T6] was studied to characterize the interfacial corrosion between the composite and the aluminum substrate. Samples were exposed at 5 locations around the islands of Hawai'i that represented alpine, marine, severe marine, rainforest, and volcano environments over 1-month, 6-month, and 12-month time periods. After exposure, the samples were then adhesion strength tested by conducting pull test to remove the composite laminate from the aluminum substrate to determine the loss (if any) of the composite laminate adhesion to their respective aluminum substrates. The delaminated samples were then analyzed with a scanning electron microscope and energy dispersive X-ray analysis to determine the distribution of corrosion products and ionic species at the aluminum substrate - composite laminate interfaces. The decay in adhesion strength was correlated to the amount of corrosion at the interface that was dependent on the type of composite and type of aluminum alloy.

Table of Contents

Page

List of Figures

List of Tables

Chapter 1

INTRODUCTION

1.1 Purpose of Research

Figure 1: Ticonderoga Class Guided Missile Cruiser, USS Lake Erie (CG-70) [1]

The United States Navy has used aluminum alloys in the superstructures and deckhouses of its surface ships for more than 70 years to reduce their weight and center of gravity [2]. Aluminum alloy (Al) 5456-H116 was selected as the primary building material of the Navy's Ticonderoga Class Guided Missile Cruiser's superstructure (Figure 1 above). The alloy's high strength (strong enough to support the AEGIS ballistic missile defense system), corrosion resistance, and low weight made it ideal for the 27 cruisers that would eventually be built [2]. Of the 27 built, 22 are still in active service today.

Almost immediately after reaching initial operational capability (IOC), cracks started forming in the structure. Initially, fatigue cracking was observed in stress concentration or highly restrained welded

structure transitions [2]. Figure 2 below shows a typical example of fatigue cracking in a welded joint on the CG-47 class cruiser.

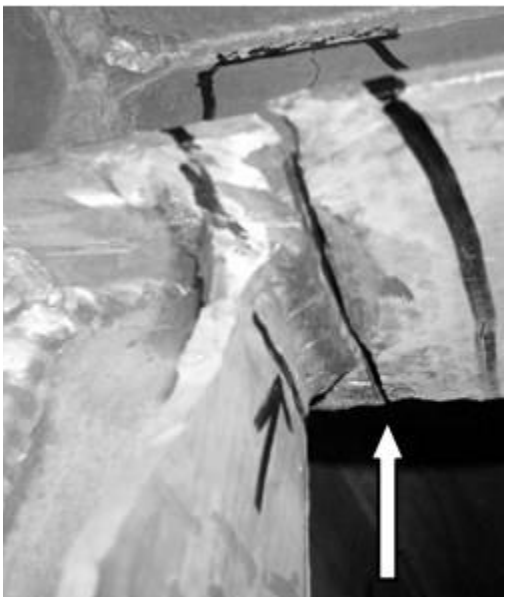

Figure 2: Fatigue Cracking in Al 5456-H116 Welded Joint [2]

Since 2006, cracking in non-structural areas of the ships were found, and naval engineers quickly realized that these cracks were due to stress corrosion cracking (SCC) [2]. After an average of 26 years in service, the Al 5456-H116 in the superstructure was becoming sensitized when exposed to moderately high temperatures (e.g., direct sunlight for long periods or next to hot ship-board equipment) [2]. Figure 3 below shows an example of SCC on a deck plate of the CG-47 class cruiser.

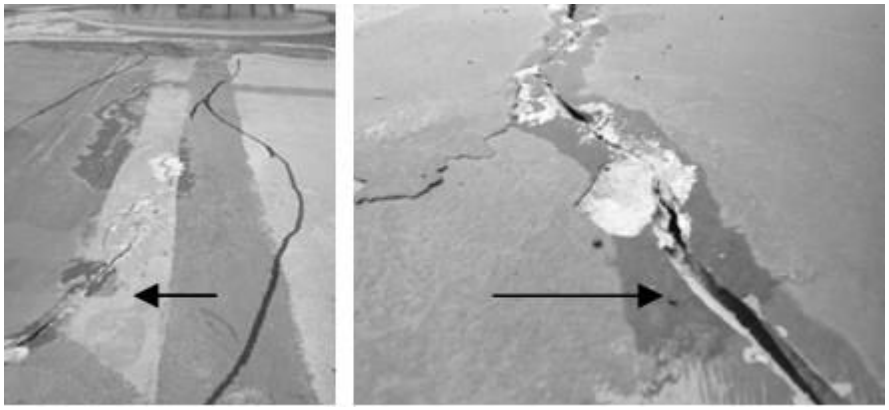

Figure 3: Stress Corrosion Cracking on CG-47 Deck Plate [2]

Al 5456-H116 is considered to be super saturated with magnesium and when heated slightly, becomes sensitized and forms Mg_2Al_3 particles that precipitate on the alloy grain boundaries [3]. These Mg_2Al_3 precipitates have a higher anodic potential than the surrounding grains and are attacked preferentially when put in a galvanic couple in a process called intergranular corrosion [4]. Figure 4 below illustrates the difference in the grain structure between a sensitized and non-sensitized Al 5456-H116 alloy.

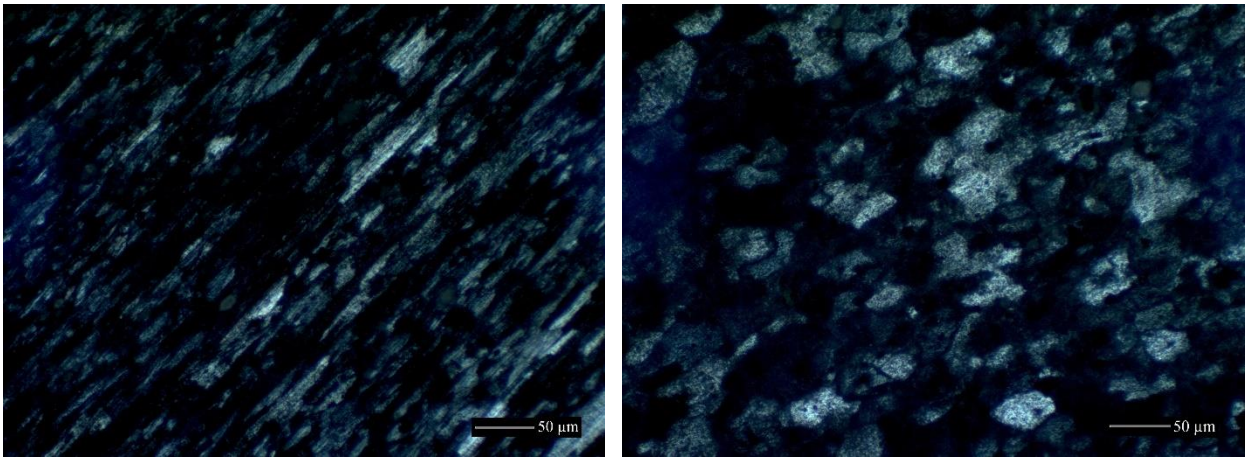

Figure 4: Microstructures of Non-Sensitized (Left) and Sensitized (Right) Al 5456-H116

Figure 5 below illustrates how the migration of Mg_2Al_3 precipitates to the grain boundaries can dissolve to form large cracks in the parent material.

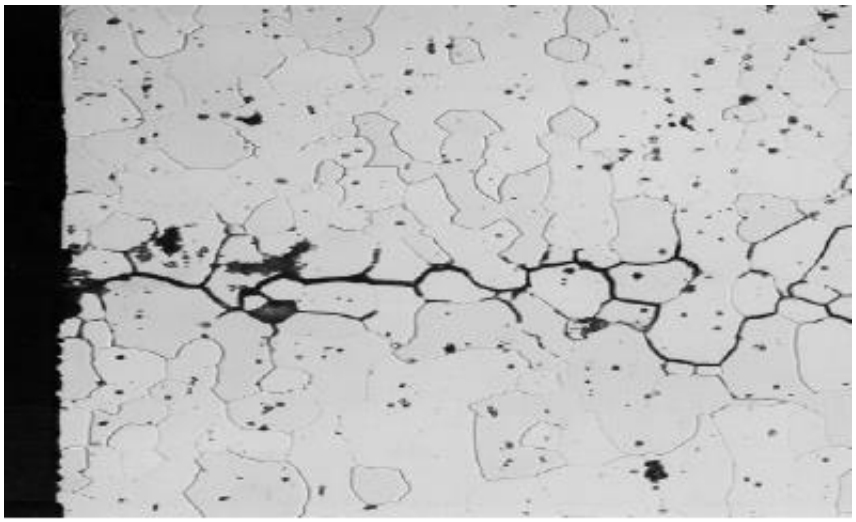

Figure 5: Sensitized AL 5456-H116 Intergranular Stress Corrosion Crack [2]

The costs to repair ongoing superstructure cracks in the ships are high, and increasing as time in service increases [2]. Most permanent crack repairs require the ship to be in port, and an increasing trend in emergent repairs (a type of repair that requires an immediate fix in port) have jeopardized the planned deployment schedule of several ships [2]. Simplified illustrations of permanent crack repairs are shown in Figure 6 and Figure 7 below.

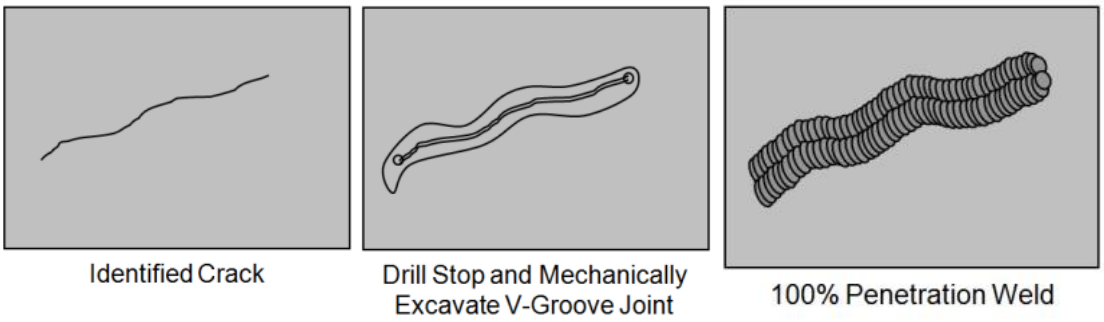

Figure 6: Permanent Crack Repair via Excavation [2]

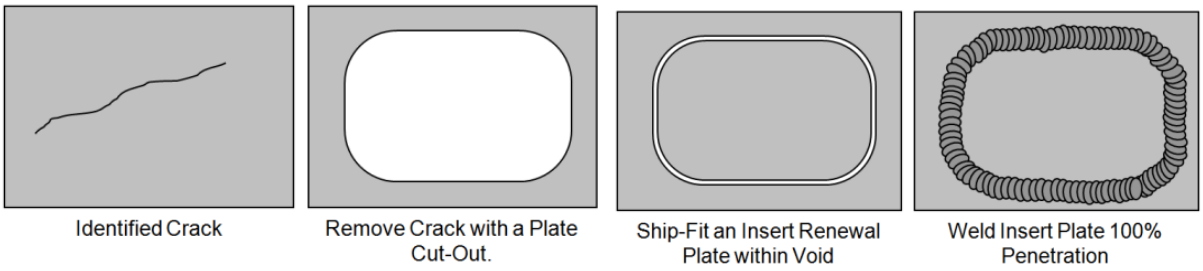

Figure 7: Permanent Crack Repair via Insert Plate [2]

There has been a push to design a more immediate, temporary repair that could be done shipboard at a reduced cost until such time that the ship goes back to port for a scheduled maintenance period. Current temporary repairs are designed to either keep the interior water-tight, or to arrest crack propagation, but not both at the same time [5]. Several temporary repair methods that are currently approved for use include polysulfide, doubler plates, compression bolts, and composite patches. Figure 8 and Figure 9 below illustrate several temporary repair methods.

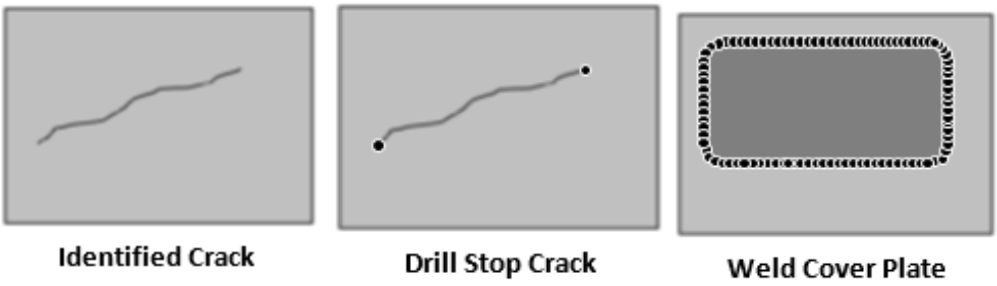

Figure 8: Temporary Crack Repair via Doubler Plate [6]

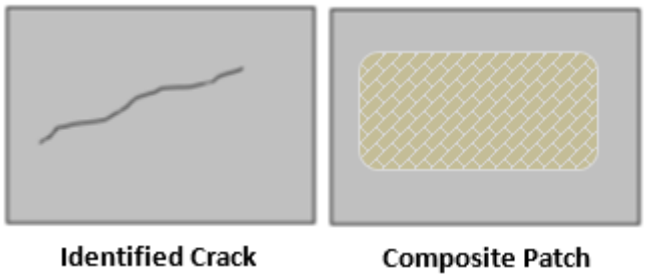

Figure 9: Temporary Crack Repair via Composite Patch [6]

Several issues arise when using temporary repair like a welded or adhesively bonded doubler plate that include the addition of residual stresses around the welded joint that can cause further cracking, or failure to arrest crack growth with adhesive bonding [5]. Compression bolts successfully halt crack propagation, but can only be applied in limited situations (e.g., flat surfaces) and do not restore water tightness [5]. Polysulfide resins can be applied by the ship's force, but only restores water tightness to the crack [5]. Composite patches have issues as well, including high installation and non-recurring engineering costs [5]. Currently, the resins used in composite repair cannot be stored shipboard, nor can they be properly applied by the ship's force [5].

There are several advantages to using composite patches that warrants further research and development to their use shipboard. Their high strength-to-weight ratio (higher than most traditional metal alloys), flexibility in use over complex and curved surfaces, and ease of application have made them the go-to choice for the aviation and automotive industries [7].

Further research could provide an easy to apply, long lasting repair that is both crack arresting and water tight. This research aims to expand knowledge and develop new techniques for composite patching by evaluating the performance of Glass Fiber Reinforced Polymer (GFRP) laminates and Carbon Fiber Reinforced Polymer (CFRP) laminates applied to several alloys of aluminum and subjected to varying corrosive environments.

1.2 Research Objectives

The primary purpose of this research was to determine the advantages and disadvantages of GFRP and CFRP composite laminates on various alloys of aluminum (e.g., Al 1100-H14, Al 5456-H116 (non-sensitized), Al 5456-H116 (sensitized), and Al 7075-T6) when subjected to various levels of environmental corrosion, as well as accelerated corrosion. Testing and evaluating these samples required the use of several different methods.

One set of the samples were placed in a Singleton Corporation E-710 Cyclic Corrosion Test Chamber (CCTC) and subjected to a modified GM-9540P accelerated corrosion test procedure. This modified test procedure subjects the samples to multiple test-chamber environments including both hot and cold while keeping the chamber humidity high for varying durations. The chamber also periodically sprays the samples with a salt solution containing 0.9% by weight sodium chloride (NaCl), 0.1% by weight calcium chloride ($CaCl_2$), and 0.25% by weight sodium bicarbonate ($NaHCO_3$). This process was repeated on a 16 hour cycle over durations running from 1 week to a maximum of 3 weeks. After removal from the CCTC, samples were subjected to adhesion strength testing.

A second set of samples were placed in five locations around the islands of Hawai'i to simulate alpine (Mauna Loa), marine (Coconut Island), severe marine (Pyramid Rock), rainforest (Lyon Arboretum), and volcano (Kilauea) environments over 1-month, 6-month, and 12-month time periods. After each of the time periods, the samples were subjected to adhesion strength testing, and select samples were analyzed with the SEM and EDX.

After the samples were removed from the CCTC and returned from the field, they were subjected to adhesion strength testing using a PosiTest AT-A Adhesion Tester. The purpose of this test was to evaluate the remaining CFRP and GFRP composite laminate adhesive strength to its respective aluminum alloy substrate. The data were then compared to adhesion tests done on unexposed samples by Daniel Jensen in his thesis "*Corrosion of Aluminum Alloys-Polymer Matrix Composite Interfaces*" [6].

Once the samples had been successfully adhesion tested, the now exposed aluminum substrate was analyzed by the Scanning Electron Microscope (SEM) and Energy Dispersive X-ray Analysis (EDXA) using INCA software. This method allowed the study of the corrosion rate and constituent corrosion products as they penetrated the composite-aluminum interfaces that had formed during the CCTC and natural environment exposure experiments.

After the field-exposed samples were analyzed in the SEM, one of the adhesion test sites was cut off from a selection of samples. The laminate was removed and the aluminum substrate was cleaned using the American Society for Testing and Materials G1 (ASTM G1) cleaning standard [8]. The selected samples were then profiled in a Nanovea ST400 3D profilometer. This experiment allowed

the study of surface roughness due to corrosion, as well as the degree of pitting in the aluminum substrate.

Following the profilometer, the Al 5456-H116 sensitized and Al 5456-H116 non-sensitized cut aluminum field samples were subjected to a nitric acid mass loss experiment that followed the ASTM G67-13 procedure [8]. The exposed samples were then compared to non-exposed 5456-H116 sensitized and Al 5456-H116 non-sensitized aluminum samples subjected to the same nitric acid mass loss experiment. The purpose of this experiment was to determine the amount of extra sensitization each of the exposed samples went through during its environmental exposure.

Small samples of each aluminum alloy (including both Al 5456-H116 sensitized and non-sensitized) were set in epoxy and polished on a Buehler Ecomet 6 variable speed grinder-polisher down to a mirror finish (0.05μm). After polishing, the samples were analyzed for their constituent elements and inclusions using SEM and EDX Analysis with INCA software. The samples were then electrolytically etched using a dilute solution of fluoroboric acid (Barker's reagent) and a 20V Direct Current (DC) power source. After the samples were etched, they were evaluated using polarized light microscopy on a Zeiss Axioplan microscope.

Lastly, samples of each aluminum alloy (including both Al 5456-H116 sensitized and non-sensitized) were cut to 1 cm x 1 cm squares, had copper lead wires attached and were set in epoxy. These samples were then polished on a Buehler Ecomet 6 variable speed grinder-polisher down to a 0.25 μm finish and were subjected to potentiodynamic polarization tests using a Parstat 2273 Advanced Electrochemical system coupled with PowerSuite software.

1.2 Thesis Format

A literature survey of corrosion on various aluminum alloys, coatings to prevent aluminum corrosion, as well as fiber reinforced composite patches in various applications is discussed in **chapter 2**. The process of fabricating the test samples is given in **chapter 3**. Experimental methods for the accelerated corrosion testing experiment in the CCTC, the field experiments, adhesion test experiment, SEM and EDX analysis, profile analysis, nitric acid mass loss experiment, microstructure analysis, and polarization experiments are discussed in **chapter 4**. Results from each of the above experiments and analyses are exhibited in **chapter 5**. A discussion of the results are discussed in **chapter 6**. Finally, all overall conclusions are presented in **chapter 7**.

Chapter 2

LITERATURE SURVEY

2.1 Corrosion of Aluminum Alloys

Both neutral salt fog (NSF) using the ASTM B 117 model and cyclic testing using the GM-9540P model have been used in previous studies to determine the corrosion resistance of various aluminum alloys. In 2009, a study conducted by the U.S. Army Research Laboratory tested the corrosion characteristics of 19 different aluminum alloys from the 2xxx, 5xxx, 6xxx, and 7xxx series [9]. Each of the alloys were subjected to both the ASTM B117 (18, 72, and 168 hours), and the GM-9540P (1, 5, and 10 cycles) [9].

The 2xxx and 7xxx alloys were observed to have the most corrosion, mainly from pitting attack, due to their high copper (2xxx alloys) and zinc (7xxx alloys) content [9]. Both the 2xxx and 7xxx series alloys are used extensively in the military in aviation and missiles as well as in armor plating [9]. The 2xxx series alloys exhibited major surface degradation due to widespread pitting and the rapid formation of corrosion products [9]. In this test, the 2xxx fared the worst overall when compared to all other alloys in the experiment with the notable exception of the Al 2195-BT alloy which performed similarly to the 5xxx series due to its high lithium content [9]. The 7xxx series alloys are known for their tendency to catastrophically fail due to stress corrosion cracking, especially in aviation, but in this study performed better overall than the 2xxx series [9]. The study notes that the more recently developed 7xxx series alloys (e.g. 7022-T651) attempt to address the stress corrosion cracking issue [9].

The 5xxx and 6xxx alloys had very good corrosion resistance overall, with the high magnesium (Mg) content in the 5xxx alloys giving the greatest corrosion resistance [9]. The study notes that the high Mg content in the 5xxx alloys is its greatest strength; as well as its greatest weakness. Over extended periods at increased temperatures the 5xxx alloys experience intergranular corrosion due to the formation of Mg_2Al_3 at the grain boundaries [9]. The 6xxx alloys performed well with one exception being the Al 6013-T651, which exhibited significant pitting damage under the ASTM B117 test, as well as staining and pits after ten cycles of the GM-9540P [9].

In a 2001 study conducted for the Air Force Research Laboratory, Materials and Manufacturing Directorate determined the fatigue behavior of Al 7075-T6 after being subjected to pitting corrosion via the ASTM G85, Annex 5, dilute electrolyte cyclic fog-dry spray test procedure [10]. Each of the test specimens were exposed for between 24-1536 hours in a prohesion chamber, and 200 randomly chosen pits were measured for their length, width and depth after exposure [10]. The corroded specimens were then cut to fit in a constant amplitude S-N fatigue tester for further testing [10]. The specimens were subjected to maximum stress levels up to 414 MPa at 15 Hz in the fatigue tester [10]. As can be expected, the longer the specimens were exposed to the cyclic fog-dry spray test procedure, the larger and deeper the pits on the surface became. The average pit depth over the complete test obeys a power law with a time exponent close to 1/3 [10]. For the fatigue testing, the 7075-T6 alloys fatigue life was reduced by a factor of six to eight overall [10].

2.2 Corrosion of Composite Laminated Aluminum Alloys

In a 2011 study conducted by the Mechanical and Aerospace Engineering Department at the University of California, Davis, galvanic corrosion between Al 7075-T6 and GFRP's with an epoxy resin modified with multi-walled carbon nanotubes [11]. Nanotubes were added to help diagnose

damage to the composite-substrate interface in real-time without resorting to destructive testing techniques [11]. The samples were constructed using varying area ratios of aluminum to laminate of 1:1, 2:1, 4:1, and 4.2:1 [11]. These samples were subjected to three separate tests to determine the rate of galvanic corrosion in the couple [11]. The first consisted of exposing the samples to a test chamber of 95% relative humidity at 23° C and measuring the volumetric resistance between the laminate and substrate aluminum for up to 20 days [11]. The second test consisted of immersing the samples in a 2% by weight NaCl solution which was heated to 40° C for 26 days [11]. The final test consisted of creating two galvanic half-cells: Al 7075-T6 and carbon nanotube-modified GFRP [11]. Each of these half-cells were immersed in a 2% by weight NaCl solution heated to 40° C and coupled together using coated wire [11]. In both the second and third test, the volumetric resistance was measured for the entire test period and the samples were cleaned and weighed using the appropriate ASTM standard to determine the mass loss rate [11]. Each of these tests used an ordinary GFRP laminated aluminum as the control [11].

The results of the study indicate that the first test (high humidity) did not show significant changes in resistance over time, and the carbon nanotube-modified GFRP and aluminum couples had a much lower resistance overall when compared to the GFRP laminated aluminum control [11]. The second and third tests show that the carbon nanotubes do indeed cause galvanic corrosion when added to the GFRP laminate [11]. Corrosion rates of approximately 1.25 mm/year were observed in coupled carbon nanotube-modified GFRP and aluminum samples versus approximately 0.7 mm/year in the control GFRP and aluminum couple [11]. The authors suggest using an insulator to mitigate the galvanic corrosion tendency, but concede that doing so could affect the ability of the carbon nanotubes to detect damage in the aluminum [11].

Several studies have been conducted on glass fiber reinforced aluminum (GLARE) by the Delft University of Technology between 2003 and 2013. GLARE is a lay-up of thin aluminum sheets (usually Al 2024-T3) and glass fiber sheets suspended in an epoxy resin [12]. The aluminum sheets are on both the outer most top and bottom layer, with alternating GFRP and aluminum sheets in the middle [12]. Overall, GLARE takes the best corrosion resistance properties of both GFRP and aluminum, and combines them into a material that is greater than the sum of its parts [13]. Thin aluminum sheets (0.3 mm – 0.5 mm) have better corrosion resistance than standard thickness sheets (2 mm – 4 mm) due to higher quenching rates [13]. Corrosion of the aluminum also isolated to a single sheet due to the GFRP acting as a corrosion barrier [13].

Moisture ingress and saturation is inherent to any polymer based epoxy, but is limited in a material such as GLARE due to its design [12]. Since GLARE is laminated with the aluminum sheets on the outside layers, moisture ingress can only occur in sheet edges or at bore holes in the material [12]. The effect of moisture ingress (85% relative humidity for up to 3000 hours) coupled with temperature increase (20-130° C for up to 3000 hours) was studied to see the effects on inter-laminar shear strength [12]. The study concluded that both temperature and moisture ingress had a detrimental and linear effect on inter-laminar shear strength [12]. A 15% drop in inter-laminar shear strength was noted after 3000 hours of exposure across the entire temperature range [12].

In a pair of studies conducted in 1991 and 1992 by the University of Naples, the galvanic corrosion between graphite-epoxy composite materials and metals in relation to metal type, temperature, area ratio, and environmental degradation. Their study included multiple alloys of aluminum, steel,

titanium, and bronze, but this review will focus on the Al 7075-T6 and Al 5052 aluminum alloys [14]. In the temperature experiment, the alloys were either coupled or uncoupled to graphite-epoxy composite materials and submerged in 3.5% by weight NaCl solution at varying temperatures from 25° C to 60° C for 24 hours [14]. In the area ratio experiment, the alloys were coupled to graphite-epoxy composite materials and submerged in 3.5% by weight NaCl solution for 24 hours at area ratios of 1:1 to approximately 1:22 (anode to cathode) [15]. In the environmental degradation experiment, the graphite-epoxy composite material was submerged in 3.5% by weight NaCl solution for 2 years, and then coupled to the Al 7075-T6 samples [15]. During each of these experiments, the galvanic current and galvanic potential were measured using a zero resistance ammeter (ZRA) [14]. After the experiments, the samples were cleaned of corrosion product and weighed to determine the corrosion rate [14].

In the variable temperature experiment, the author concluded that there were significant galvanic currents when the Al alloys were coupled to the graphite-epoxy composite materials, and an increase in temperature caused an increase in galvanic current in the Al 7075-T6 [14]. Corrosion rates for the Al alloys ranged from approximately 18-25 milligrams per square decimeter per day (mdd) [14]. For the area ratio experiment, the author found that the extent of corrosion on the Al alloy and graphite-epoxy composite material couples was linearly dependent on the cathodic to anodic area ratio [15]. For the environmental degradation experiment, the author found that aging the graphite-epoxy composite material in the 3.5% NaCl solution increases the corrosion rate of the Al 7075-T6 alloy [15].

2.3 Corrosion of Coated Aluminum Alloys

A 2003 study conducted by the Army Research Laboratory tested the effectiveness of eight chromate (Cr^{6+}) free pretreatments on four different aluminum alloys (Al 2024-T3, Al 2219-T87, Al 5083-H131, and Al 7075-T6) [16]. One pretreatment containing Cr^{6+} was used as a control for the test. Each of the aluminum alloys were then coated with one of five epoxy primer and polyurethane topcoat systems and were subjected to the GM-9540P cyclic corrosion test for 120 cycles with evaluations done every 20 cycles [16]. Prior to exposure, each of the samples was scribed with an "X" using a carbide tipped steel scribe [16].

For the Al 2219-T87 alloy with its high copper content, creating a pretreatment/coating system to halt the corrosion process proves tremendously difficult [16]. None of the chromate free pretreatment and coating systems survived the full 120-cycle duration [16]. The best performing system for the Al 2219-T87 were the Alodine 1200S pretreatment and MIL-PRF-23377 and MIL-PRF-85285 coatings [16]. The Al 2024-T3 alloy performed better overall than the 2219-T87, with the TCP10 pretreatment with MIL-P-53030 and MIL-C-53039 actually performing better than the control Cr^{6+} pretreatment [16].

The Al 5083-H131 performed the best of all alloys tested, mainly due to its very stable and protective oxide layer [16]. Most of the pretreatment and coating system combinations were able to complete the 120 cycles without any noticeable damage with the MIL-PRF-23377 and MIL-PRF-85285 coatings exhibiting the best performance [16]. For the Al 7075-T6 alloy, none of the non-Cr^{6+} containing coating systems lasted the entire 120 cycles.

Overall the performance of the Cr^{6+} containing pretreatment and coating systems were much more corrosion resistant than the non-Cr^{6+} containing systems, but since government agencies are transitioning away from Cr^{6+}, a comparable replacement needed to be found [16]. The best overall performance for a non- Cr^{6+} system was obtained with the Alodine 5200 pretreatment with any of the chromium-free organic coatings, which provided sufficient corrosion protection [16].

Chapter 3

FABRICATION AND PREPARATION OF SAMPLES

3.1 Composite Laminated Aluminum Alloy Samples

Each of the composite laminated aluminum alloy samples used in the experiments were created using a wet lay-up and vacuum bagging technique. The following description of the fabrication of the composite laminated aluminum alloy samples is just a general overview, for a complete and detailed description please refer to Daniel Jensen's work in his thesis "*Corrosion of Aluminum Alloys-Polymer Matrix Composite Interfaces*" [6]. The aluminum alloy substrate started as a 3 mm x 30 cm x 30 cm plate that was immersed in Alumiprep for one minute and then sanded with 600 grit silicon-carbide sandpaper. After sanding, the aluminum alloys were rinsed with ultra-pure deionized water, dried carefully, and placed in dry box storage (1% relative humidity) until needed. The sensitized Al 5456-H116 plates were then heat treated at 150° C for 50 hours.

The composite laminates that were chosen for lay-up on the aluminum substrates were plane weaved carbon fiber and glass fiber fabrics. Each of these laminates were placed in two layers on each of their respective alloys, using an equal mix of Aeropoxy PH3660 resin and PH3636 hardener on each of the layers. After lay-up, the laminate coated aluminum alloy samples were vacuum bagged and cured in an oven at 51° C for four hours. After curing in the oven, the samples were left to cure for an additional 24 hours in ambient conditions.

After curing, the samples were water jet cut by the University of Hawai'i machine shop. Each plate was cut into nine triangular shapes; then placed in a vertical mill to diamond cut three evenly-spaced 20 mm diameter reliefs into the composite layers. Figure 10 below shows a completed CFRP sample.

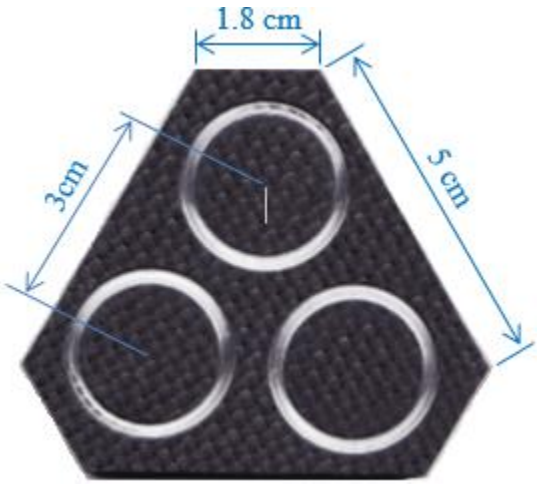

Figure 10: Triangular-Shaped Composite Al Alloy Sample [6]

The electrical resistance between the carbon fiber composite reliefs and the aluminum substrate was usually less than 50 ohms [6].

3.2 Microstructure Analysis Samples

Each small microstructure analysis sample was created by setting a small piece of each alloy (Al 1100-H14, Al 5456-H116 (non-sensitized), Al 5456-H116 (sensitized), and Al 7075-T6) in epoxy. After the epoxy was cured, the samples were polished to a mirror finish (0.05 µm abrasive) and then electrolytically etched for further analysis. The manufacturing process used is listed below.

3.2.1 Material Preparation

Small samples (approx. 13 mm x 3 mm x 3 mm) of each alloy were cut using a Buehler IsoMet low speed saw in order to minimize tempering the alloys due to cutting friction. The alloy samples were

placed in a ring mold and Buehler EpoxiCure 2 resin and hardener were poured (in a four to one ratio of resin to hardener, measured on an electronic balance) to fill the ring molds. The samples were left to cure for 24 hours before being removed from the mold.

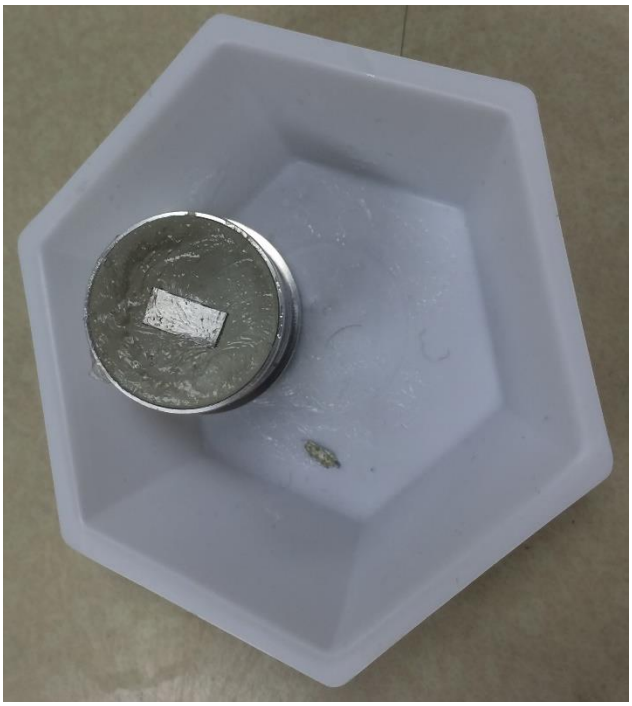

Figure 11: Al alloy Sample Set in Epoxy

Figure 11 above illustrates how the aluminum sample was set in epoxy just before being removed from the ring mold.

3.2.2 Material Polishing Process

Each of the samples were wet sanded with silicon-carbide grinding paper in 180, 320 and 600 grits on a Buehler Ecomet 6 variable speed grinder-polisher. The samples were sanded for 2 minutes on each grit of grinding paper at 150 rpm on the Ecomet 6 while being constantly sprayed with a fine stream of water. After the initial grinding was finished, the grinding paper was switched in favor of polishing pads that were sprayed with Buehler Metadi Supreme polycrystalline diamond suspensions in 9µm, 3µm, 1µm, 0.25µm, and 0.05µm grits. The samples were polished for approximately 2

minutes at each grit level, and carefully washed between grits to ensure no cross contamination occurred between polish levels.

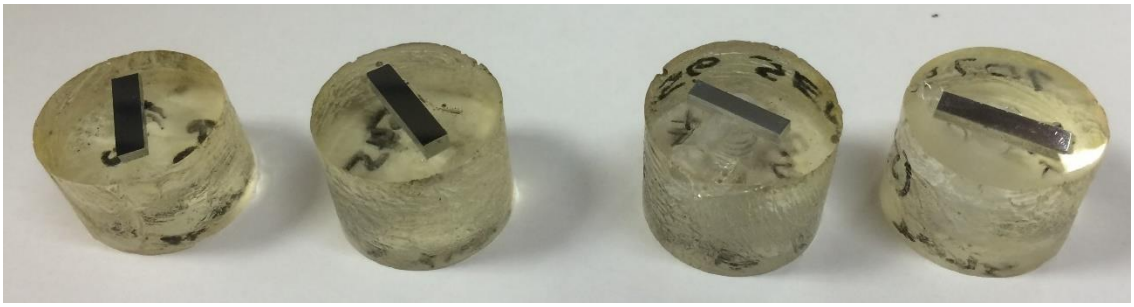

Figure 12: Fully polished Al Alloy Microstructure Samples

Figure 12 above displays the fully polished Al alloy samples (Al 1100-H14 far left, Al 5456-H116 (non-sensitized) center left, Al 5456-H116 (sensitized) center right, and Al 7075-T6 far right).

3.3 Polarization Experiment Samples

Each of the small polarization experiment samples were created by setting a 1 cm^2 piece of each alloy (Al 1100-H14, Al 5456-H116 (non-sensitized), Al 5456-H116 (sensitized), and Al 7075-T6) and a copper wire lead surrounded by a glass tube in epoxy. After the epoxy was cured, the samples were polished to a near-mirror finish (0.25 µm abrasive). The manufacturing process used is listed below.

3.3.1 Material Preparation

Small samples (approx. 1 cm x 1 cm x 3 mm) of each alloy were cut using a Buehler IsoMet low speed saw in order to minimize plastic deformation and tempering the alloys due to cutting friction. Copper wires were attached to each of the alloy samples using conductive high-purity silver paint and then set in Loctite 0151™ Hysol epoxy to ensure adherence. A glass tube was then sealed with

epoxy around the copper wire to ensure a water tight seal. After each epoxy application, a cure time of 2 hours at 60° C was given.

Figure 13: Polarization Experiment Samples

Figure 13 above displays the completed Al alloy polarization samples (Al 1100-H14 bottom, Al 5456-H116 (non-sensitized) second from bottom, Al 5456-H116 (sensitized) second from top, and Al 7075-T6 top).

3.3.2 Material Polishing Process

This process is the same as listed above in *3.2.2 Material Polishing Process* with the notable exception of only polishing down to the 0.25 µm level.

3.4 CCTC Steel Coupons

The steel coupons used in the CCTC were made of 25.4 mm x 50.8 mm x 0.79 mm AISI 1009-1010 steel in accordance with the GM-9540P test procedure.

3.5 Profile Analysis Samples

After performing the adhesion test experiment listed in section *4.4 Adhesion Testing Experiment*, the samples were sent to the University of Hawaii machine shop where one of the test areas was cut off and the composite layer was mechanically removed (Figure 14).

Figure 14: Composite-Al Sample Before (left) & After (right) Removal of Profile Test Sample

After the composite layer was carefully mechanically removed, the corrosion products were removed in accordance with the International Standard Procedure ISO 8407:1991 (E) C.1.1 [17]. The cleaning solution was produced by adding 50 mL of Phosphoric Acid (H_3PO_4; $\rho = 1.69$ g/mL) and 20 g of chromium trioxide (CrO_3) to 1 L of nano-pure water. This solution was heated to 80°C using a Corning PC-620D hotplate and stirrer with an attached temperature probe. Test specimens were submersed in the solution for a total of 5 minutes, then were rinsed with deionized water in a Fisher Scientific FS220H ultrasonic cleaner for 20 minutes. After cleaning and drying, the samples were weighed on a Mettler Toledo XP504 analytical balance to within ± 0.0001 g.

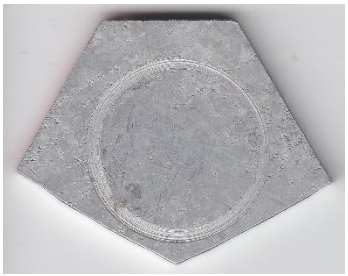

Figure 15: Profile Testing Sample After Cleaning

Figure 15 above shows an example of the results from cleaning the profile samples. The samples were then profiled on a Nanovea ST400 3D profilometer.

3.6 Nitric Acid Mass Loss Samples

There was no major preparation of the samples between the profile test and the nitric acid mass loss test.

Chapter 4

EXPERIMENTAL METHODS

4.1 Substrate Aluminum Composition

The 3 different aluminum alloys used in this study were Al 1100-H14, Al 5456-H116, and Al 7075-T6. The elemental compositions of each of the alloys can be seen in Table 1 below.

Table 1: Elemental Makeup of Aluminum Alloys in Atomic % [18]

Alloy	Mg	Cu	Mn	Si	Fe	Zn	Ti	Cr	Al
1100		0.05-0.20	≤ 0.05	≤0.95	≤0.95	≤ 0.10			Balance
5456	4.7-5.5	≤ 0.10	0.5-1.0	≤ 0.25	≤ 0.40	≤ 0.25	0.05-0.20	0.05-0.20	Balance
7075	2.1-2.9	1.2-2.0	≤ 0.30	≤ 0.40	≤ 0.50	5.1-6.1	≤ 0.20	0.18-0.28	balance

Half of the Al 5456-H116 samples were then heat treated at 150° C for 50 hours to sensitize the metal.

4.2 Accelerated Corrosion Experiment

4.2.1 General Background

Each of the GFRP and CFRP laminated aluminum samples (Al 1100-H14, Al 5456-H116, and Al 7075-T6) were subjected to accelerated corrosion with a modified version of the GM-9540P test procedure. This revised procedure will be discussed in-depth below. This test was compared to experiments done by Daniel Jensen in his thesis "*Corrosion of Aluminum Alloys-Polymer Matrix Composite Interfaces*" [6], and was used to help identify any major trends in corrosion ahead of field experiments.

4.2.2 Preparation of Samples

Each of the GFRP and CFRP laminated aluminum samples were labeled and mounted to a powder coated aluminum plate with nylon bolts and spacers to electrically isolate them from the rest of the test chamber. Figure 16 below refers.

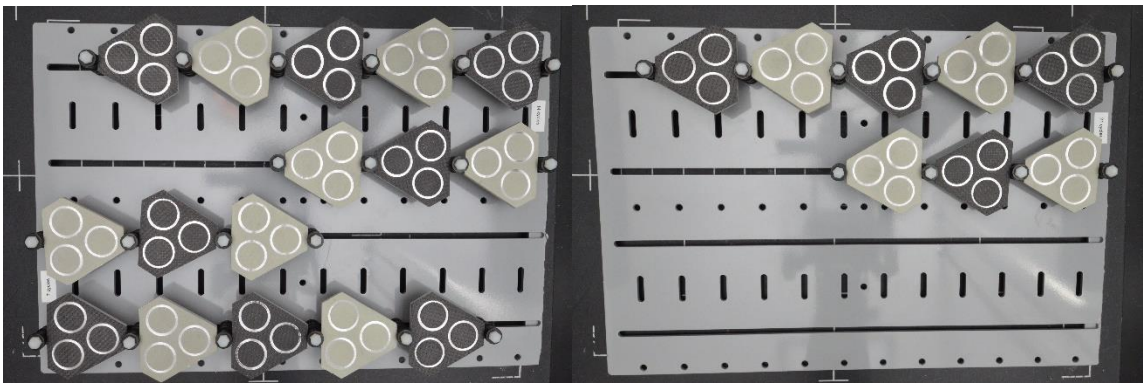

Figure 16: Composite-Al Samples Mounted for Accelerated Corrosion Experiment

The steel coupons were drilled for identification purposes and weighed before installation to help verify the accuracy of the test procedure.

4.2.3 Experiment Procedure, Conditions, & Set-up

The mounted samples were installed in the Singleton Corporation E-710 CCTC, as shown in Figure 17 below.

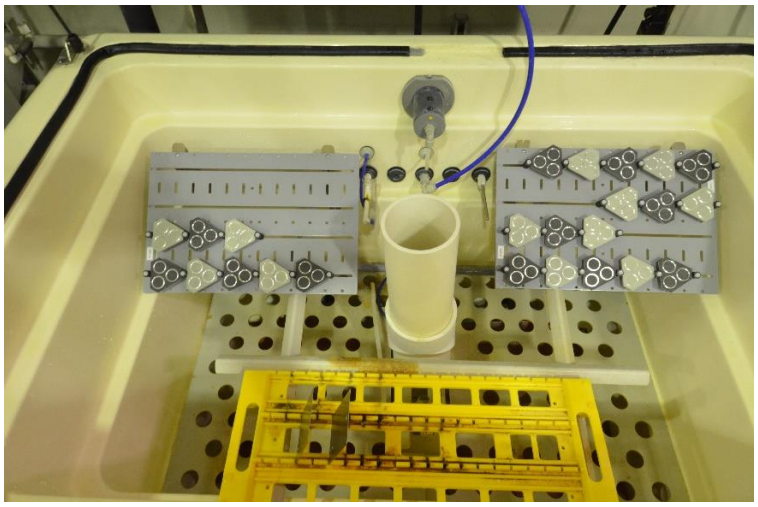

Figure 17: Composite-Al Laminate Samples and Steel Coupons Installed in the CCTC

The spray tank was then filled with a solution containing 0.9% by weight NaCl, 0.1% by weight $CaCl_2$, and 0.25% by weight $NaHCO_3$, and the CCTC was programmed with a modified version of the GM-9540P test procedure shown in Figure 18 below.

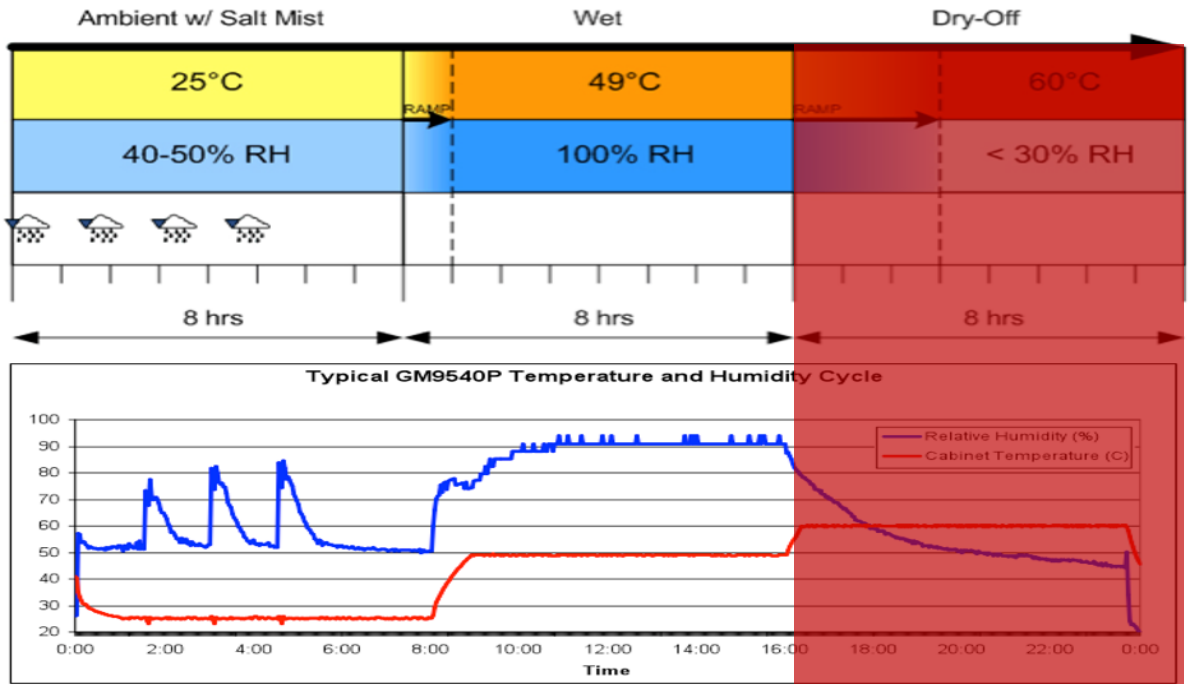

Figure 18: GM-9540P Test Procedure with Modifications in Red

The last 8 hour cycle was truncated in order to keep the samples constantly wetted, and was done as a comparison of corrosion and delamination rates compared to the full 24 hour cycle. The CCTC was programmed to run for an overall duration of 21 cycles (approximately 14 calendar days), and was stopped at 7 and 14 cycles to remove and inspect the appropriate GFRP and CFRP laminated aluminum samples. The steel coupons were removed, sandblasted, weighed, and replaced with new steel samples every 7 cycles to ensure accuracy of the GM-9540 test. All samples were stored in a 1 % relative humidity dry box once removed from the CCTC.

4.3 Field Experiment

4.3.1 General Background

Each of the GFRP and CFRP laminated aluminum samples (Al 1100-H14, Al 5456-H116, and Al 7075-T6) were subjected to environmental exposure at 5 different locations around the islands of Hawai'i for periods of 1 month, 6 months, and 1 year. Subjecting the samples to a variety of real world environments allowed for a very complete evaluation of the resiliency and bonding strength of the composite laminate and aluminum interface.

4.3.2 Preparation of Samples

Each of the GFRP and CFRP laminated aluminum samples were labeled and mounted to a powder coated aluminum plate with nylon bolts and spacers to electrically isolate them from the rest of the test stands (Figure 19).

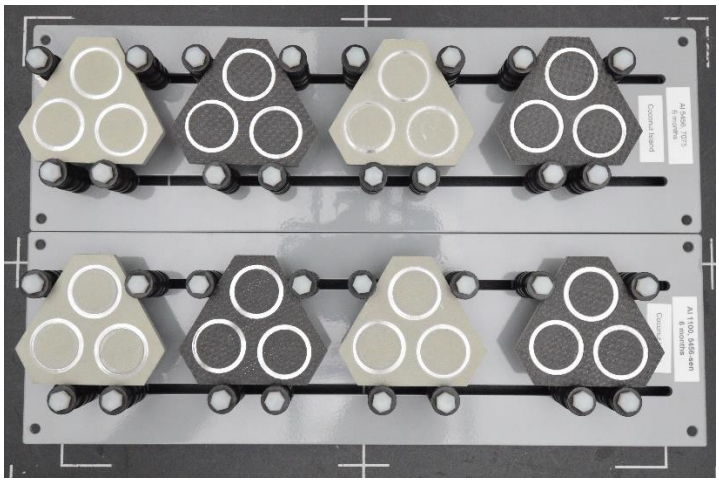

Figure 19: Composite-Al Samples Mounted for Environmental Corrosion Experiment

4.3.3 Experiment Procedure, Conditions, & Set-up

After the samples were mounted to the powder-coated plate, they were taken to 5 different locations around the islands of Hawai'i. These locations were Lyon Arboretum, Pyramid Rock, Coconut

Island, Mauna Loa and Kilauea Volcano. Figure 20 below shows each of the locations, as well as a picture of the test site.

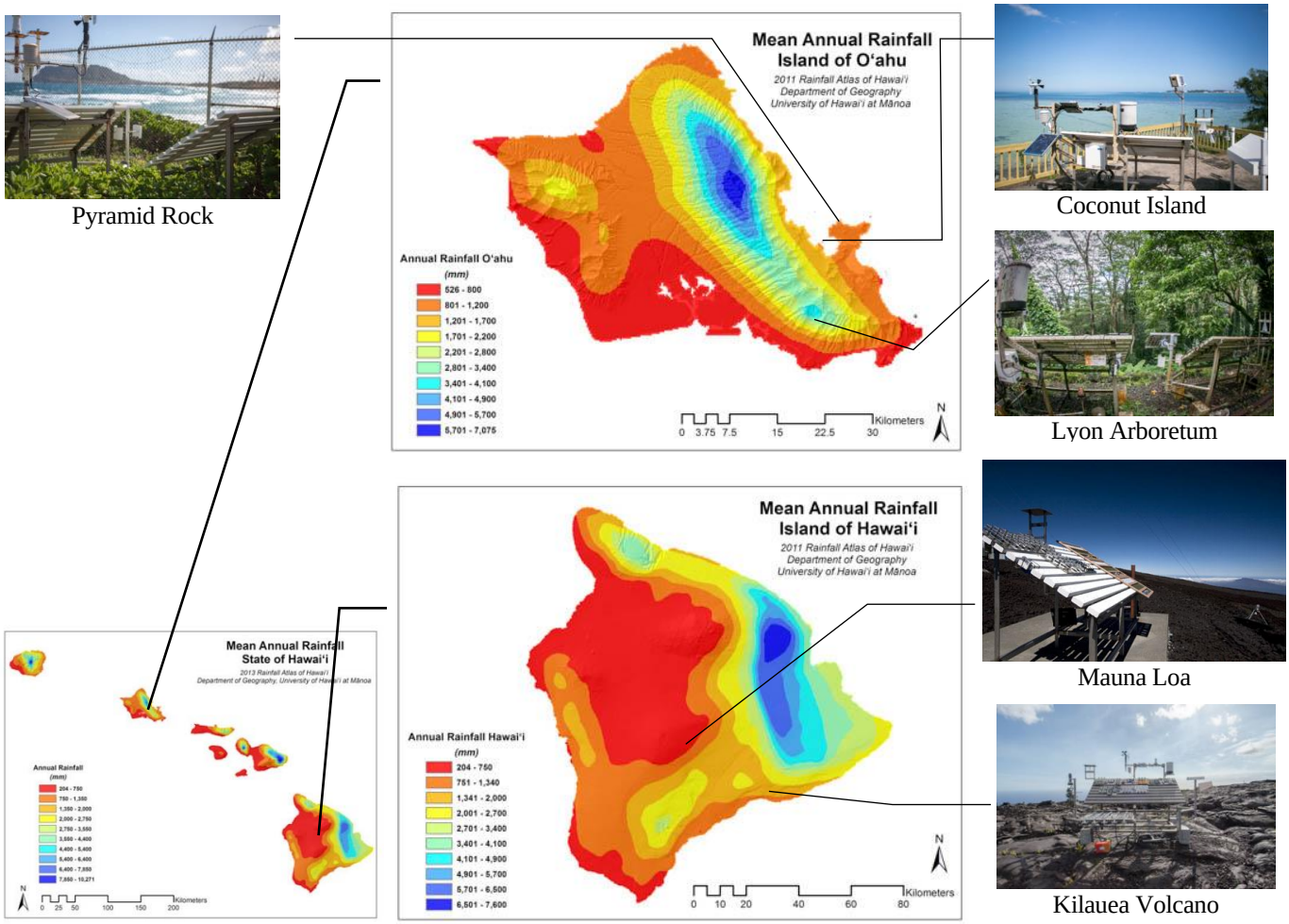

Figure 20: Atmospheric Testing Locations around the Islands of Hawai'i [19]

The Lyon Arboretum test site is located in a tropical rainforest and represents high rainfall and low chloride and sulfate deposition location. Lyon Arboretum is owned and has been used extensively by the University of Hawaii to study tropical and sub-tropical plants. Annual weather data for Lyon Arboretum can be found in Table 2 below.

The Pyramid Rock test site is located on a beach on the north side of Marine Corps Base Hawaii (MCBH) and faces northeast toward the Pacific Ocean. Pyramid Rock represents a severe marine

environment with moderate rainfall and extremely high chloride and sulfate deposition. Annual weather data for Pyramid Rock can be found in Table 2 below.

The Coconut Island test site is located on a beach on the north side of Coconut Island. The test site represents a moderate rainfall and moderate chloride and sulfate deposition site due to its secluded location in Kaneohe Bay. Annual weather data for Coconut Island can be found in Table 2 below.

The Mauna Loa test site is located at the National Oceanic and Atmospheric Administration (NOAA) observatory on Mauna Loa volcano. Mauna Loa represents a dry-alpine environment with its high altitude (11,145 feet above sea-level), low rainfall, and low chloride and sulfate deposition. Annual weather data for Mauna Loa can be found in Table 2 below.

The Kilauea volcano test site is located on a cooled lava flow near the erupting caldera of Kilauea. Kilauea represents a volcanic site with moderate rainfall and low chloride and sulfate deposition. Of note, the sulfur dioxide (SO_2) emitted by the volcanic vents reacts with water vapor in the air and sunlight to form sulfuric acid (H_2SO_4) which causes a severe acid rain environment. Annual weather data for Kilauea volcano can be found in Table 2 below.

Table 2: Annual Average Weather Data for Atmospheric Test Sites

Test Site	Avg. Temp (°C)	Avg. Humidity (%RH)	Avg. Monthly Rainfall (mm)	Cl^- Depos. ($mg/m^2/day$)	SO_4^{2-} Depos. ($mg/m^2/day$)
Lyon Arboretum	23.3	85.0	362.0	2.0	0.5
Pyramid Rock	24.6	79.3	61.2	2267.2	326.3
Coconut Island	25.0	78.1	91.2	49.3	7.7
Mauna Loa	6.1	36.3	37.7	0.1	1.4
Kilauea Volcano	21.0	80.6	130.9	52.8	30.8

As an aid to the maps presented in Figure 20 above, Table 3 below shows the exact location of each test site and their microclimate representation.

Table 3: Test Site Locations

Test Sites	Microclimate Representation
Lyon Arboretum	Tropical Rainforest
Pyramid Rock	Marine (severe)
Coconut Island	Marine (mild)
Mauna Loa	Alpine (arid)
Kilauea Volcano	Volcano/Acidic (acid rain)

One test sample of each laminate (GFRP and CFRP) coupled to each alloy of aluminum (Al 1100-H14, Al 5456-H116 sensitized, Al 5456-H116 non-sensitized, and Al 7075-T6) for each of the exposure periods (1 month, 6 months, and 1 year) for a total of 24 samples were brought to each test site. The one notable exception to the exposure periods was at Pyramid Rock. The environment was so severe the CFRP laminated aluminum samples were returned to the lab at 20 days, 80 days, and 110 days in order to get meaningful data when performing the adhesion test. Another notable exception was at the Mauna Loa test site, there were no CFRP laminated Al 5456-H116 sensitized

samples for the 1 month and 6 month time period due to a shortfall in production of those samples. A typical test sample orientation at a test site is shown in Figure 21 below.

Figure 21: Typical Field Exposure Sample Layout

4.4 Adhesion Testing Experiment

4.4.1 General Background

Once the laminated aluminum alloys returned from field exposure, they were subjected to adhesion testing to determine the residual strength of the epoxy bond to the aluminum substrate. Each of the 20 mm diameter composite reliefs were removed from substrate aluminum using a DelFelsko PosiTest AT-A Automatic adhesion tester and 20 mm diameter aluminum dolly. After the composite reliefs were removed, further analysis including SEM and EDX analysis could be accomplished.

4.4.2 Preparation of Samples

Before being adhered to the composite test relief on each sample, the 20 mm dolly was scuffed with a red Scotch-Brite pad and cleaned with acetone to allow the epoxy maximum bonding strength. The surface of each composite relief was lightly scuffed using a Dremel 200 rotary tool and a round

carbide bit to remove some of the corrosion products on the composite surface to allow maximum bonding strength.

Once all the dollies and composite reliefs were cleaned and scuffed, the dollies were epoxied onto the reliefs using 3M Scotch-Weld Epoxy Adhesive 1838 B/A. The freshly epoxied samples were then put in a Lindberg/Blue mechanical oven to cure at 60° C for 2 hours to fully cure the epoxy. Figure 22 below shows an example of a fully cured dolly on a composite relief test site.

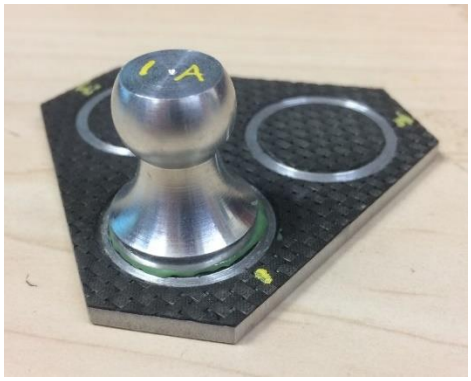

Figure 22: 20 mm Aluminum Dolly Epoxied to Composite-Laminated Aluminum Sample

After the samples had cured in the oven, each test relief was labeled with a number corresponding to the relief location and letter corresponding to the number of adhesion tests done on that relief. Many of the test samples took several attempts to successfully remove the composite laminate from the aluminum surface, so this method made it easy to track which dolly went to each relief site.

4.4.3 Experiment Procedure, Conditions, & Set-up

The cured and labeled samples were then put into the DelFelsko PosiTest AT-A Automatic adhesion tester, which was set to 20 mm dollies and a pull rate of 30 psi/sec. This pull rate was the slowest the adhesion tester could perform, and allowed for a more even pull and a higher success rate for

complete delamination. Figure 23 below shows how the adhesion tester was coupled to the test samples.

Figure 23: Composite-Laminated Aluminum Sample in Adhesion Tester

When the adhesion test was complete, the pressure to remove the dolly (in psig) and whether or not the test was successful in completely removing the composite from the substrate was recorded. Figure 24 below illustrates a successful and unsuccessful adhesion test.

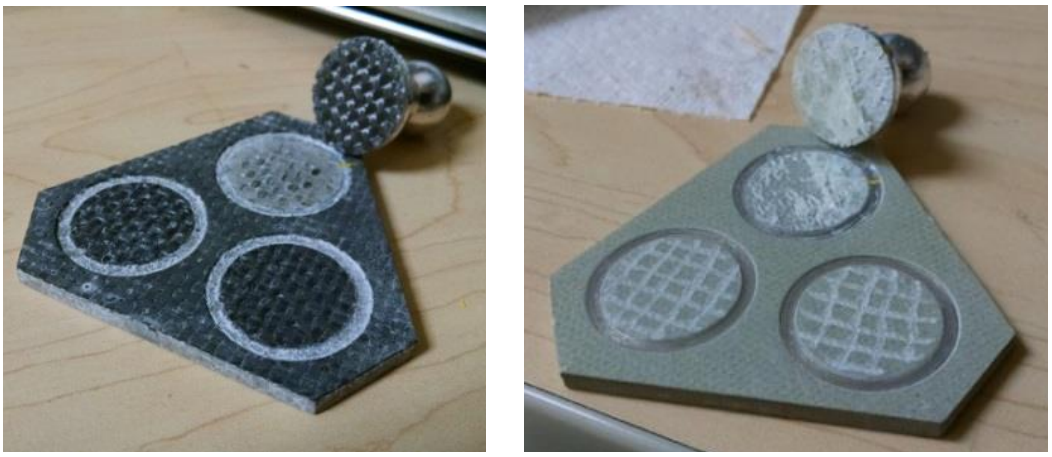

Figure 24: Successful (left) and Unsuccessful (right) Adhesion Tests [6]

Some reliefs required multiple pulls to remove all composite layers. After all reliefs were successfully pulled, the highest values for each of the three reliefs were averaged to determine the average composite adhesion strength for each composite and substrate tested.

4.5 SEM and EDX Analysis

4.5.1 General Background

The corrosion products that formed on the substrate aluminum around and below the composite reliefs were studied with a Hitachi S3400-N scanning electron microscope equipped with an Oxford Instruments energy dispersive X-ray analyzer. Figure 25 below shows the SEM and EDX.

Figure 25: Hitachi S3400-N SEM with Oxford Instruments EDX Analyzer

This analysis allowed for the study of the rate of penetration and type of corrosion products that caused a weakened bond between the laminate and substrate.

4.5.2 Preparation of Samples

Test specimens were carefully chosen that had a solid delineation between corroded and uncorroded regions under the composite reliefs. Once chosen, the samples had a strip of pure copper placed across the diameter of the relief in order to optimize the EDX INCA software for elemental analysis.

The copper strip was then marked in the center of each relief and subsequent marks were placed approximately 1 mm apart to help serve as a reference point when the sample was in the SEM (Figure 26).

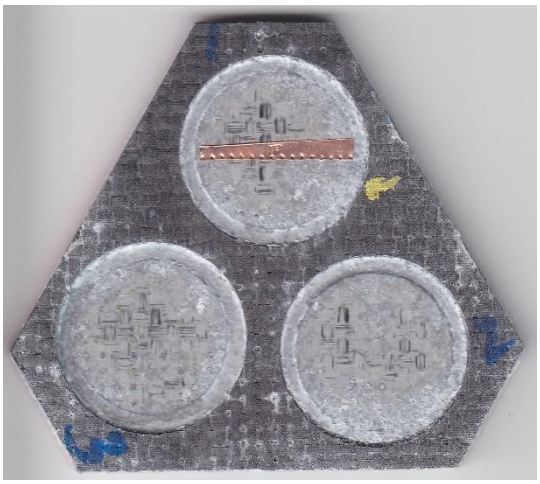

Figure 26: Composite-Laminated Al Sample with Copper Strip for SEM/EDX Analysis

4.5.3 Experiment Procedure, Conditions, & Set-up

Seventeen test specimens were selected for SEM and EDX analysis, as it would be very time consuming and impractical to test all 142 test samples (Table 5). After the specimens were marked for analysis, they were mounted in the SEM. The SEM was set for 20.0 kV and the detector was positioned approximately 10 mm from the sample surface to ensure proper alignment. After finding the center of the specimen, the microscope was set to 50x magnification and a site picture was taken. The EDX coupled with INCA software was then used to scan the surface of the sample from the center to the edge of the circle in approximately 0.2 mm increments. The INCA software allowed for the study composition of corrosion products on the aluminum substrate, and the results were presented in atomic percentage.

4.6 Profilometry Analysis

4.6.1 General Background

The profile analysis was completed off site at Nanovea using their ST400 3D profilometer after the SEM and EDX analysis was completed. This analysis allowed for the study of the amount of pitting corrosion that occurred under the composite laminate, as well as the volume lost to pitting in the substrate aluminum.

4.6.2 Preparation of Samples

After a select group of samples was selected from the SEM and EDX analysis, they were sent to the University of Hawai'i at Manoa machine shop to be cut, and then cleaned as stated in section *3.5 Profile Analysis Samples*.

4.6.3 Experiment Procedure, Conditions, & Set-up

Each of the samples were scanned by Nanovea using an x-axis spacing of 10 μm and a y-axis spacing of 40 μm on the Nanovea ST400 3D profilometer.

4.7 Nitric Acid Mass Loss Experiment

4.7.1 General Background

Once the aluminum samples had been profiled, they were subjected to a nitric acid (HNO_3) bath in order to determine the amount of sensitization the Al 5456-H116 alloy underwent. This test was

also used to compare sensitized and exposed samples to sensitized and unexposed samples to determine if there was additional sensitization that occurred due to extended periods in hot climates.

4.7.2 Preparation of Samples

There was no major preparation of the samples between the profile test and the nitric acid mass loss test.

4.7.3 Experiment Procedure, Conditions, & Set-up

After performing the profile test listed in section *4.6 Profilometry Analysis* above, the Mg_2Al_3 precipitates were removed from the bulk aluminum substrate in accordance with the ASTM G67-13 procedure [8]. The all dimensions of the aluminum samples are taken to within 0.02 mm and the total surface area of each sample was calculated. Each of the aluminum samples were then desmutted by submerging in a 5% by weight NaOH solution at 80° C for 1 minute, followed by an ultrapure (18 MΩ•cm) water rinse. The samples were then submerged in a 70 wt% solution of HNO_3 at 30° C for 30 seconds, followed by the ultrapure water rinse. After drying, the samples were weighed to within ± 0.0001 g, and then submerged in the 70 wt% HNO_3 solution at 30° C for 24 hours. The nitric acid experiment setup is shown in Figure 27 below.

Figure 27: Nitric Acid Mass Loss Experiment Setup

After the 24 hour immersion, the samples were rinsed in ultrapure water, dried, and weighed to within ± 0.0001 g.

4.8 Microstructure Analysis

4.8.1 General Background

Small samples of each substrate aluminum alloy [Al 1100-H14, Al 5456-H116 (non-sensitized), Al 5456-H116 (sensitized), and Al 7075-T6] were cut, set in epoxy, polished, and then electrolytically etched to study the microstructure of each alloy. The polished samples were subjected to SEM and EDX analysis before being etched and subjected to optical microscopy. The SEM and EDX analysis allowed for the comparison of the test sample aluminum elemental makeup compared to scientific standard elemental makeup. The samples that were etched and subjected to optical microscopy allowed for the study of grain orientation, size, and shape between each of the alloys.

4.8.2 Preparation of Samples

The samples that were subjected to SEM and EDX analysis were prepared as stated in section *3.2 Microstructure Analysis Samples* above.

The samples that were etched were prepared as follows. The etching process started with drilling a small hole in the back of the samples to connect a wire lead to the aluminum alloy. Each alloy was then submerged in a dilute solution of fluoroboric acid, also known as Barker's reagent (5 mL HBF_4 (48%) in 200 mL water) as the anode with a stainless steel cathode also submerged in the acid etchant. An Xpower 305D DC power supply was connected to each of the electrodes (positive side to the Al alloy and negative side to the stainless steel) and a 30 V potential across the electrodes was applied for 120 seconds. The Al alloy samples were then immediately taken out of the Barker's reagent and cleaned with ultrapure water.

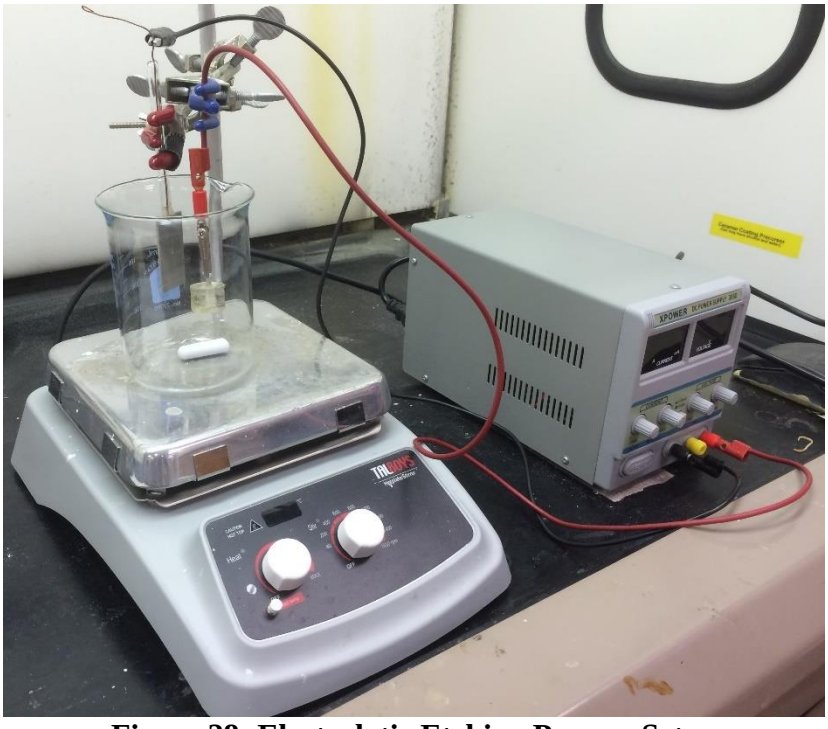

Figure 28: Electrolytic Etching Process Setup

Figure 28 above shows the setup process for electrolytic etching of each Al alloy microstructure analysis sample.

4.8.3 Experiment Procedure, Conditions, & Set-up

After polishing, the samples were mounted in the SEM. The SEM was set for 20.0 kV and the detector was positioned approximately 10 mm from the sample surface to ensure proper alignment. The samples were studied at varying magnifications and locations to get a representative elemental composition. The EDX coupled with INCA software was then used to scan the surface of the sample at multiple points of interest. The INCA software allowed for the study composition of elements in the aluminum alloys, and the results were presented in atomic percentage.

After SEM analysis, the samples were etched as stated above and mounted in a Zeiss Axioplan optical microscope. The samples were then analyzed with a Paxcam 5 digital camera and Pax-it! software at 10x, 20x, and 50x magnification. Figure 29 below refers.

Figure 29: Zeiss Axioplan Optical Microscope and Paxcam 5 Digital Camera

4.9 Polarization Experiment

4.9.1 General Background

Each of the aluminum alloys [Al 1100-H14, Al 5456-H116 (non-sensitized), Al 5456-H116 (sensitized), and Al 7075-T6] were subjected to an open-circuit potential and potentiodynamic polarization test. These tests allowed for the study of the corrosion current (I_{corr}) which is an indicator of a normal corrosion rate for each alloy of aluminum. The results will be used to determine if the normal corrosion rates have an effect on the delamination rate of the composite layers.

4.9.2 Preparation of Samples

The samples that were subjected to polarization tests were prepared as stated in section *3.3 Polarization Experiment Samples* above.

4.9.3 Experiment Procedure, Conditions, & Set-up

Before the potentiodynamic polarization experiments were started, open-circuit potential values were obtained over a one-hour period on a Parstat 2273 Advanced Potentiostat. The electrodes were submerged in a 3.15 wt% solution of NaCl heated to 30° C, and compared against a Saturated Calomel Electrode (SCE) with KCl for both the open-circuit and potentiodynamic polarization experiments. The solution was aerated with compressed air at a volumetric rate of 320-370 mL/minute at a pressure of 1 atmosphere for both the open-circuit and potentiodynamic polarization experiments. Figure 30 below illustrates the setup for the open-circuit potential and potentiodynamic polarization experiments.

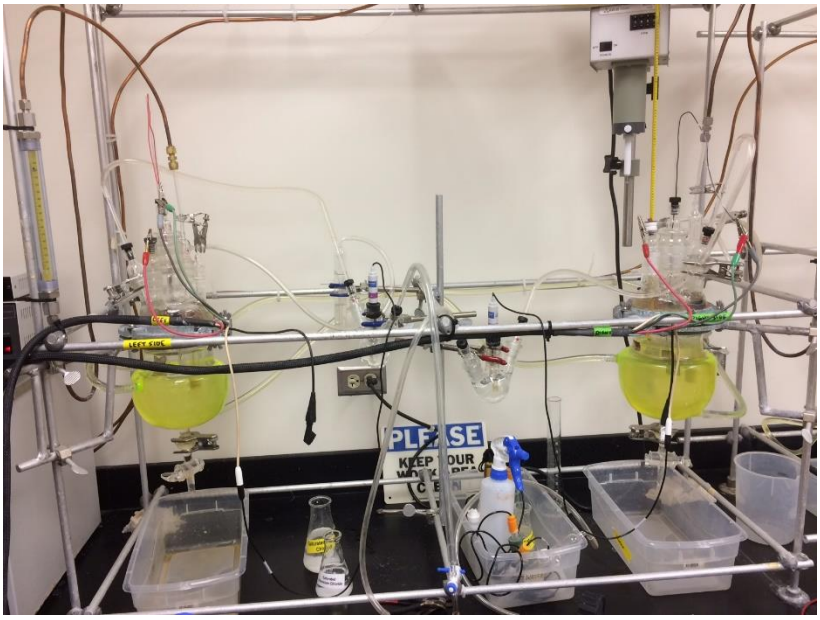

Figure 30: Potentiodynamic Polarization Experiment Setup

Immediately following the open-circuit potential experiment for each electrode, the cathodic polarization curve for each electrode could be obtained.

Chapter 5

RESULTS

5.1 Adhesion Experiment

5.1.1 Results

After the adhesion tests were complete, the highest value for each of three composite reliefs (per alloy and composite combination) was averaged together to get a composite look at the strength decay rates over the exposure period. Scatter plots with linear trend lines for each test location (to include CCTC testing) are presented in Figure 31 through Figure 36 below.

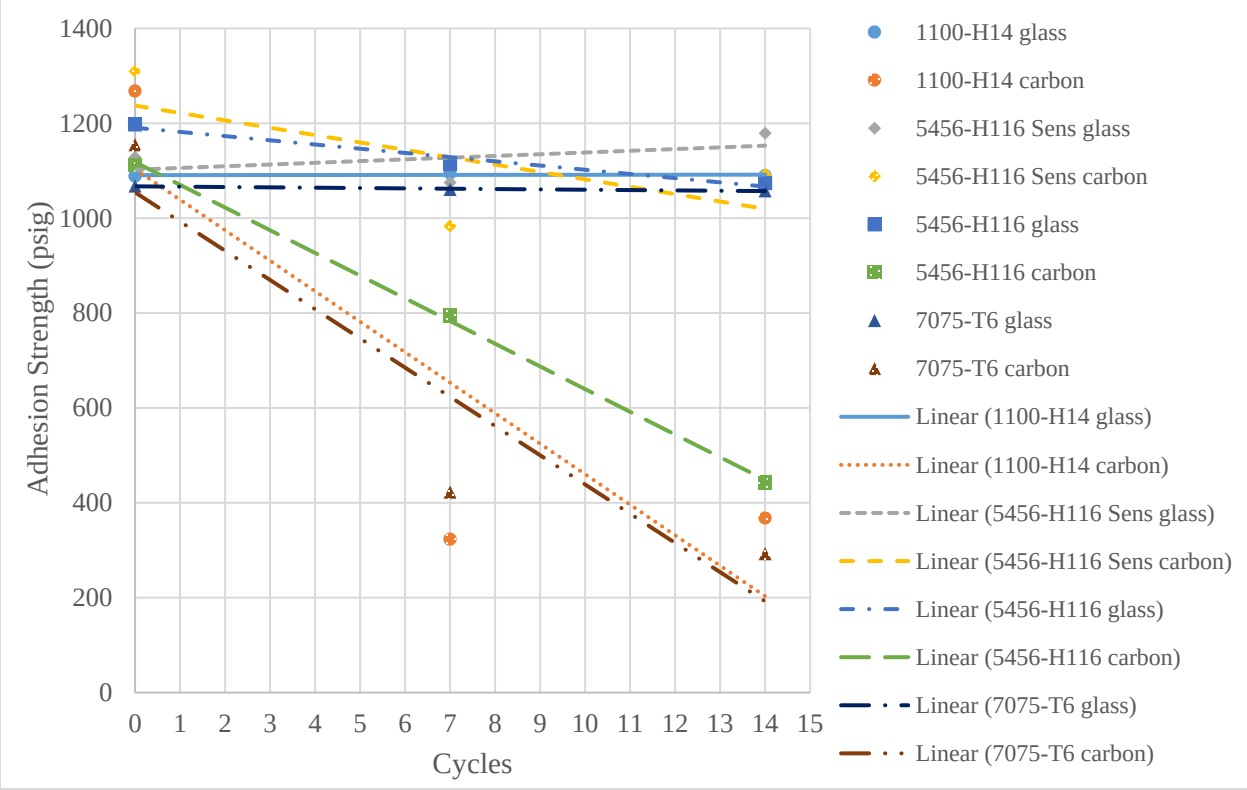

Figure 31: CCTC Adhesion Test Results

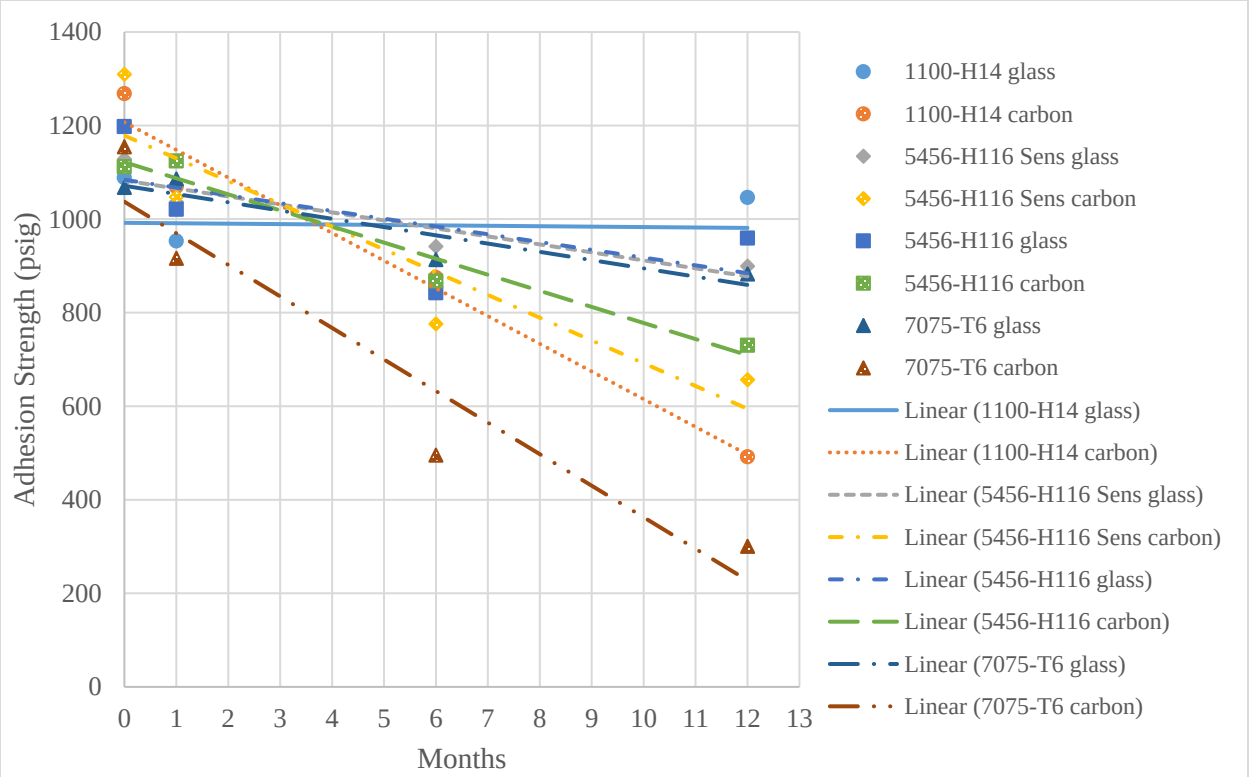

Figure 32: Lyon Arboretum Adhesion Test Results

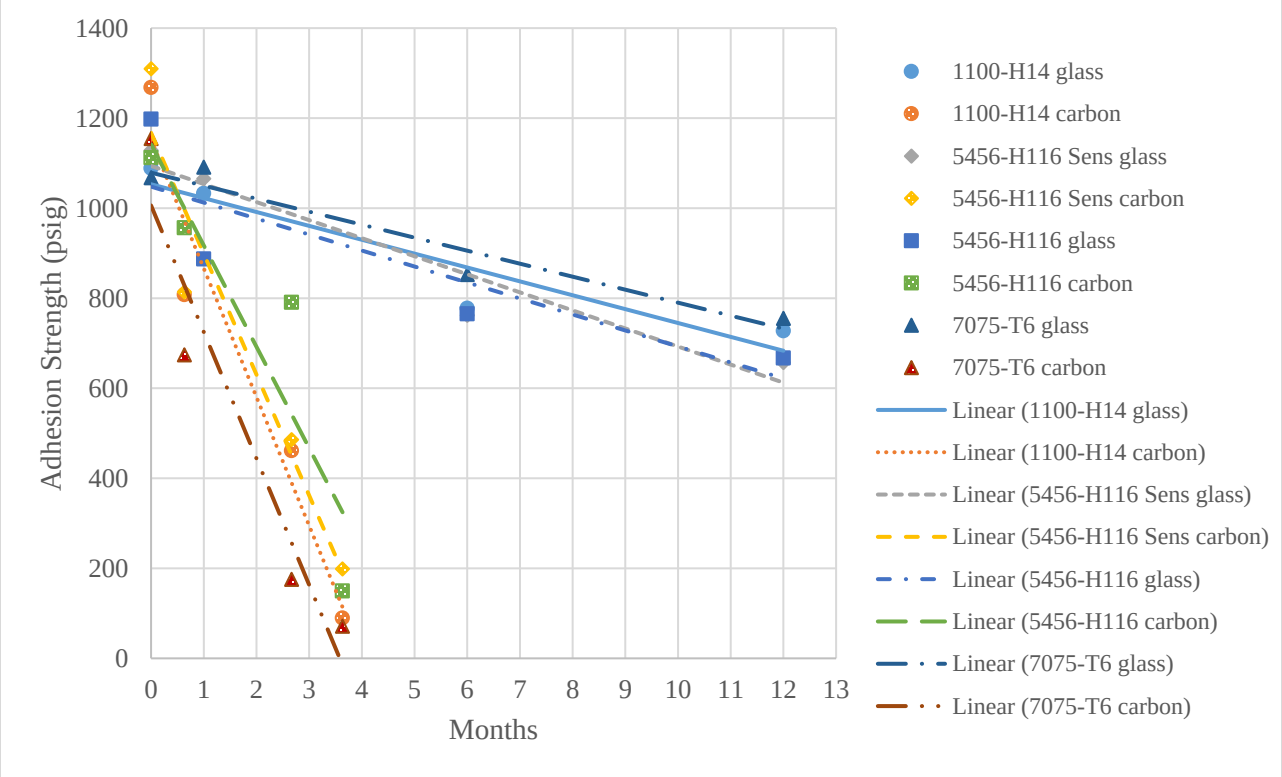

Figure 33: Pyramid Rock Adhesion Test Results

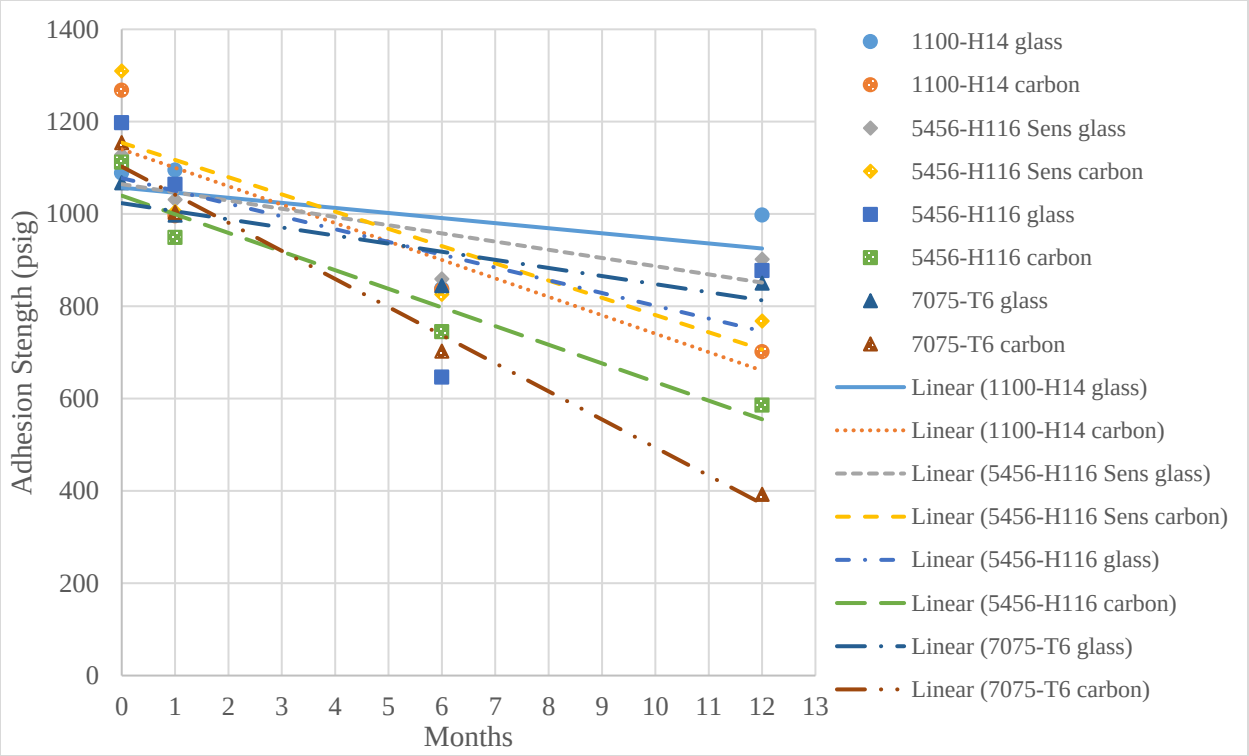

Figure 34: Coconut Island Adhesion Test Results

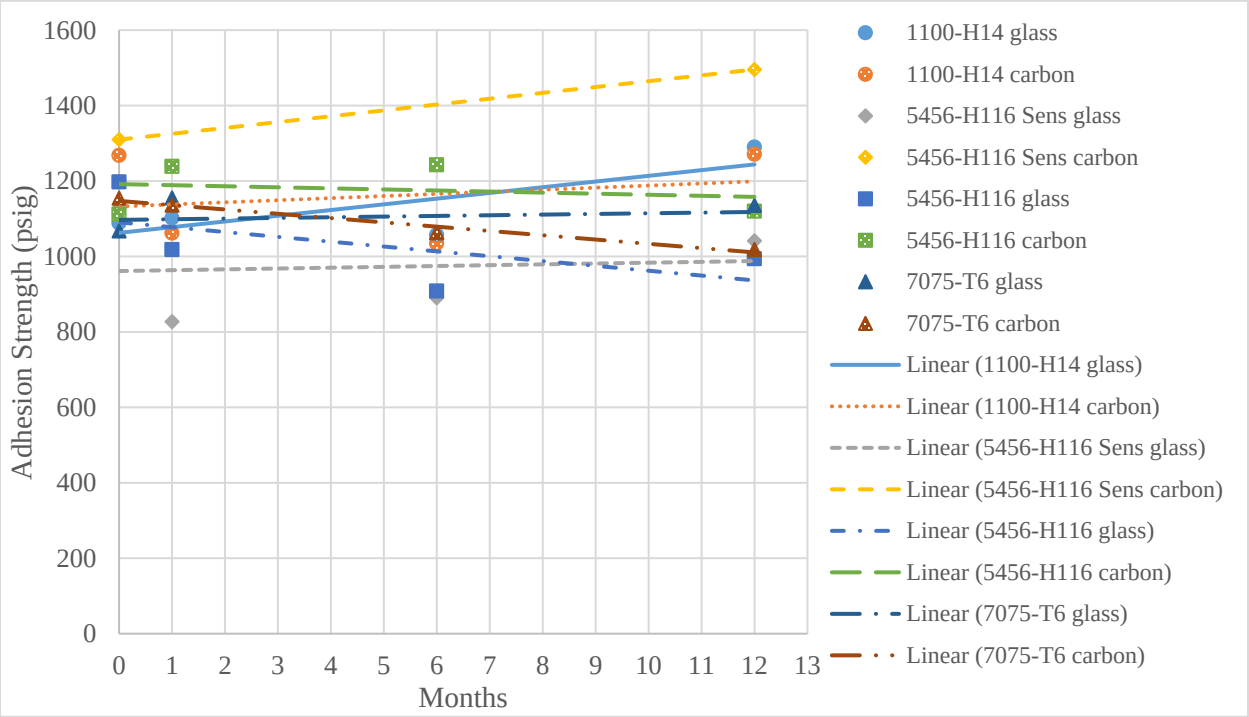

Figure 35: Mauna Loa Adhesion Test Results

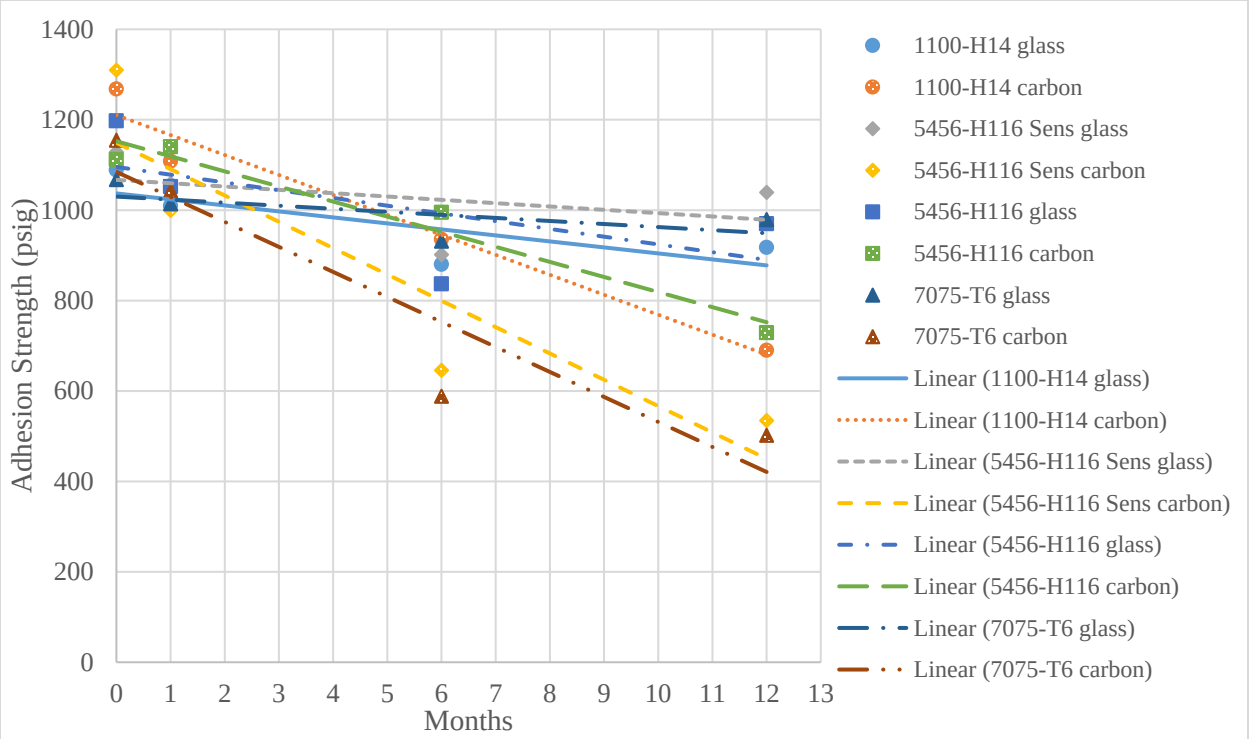

Figure 36: Kilauea Volcano Adhesion Test Results

Scatter plots in Figure 37 through Figure 40 below illustrate the decohesion rate for each alloy and composite laminate combination compared to test site location. The dotted line that is the same color as the corresponding test site location is the trend line for that data.

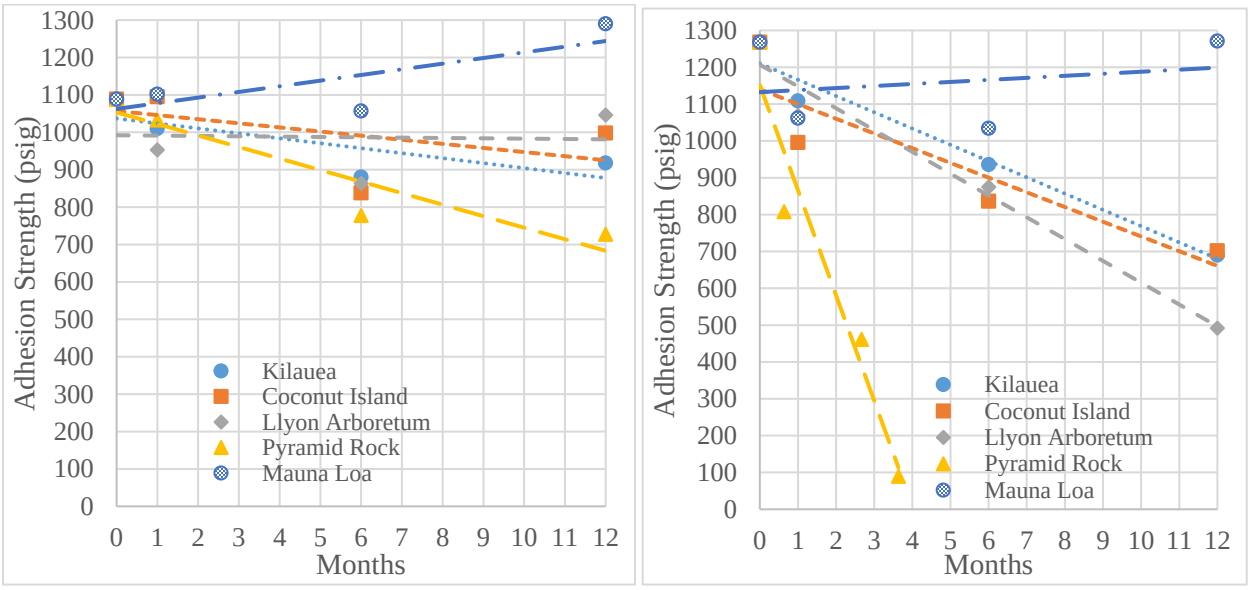

Figure 37: Al 1100-H14 GFRP (left) & CFRP (right) Adhesion Test Results

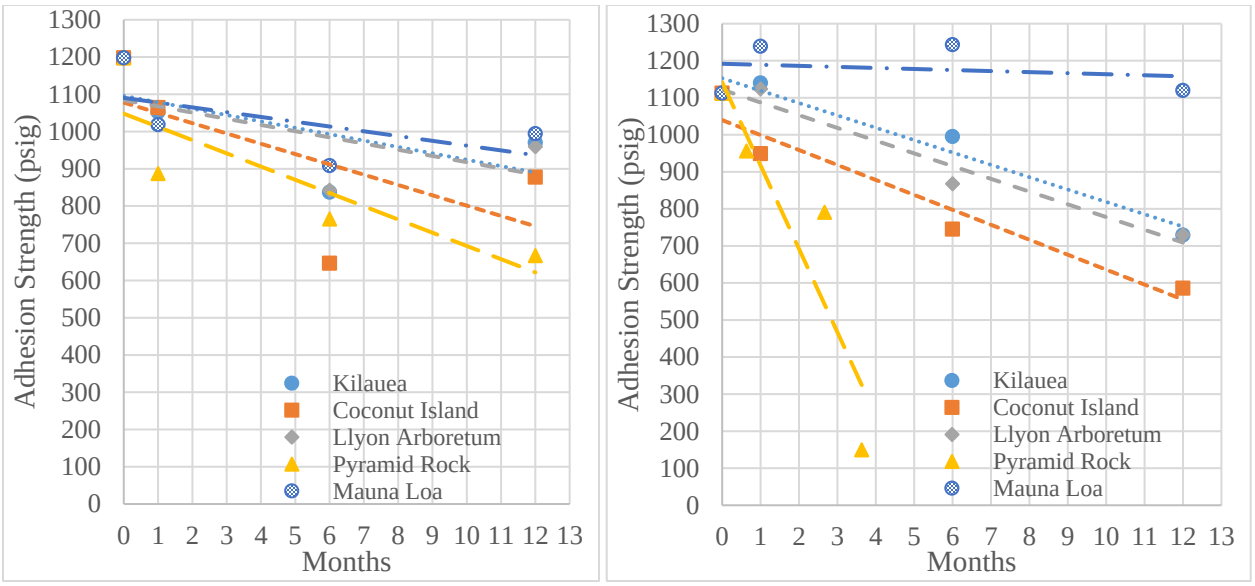

Figure 38: Al 5456-H116 Non-sensitized GFRP (left) & CFRP (right) Adhesion Test Results

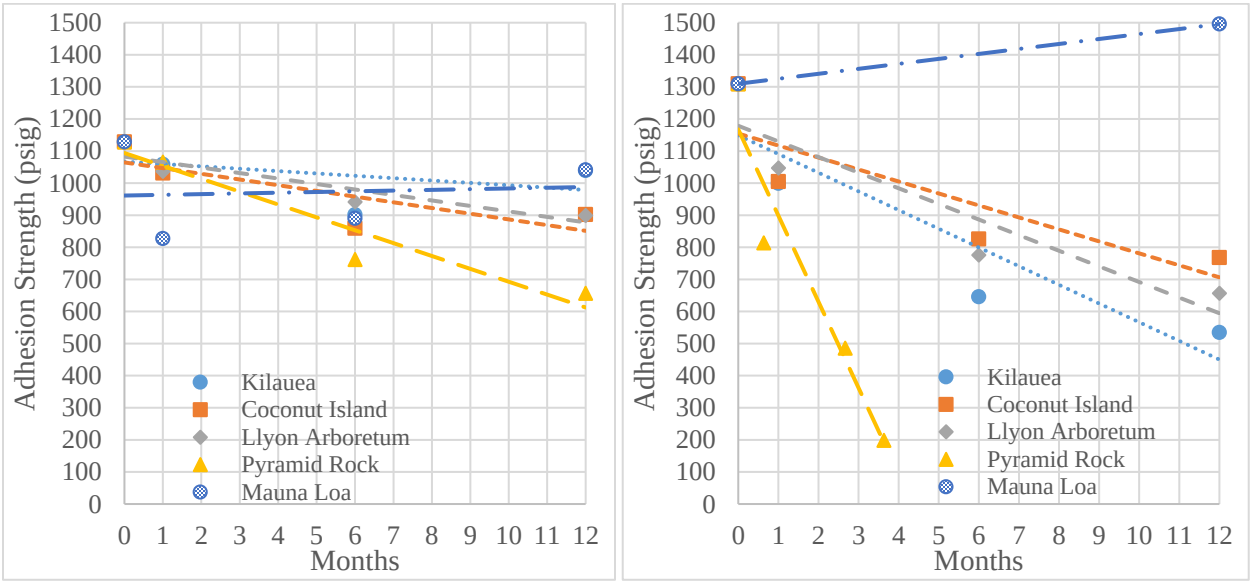

Figure 39: Al 5456-H116 Sensitized GFRP (left) & CFRP (right) Adhesion Test Results

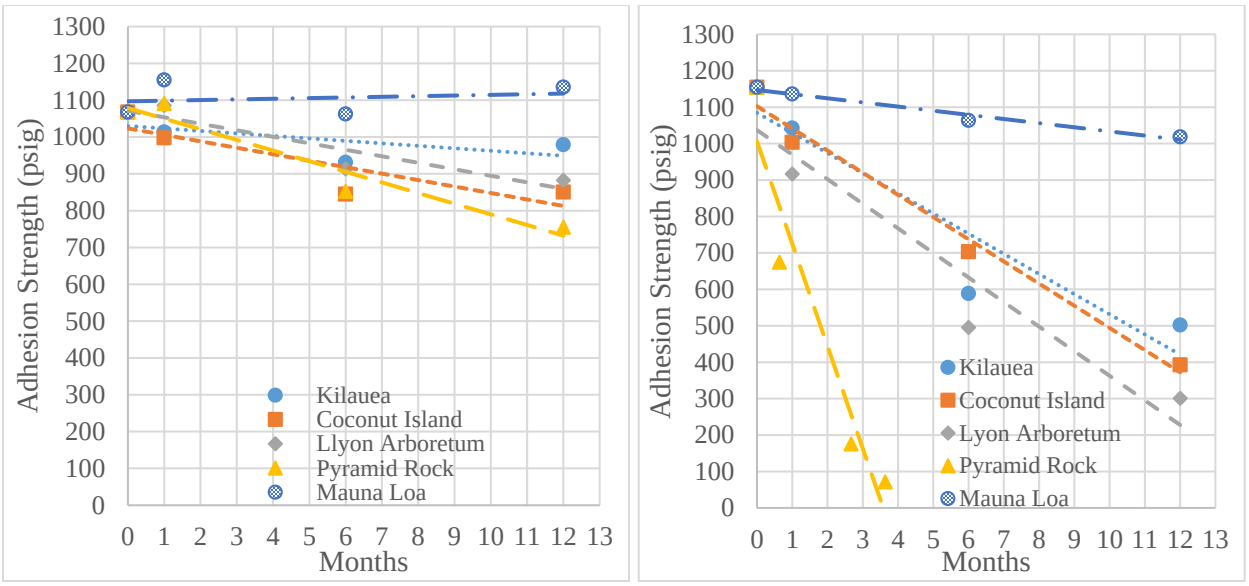

Figure 40: Al 7075-T6 GFRP (left) & CFRP (right) Adhesion Test Results

Decohesion rates in psi/month for each environmental exposure composite laminated aluminum alloy sample were taken using the slope of the adhesion test trend lines, and are listed in Figure 41 and Figure 42 below.

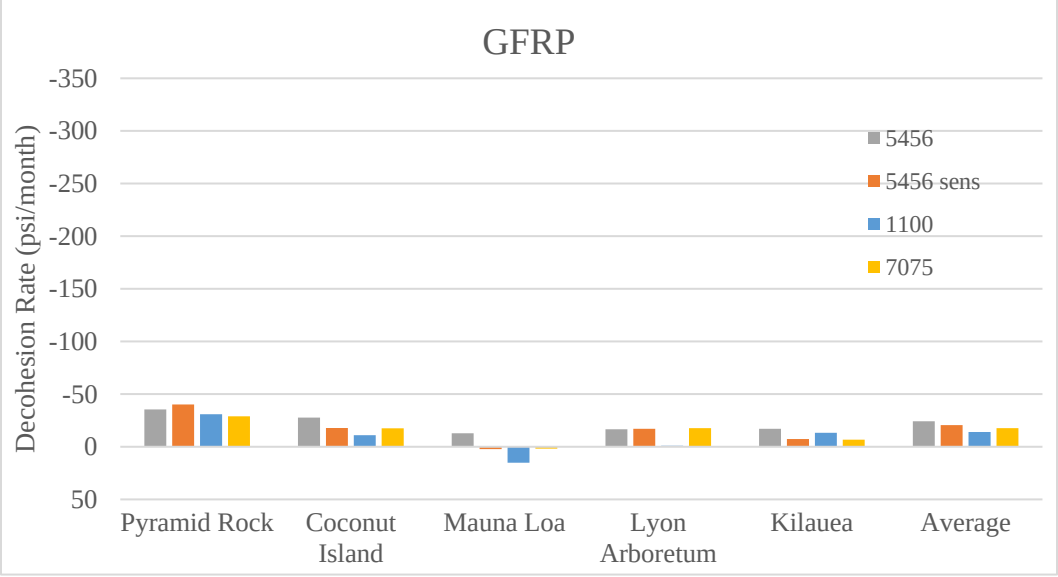

Figure 41: Decohesion Rates for Environmental Exposure GFRP Laminated Al Alloys

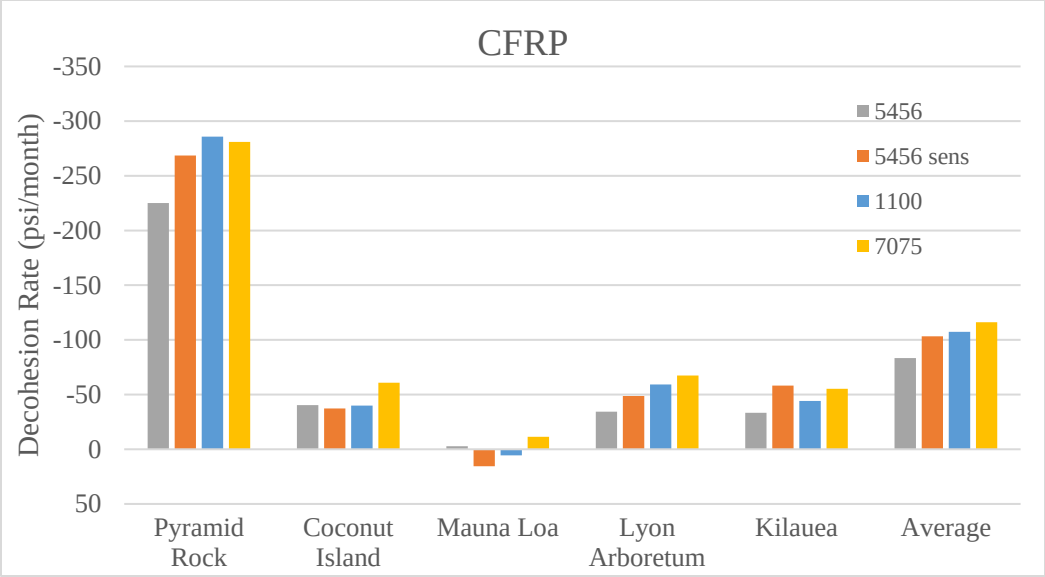

Figure 42: Decohesion Rates for Environmental Exposure CFRP Laminated Al Alloys

Table 4: Decohesion Rate of CFRP-laminated Al Alloy as a Function of Substrate Aluminum (psi/month)

Location	Alloy			
	1100-H14	**5456-H116 Sensitized**	**5456-H116 Non-sensitized**	**7075-T6**
Lyon Arboretum	-59.21	-48.68	-34.38	-67.46
Pyramid Rock	-285.85	-268.50	-225.07	-280.98
Coconut Island	-39.94	-37.33	-40.37	-60.86
Mauna Loa	5.55	15.50	-2.82	-11.37
Kilauea Volcano	-44.16	-58.24	-33.37	-55.31
Average	-84.7	-79.4	-67.2	-116.2
Standard Deviation	115.0	109.5	89.5	106.2

Decohesion rates in psi/cycle for each CCTC exposure composite laminated aluminum alloy sample are listed in Figure 43 below.

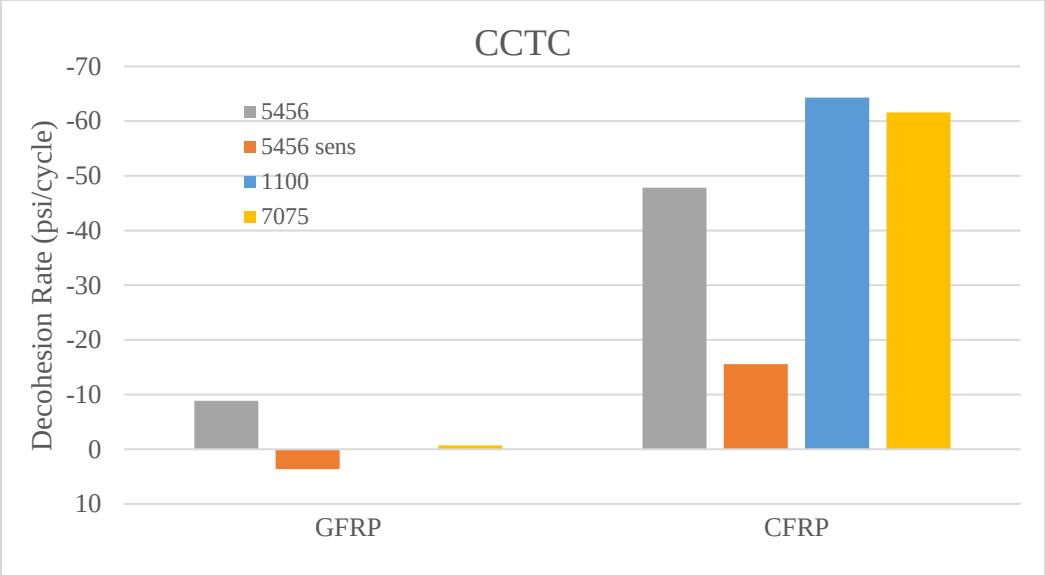

Figure 43: Decohesion Rates for CCTC Exposure GFRP and CFRP Laminated Al Alloys

5.2 SEM and EDX Analysis

5.2.1 Results

SEM and EDX analysis was conducted on 17 samples to determine the atomic percentage of elements from the center of the relief section to the exposed substrate gap on the very edge. The 17 samples tested are listed in Table 5 below.

Table 5: SEM and EDX Analysis Samples

Location	Alloy	Exposure Time	Composite
Lyon Arboretum	1100-H14	1 year	CFRP
	5456-H116 non-sensitized	1 year	CFRP
	5456-H116 sensitized	1 year	CFRP
	7075-T6	1 year	CFRP
Pyramid Rock	1100-H14	2.67 months	CFRP
	5456-H116 non-sensitized	2.67 months	CFRP
	5456-H116 sensitized	2.67 months	CFRP
	7075-T6	2.67 months	CFRP
	7075-T6	1 year	GFRP
Coconut Island	1100-H14	1 year	CFRP
	5456-H116 non-sensitized	1 year	CFRP
	5456-H116 sensitized	1 year	CFRP
	7075-T6	1 year	CFRP
Kilauea	1100-H14	1 year	CFRP
	5456-H116 non-sensitized	1 year	CFRP
	5456-H116 sensitized	1 year	CFRP
	7075-T6	1 year	CFRP

Elemental analysis scatter plots for each of the test sites and composite laminated aluminum alloy samples are illustrated in Table 6 through Table 9 below. The x-axis of each scatter plot starts at as close to the exact center of the circular relief as possible, and moves out in approximately 0.2 mm steps until it stops at approximately the first 1/3 of the open substrate gap. The graph on the left side indicates the atomic percentage of carbon (C), oxygen (O), and aluminum (Al) with the left y-axis scale (each of the values are additive to 100%), and the aluminum to oxygen ratio is represented with the yellow line and is read from the right y-axis scale. The graph on the right side indicates the atomic percentage of sodium (Na), chlorine (Cl), and sulfur (S).

Table 6: Lyon Arboretum SEM and EDX Sample Analysis

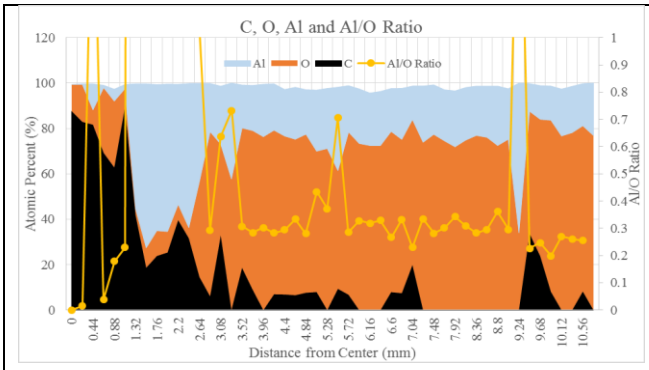	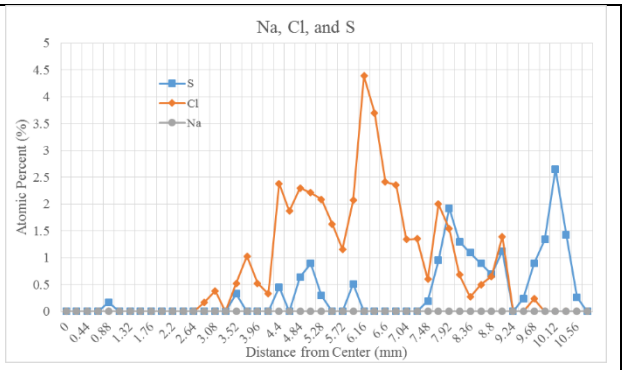
1100-H14 CFRP 1 Year	1100-H14 CFRP 1 Year
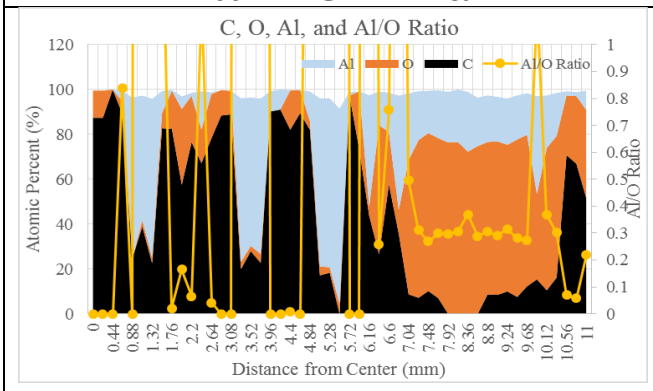	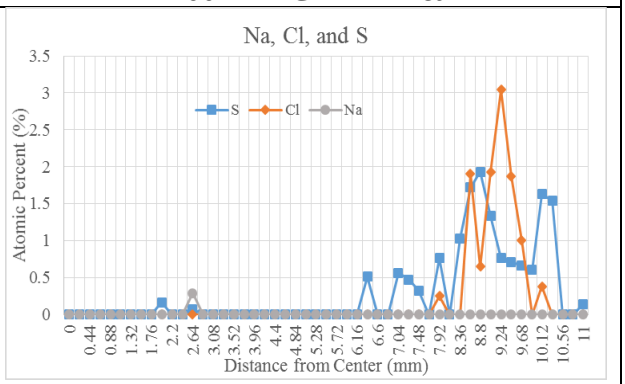
5456-H116 CFRP 1 Year	5456-H116 CFRP 1 Year
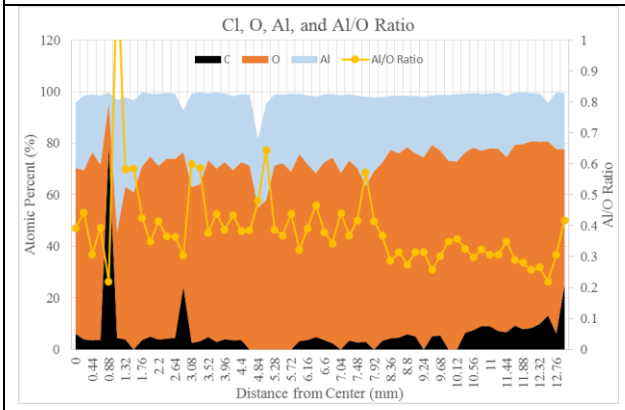	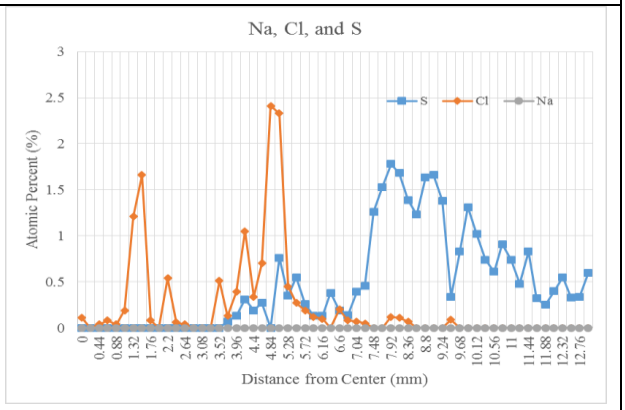
5456-H116 Sensitized CFRP 1 Year	5456-H116 Sensitized CFRP 1 Year
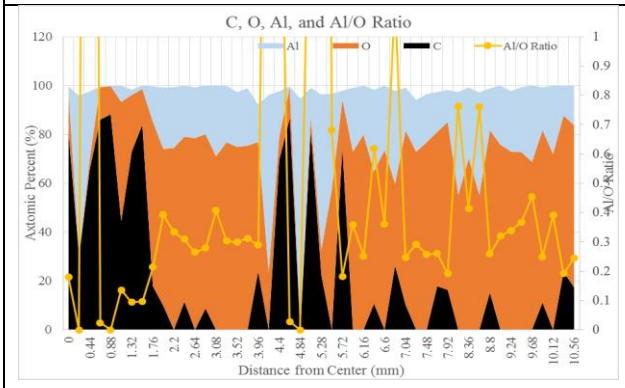	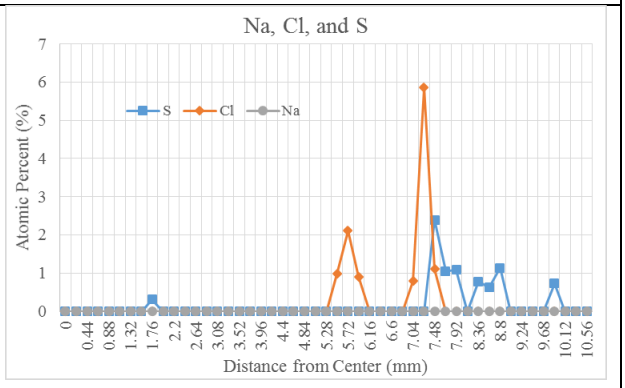
7075-T6 CFRP 1 Year	7075-T6 CFRP 1 Year

Table 7: Pyramid Rock SEM and EDX Sample Analysis

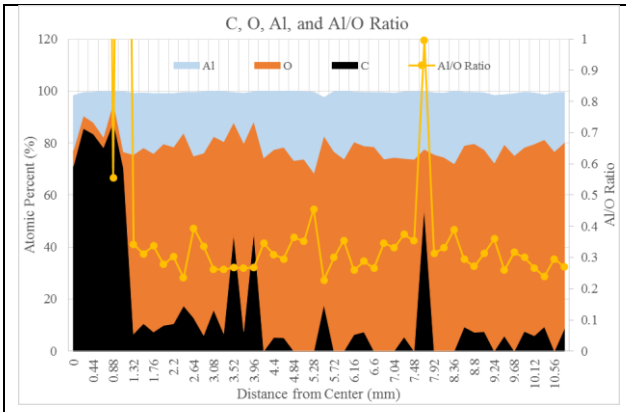

1100-H14 CFRP 2.67 Months

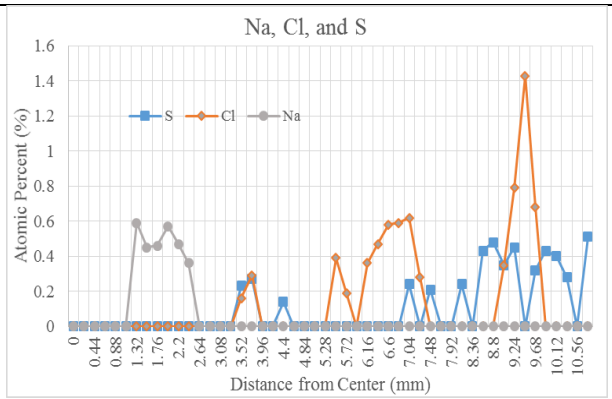

1100-H14 CFRP 2.67 Months

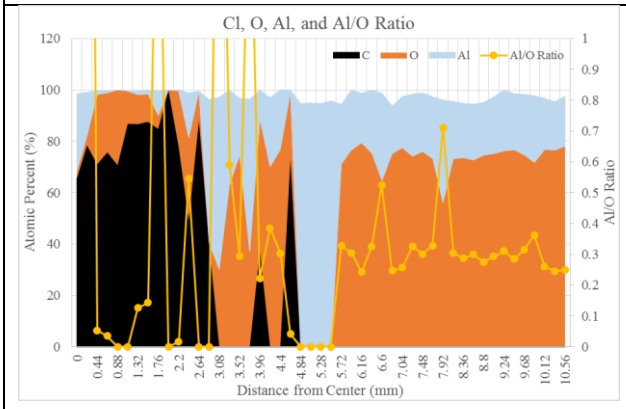

5456-H116 CFRP 2.67 Months

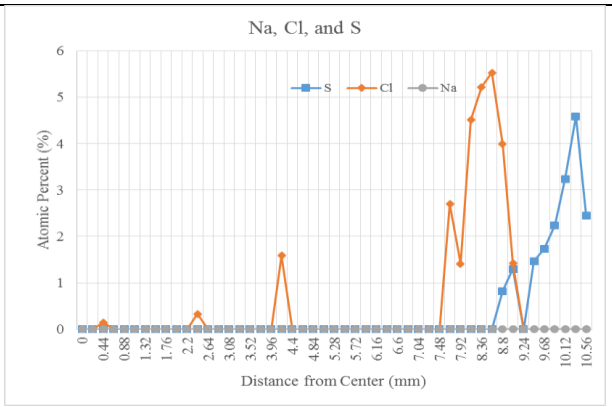

5456-H116 CFRP 2.67 Months

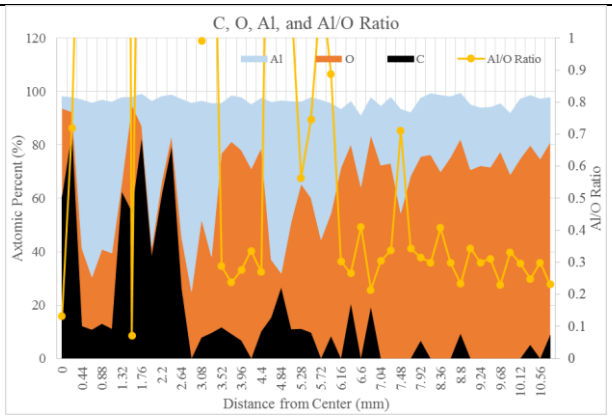

5456-H116 Sensitized CFRP 2.67 Months

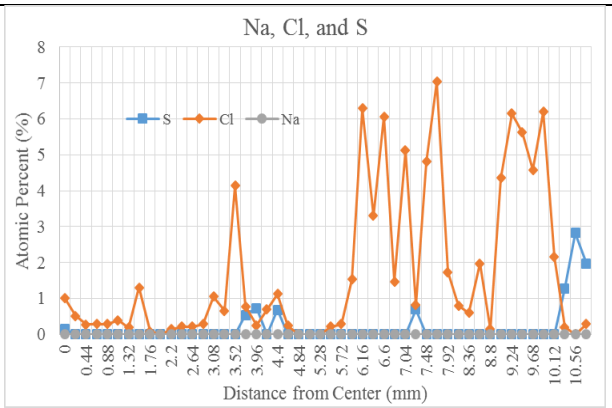

5456-H116 Sensitized CFRP 2.67 Months

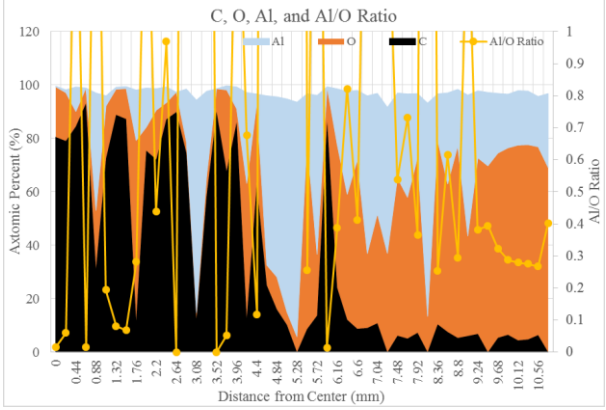

7075-T6 CFRP 2.67 Months

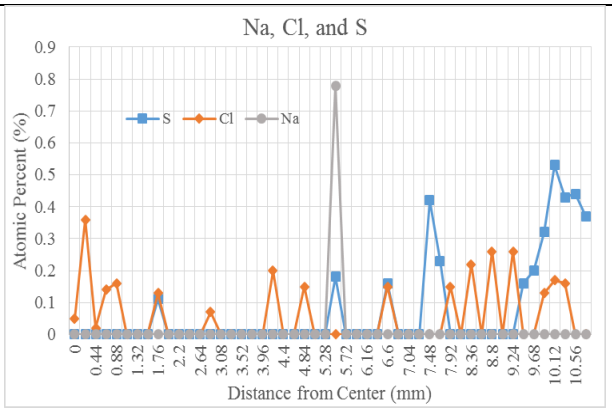

7075-T6 CFRP 2.67 Months

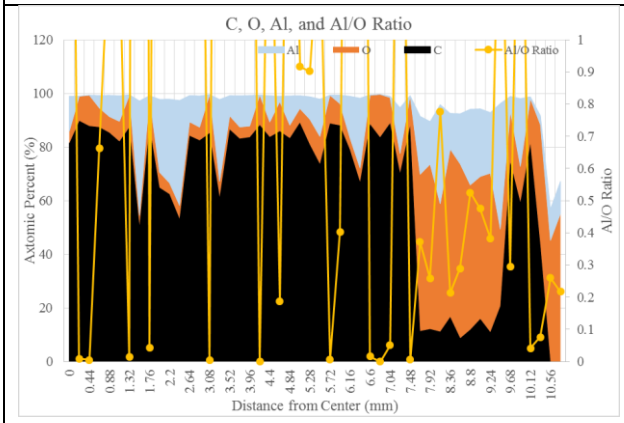

7075-T6 GFRP 1 Year

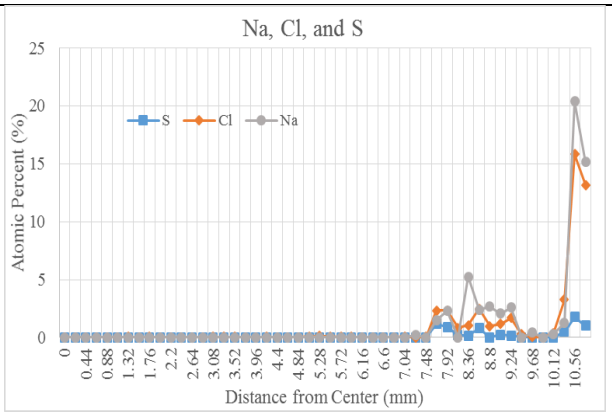

7075-T6 GFRP 1 Year

Table 8: Coconut Island SEM and EDX Sample Analysis

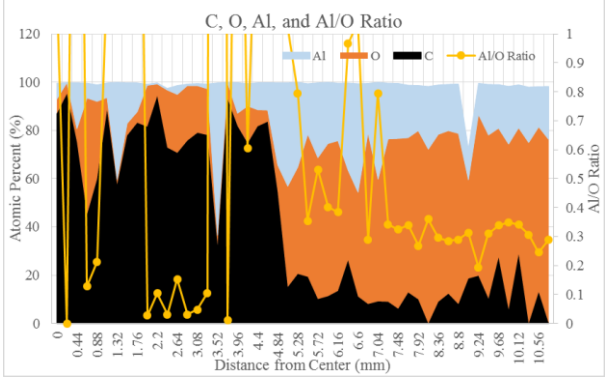

1100-H14 CFRP 1 Year

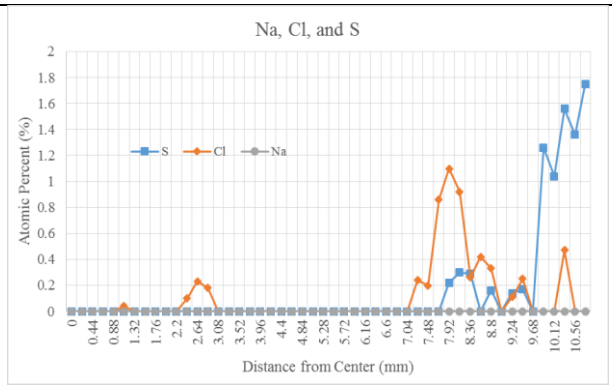

1100-H14 CFRP 1 Year

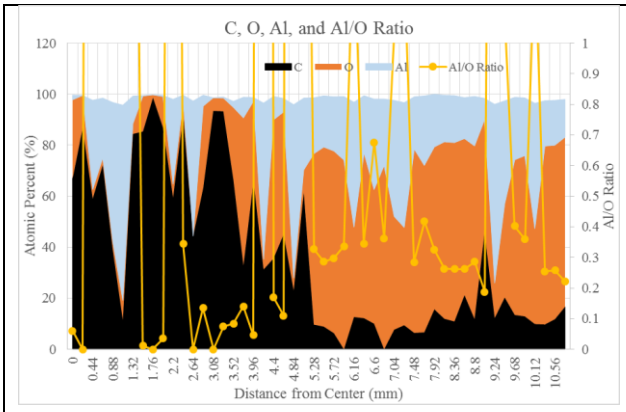

5456-H116 CFRP 1 Year

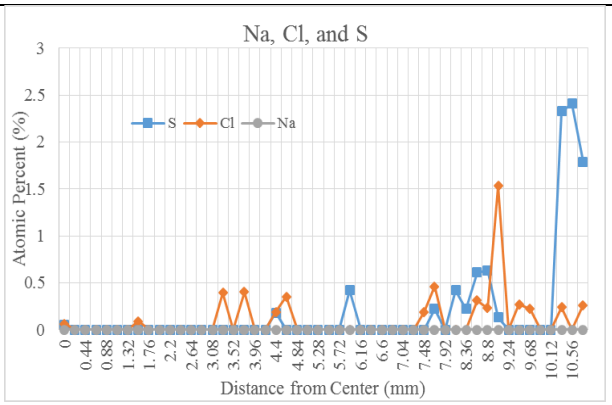

5456-H116 CFRP 1 Year

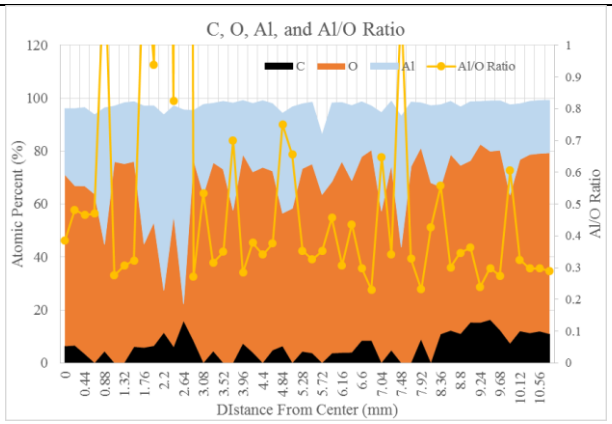

5456-H116 Sensitized CFRP 1 Year

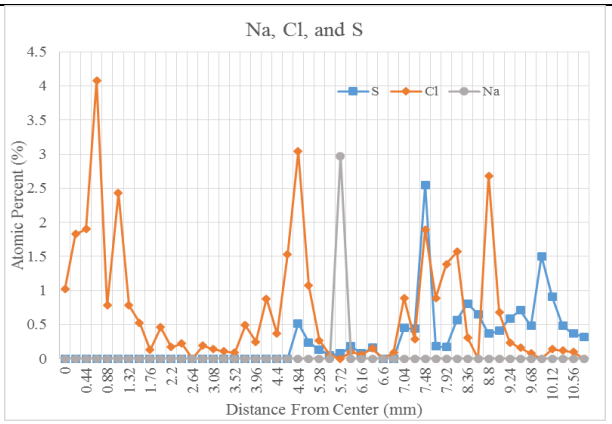

5456-H116 Sensitized CFRP 1 Year

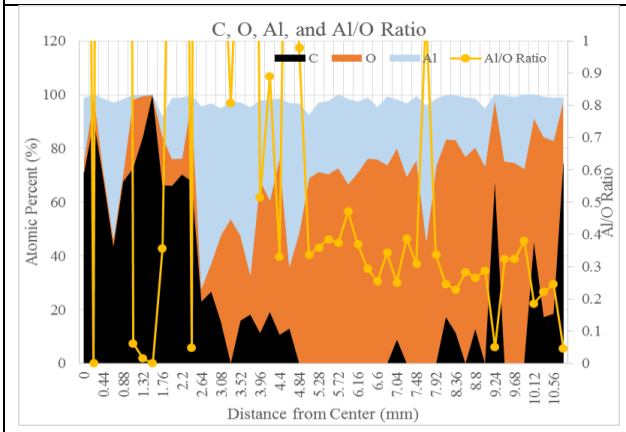

7075-T6 CFRP 1 Year

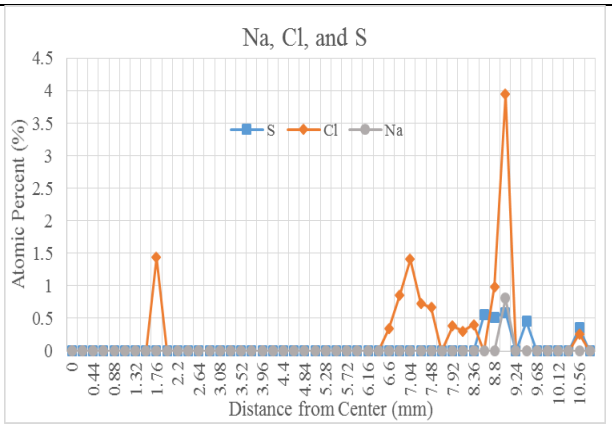

7075-T6 CFRP 1 Year

Table 9: Kilauea Volcano SEM and EDX Sample Analysis

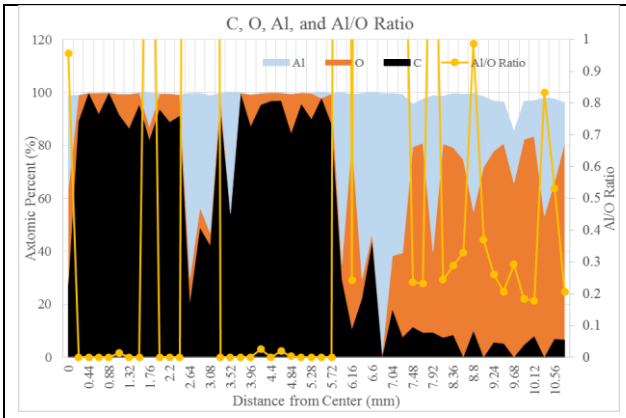

1100-H14 CFRP 1 Year

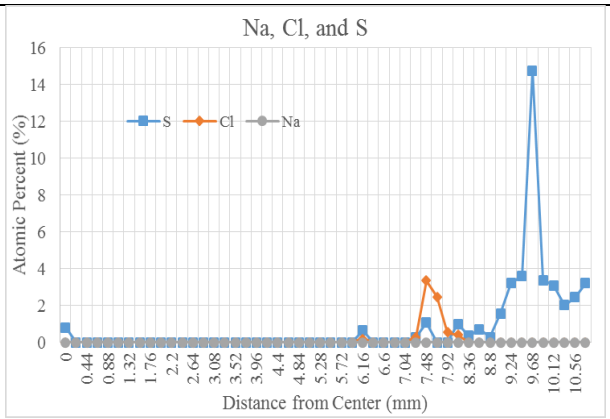

1100-H14 CFRP 1 Year

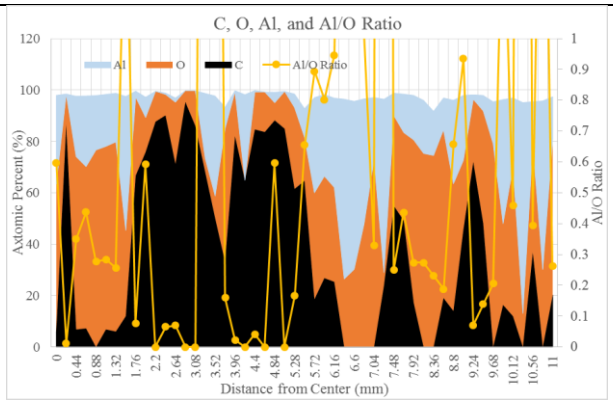

5456-H116 CFRP 1 Year

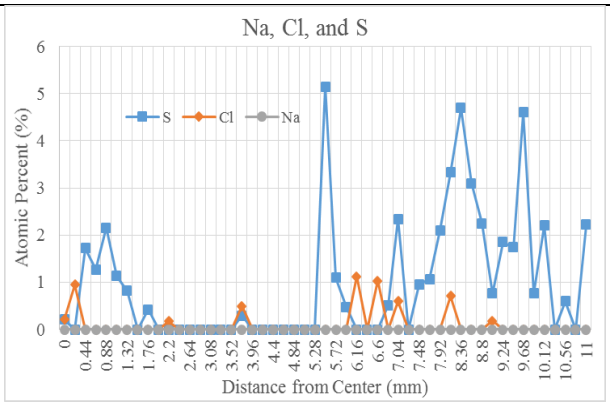

5456-H116 CFRP 1 Year

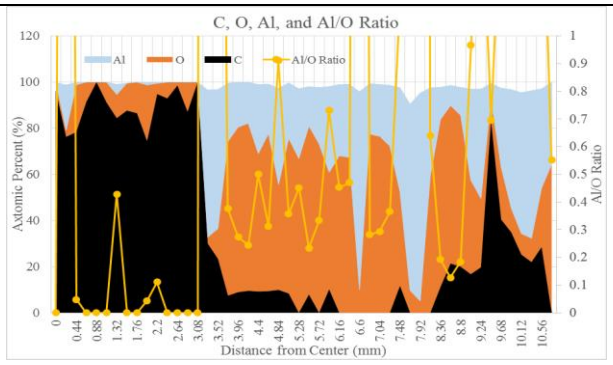

5456-H116 Sensitized CFRP 1 Year

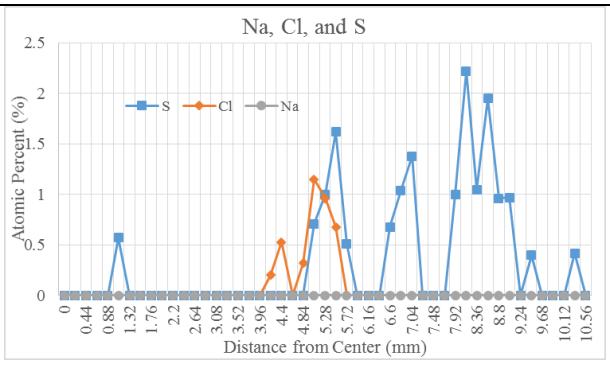

5456-H116 Sensitized CFRP 1 Year

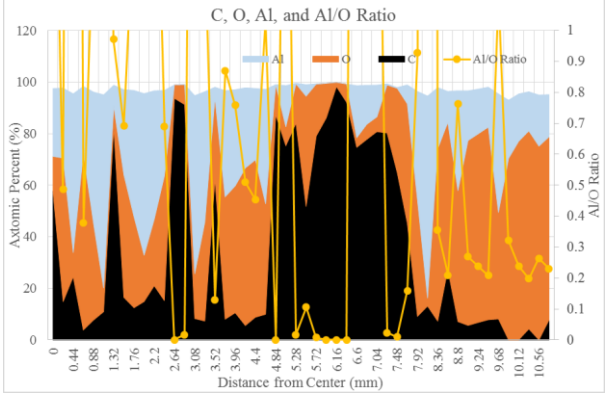

7075-T6 CFRP 1 Year

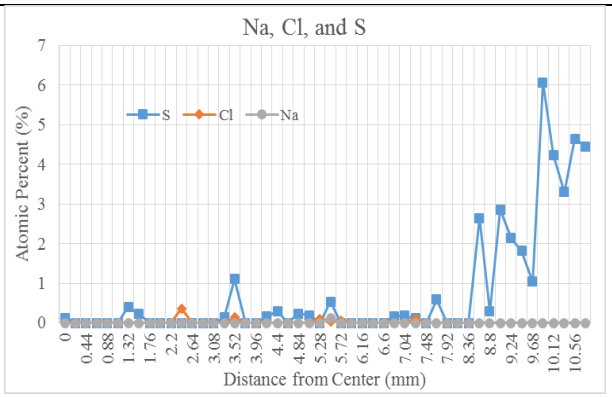

7075-T6 CFRP 1 Year

5.3 Profilometry Analysis

5.3.1 Results

Profile analysis was conducted on 8 different samples that are listed in Table 10 below.

Table 10: Profile Analysis Samples

Location	Alloy	Exposure Time	Composite
Coconut Island	1100-H14	1 year	CFRP
	5456-H116 non-sensitized	1 year	CFRP
	5456-H116 sensitized	1 year	CFRP
	7075-T6	1 year	CFRP
Kilauea	5456-H116 non-sensitized	1 year	CFRP
	5456-H116 sensitized	1 year	CFRP
Lyon Arboretum	5456-H116 non-sensitized	1 year	CFRP
	5456-H116 sensitized	1 year	CFRP

Depth profiles for each sample can be found in Figure 44 through Figure 51 below. Each depth profile starts at the red dot (corresponding to the left side of the graph) and finishes on the green dot (corresponding to the right side of the graph).

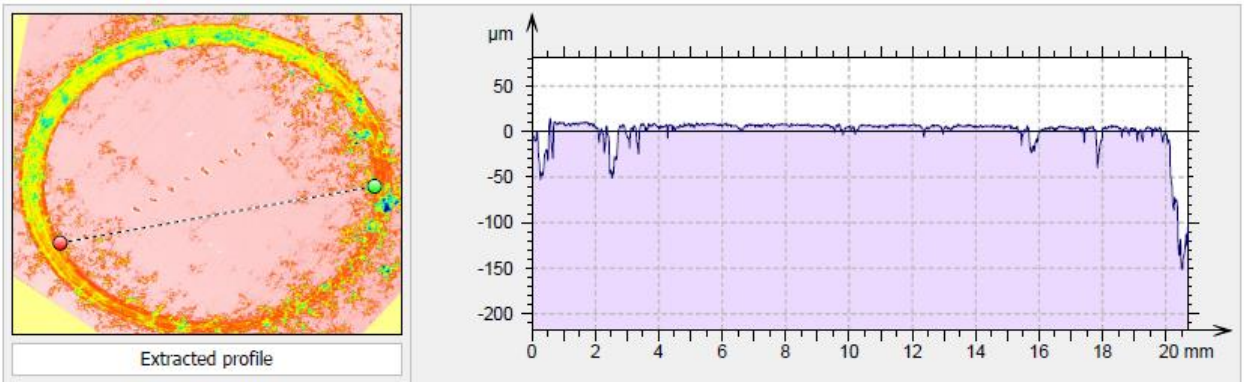

Figure 44: 1 Year Exposure CFRP Laminated Al 1100-H14 Sample from Coconut Island

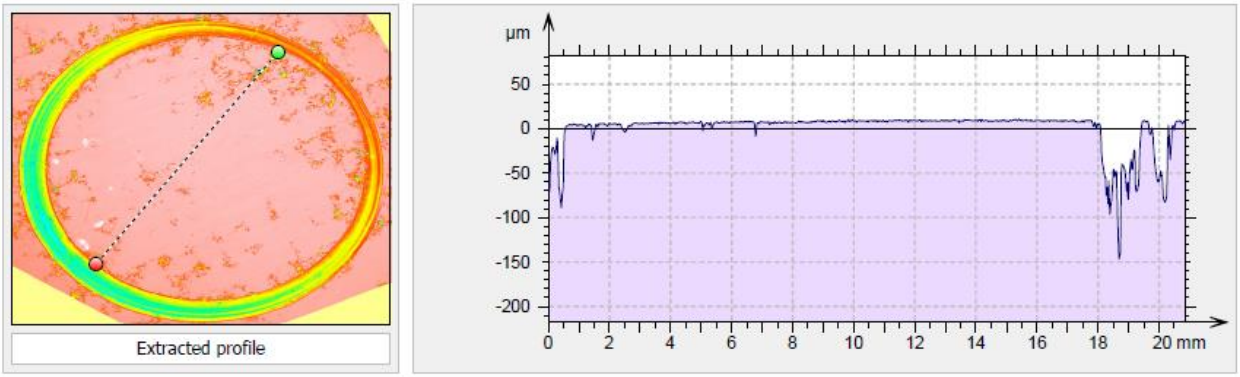

Figure 45: 1 Year Exposure CFRP Laminated Al 5456-H116 Non-sensitized Sample from Coconut Island

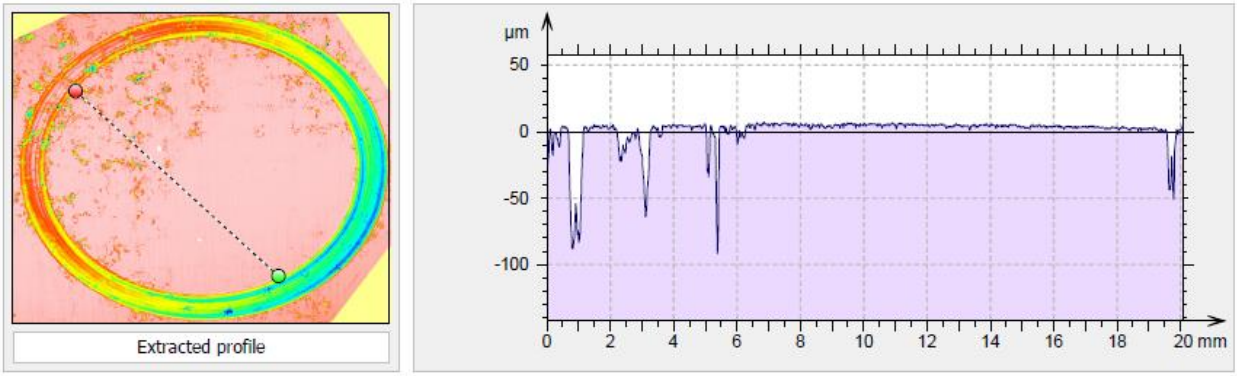

Figure 46: 1 Year Exposure CFRP Laminated Al 5456-H116 Sensitized Sample from Coconut Island

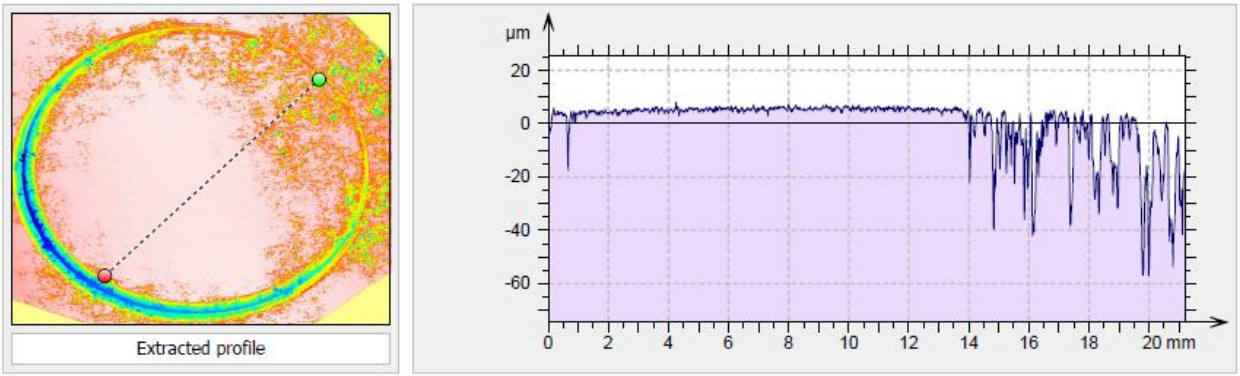

Figure 47: 1 Year Exposure CFRP Laminated Al 7075-T6 Sample from Coconut Island

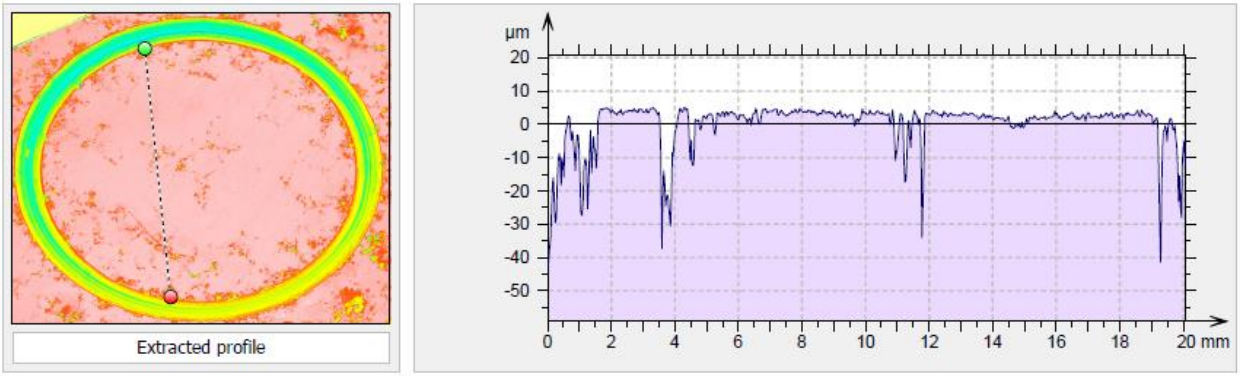

Figure 48: 1 Year Exposure CFRP Laminated Al 5456-H116 Non-sensitized Sample from Kilauea Volcano

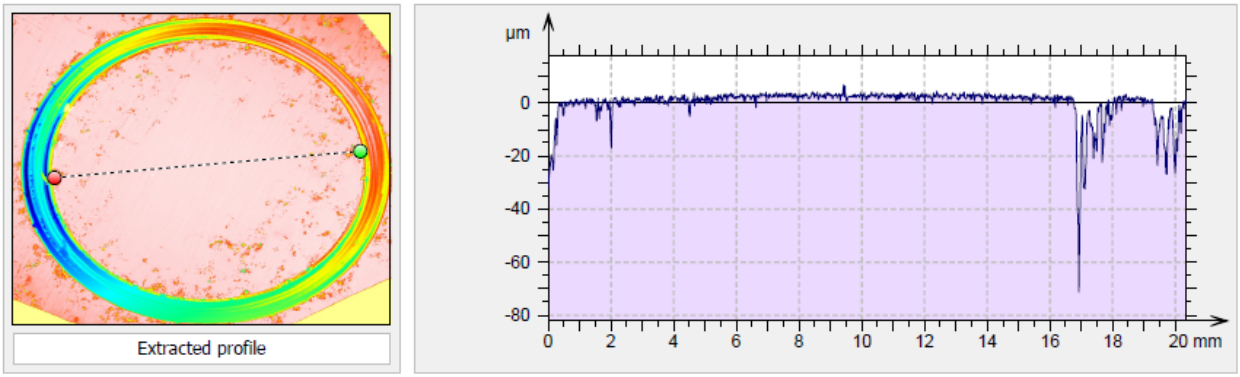

Figure 49: 1 Year Exposure CFRP Laminated Al 5456-H116 Sensitized Sample from Kilauea Volcano

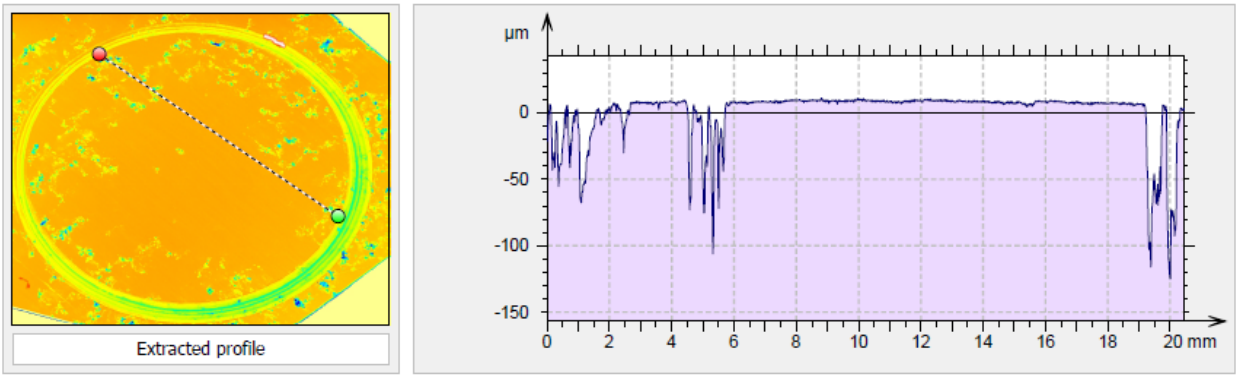

Figure 50: 1 Year Exposure CFRP Laminated Al 5456-H116 Non-sensitized Sample from Lyon Arboretum

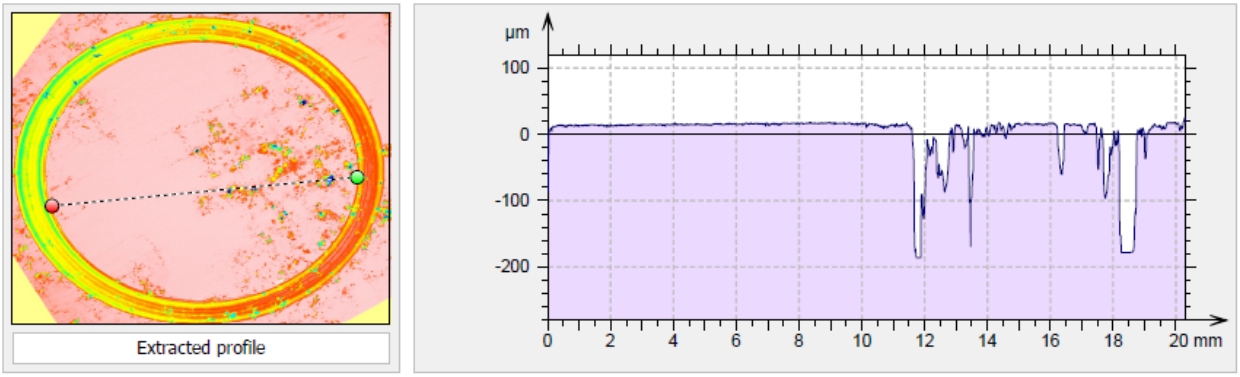

Figure 51: 1 Year Exposure CFRP Laminated Al 5456-H116 Sensitized Sample from Lyon Arboretum

The missing volume due to the pits within the relief area was also calculated using a least-square regression to determine the flat surface of each sample. An example of the calculation can be seen in Figure 52 below where green indicates the flat and level surface while red is the pit.

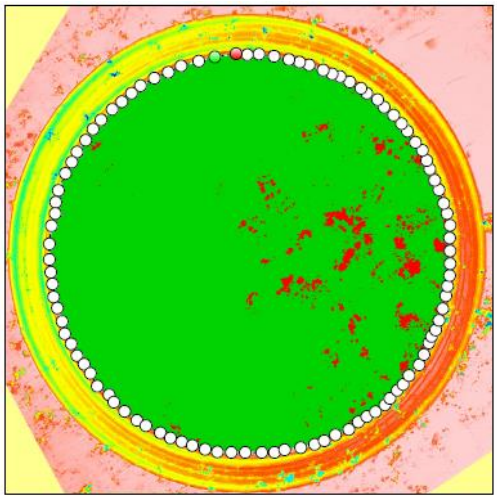

Figure 52: Volume and Surface Area Lost Due to Pitting Corrosion

The total volume lost and surface area lost due to pitting for each sample is listed in Table 11 below.

Table 11: Volume Lost Due to Pitting Corrosion

Location	Alloy	Volume Lost (mm^3)	Surface Area of Pits (mm^2)	Avg Pit Depth (mm)
Coconut Island	1100-H14	0.283	10.3	0.027
	5456-H116 non-sensitized	0.094	3.76	0.025
	5456-H116 sensitized	0.134	4.19	0.032
	7075-T6	0.258	18.2	0.014
Kilauea	5456-H116 non-sensitized	0.036	1.68	0.021
	5456-H116 sensitized	0.020	1.19	0.017
Lyon Arboretum	5456-H116 non-sensitized	0.389	13.5	0.029
	5456-H116 sensitized	0.339	8.09	0.042

A graphical comparison between the volume of each pit, average pit depth, and the percent of corroded-pit area to total relief area is presented in Figure 53 below.

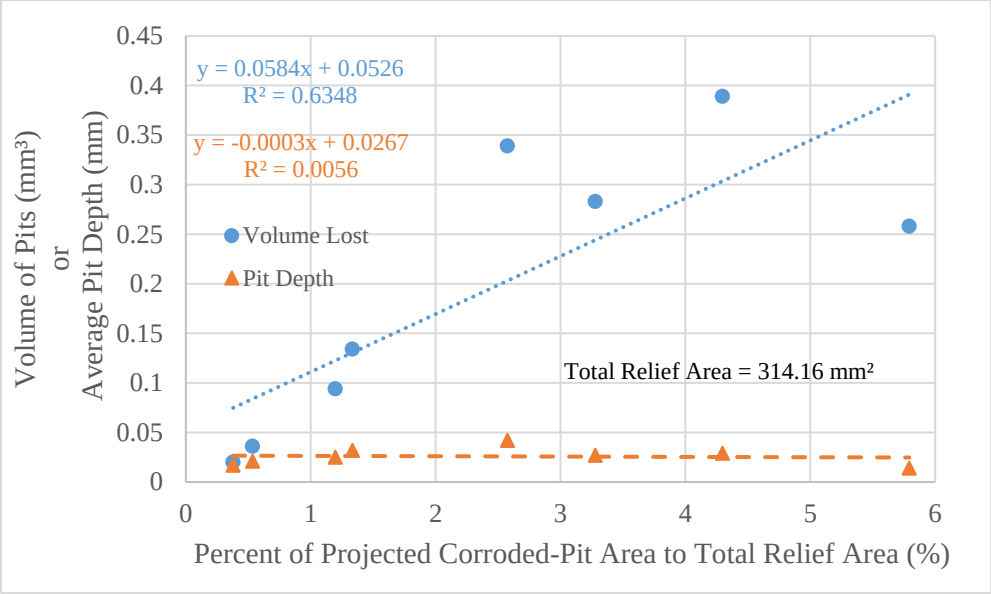

Figure 53: Pit Volume and Depth Compared to Total Relief Area

5.4 Nitric Acid Mass Loss Experiment

5.4.1 Results

Nitric acid mass loss analysis was conducted on 10 different samples that are listed in Table 12 below.

Table 12: Nitric Acid Mass Loss Analysis Samples

Location	Alloy	Exposure Time	Composite
Coconut Island	1100-H14	1 year	CFRP
	5456-H116 non-sensitized	1 year	CFRP
	5456-H116 sensitized	1 year	CFRP
	7075-T6	1 year	CFRP
Kilauea Volcano	5456-H116 non-sensitized	1 year	CFRP
	5456-H116 sensitized	1 year	CFRP
Lyon Arboretum	5456-H116 non-sensitized	1 year	CFRP
	5456-H116 sensitized	1 year	CFRP
Unexposed	5456-H116 non-sensitized		CFRP
	5456-H116 sensitized		CFRP

The total mass lost per cm^2 of surface area can be seen in Table 13 below.

Table 13: Nitric Acid Mass Loss

Location	Alloy	Sample Surface Area (cm^2)	Mass Loss (mg/cm^2)
Coconut Island	1100-H14	21.23	1.24
	5456-H116 non-sensitized	23.26	10.24
	5456-H116 sensitized	20.79	23.97
	7075-T6	21.92	2.37
Kilauea Volcano	5456-H116 non-sensitized	21.66	9.76
	5456-H116 sensitized	21.68	23.89
Lyon Arboretum	5456-H116 non-sensitized	21.73	9.85
	5456-H116 sensitized	21.41	25.53
Unexposed	5456-H116 non-sensitized	20.90	9.31
	5456-H116 sensitized	20.72	23.78

5.5 Microstructure Analysis

5.5.1 Results

The grain structure of each Al alloy is presented in Figure 54 through Figure 57 below.

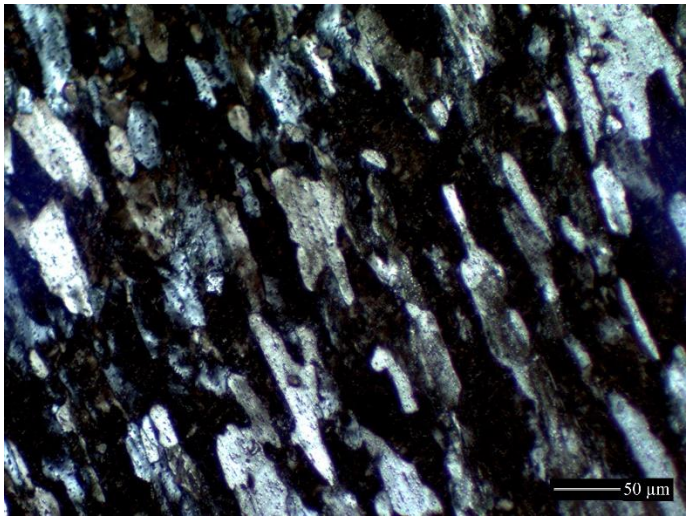

Figure 54: Grain Structure of Al 1100-H14

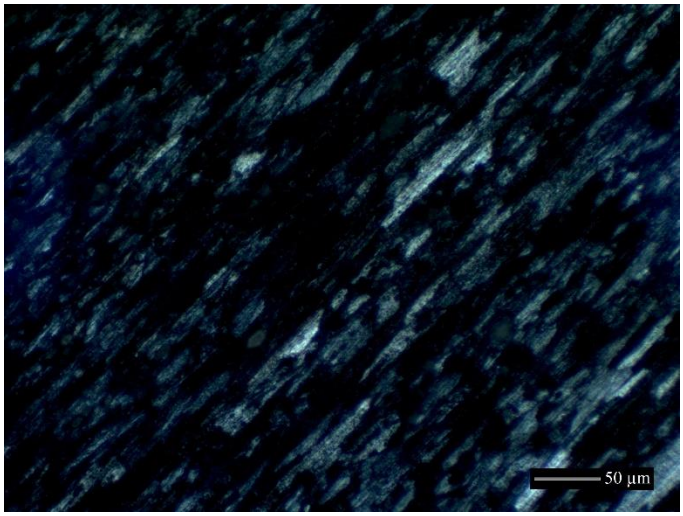

Figure 55: Grain Structure of Al 5456-H116 Non-sensitized

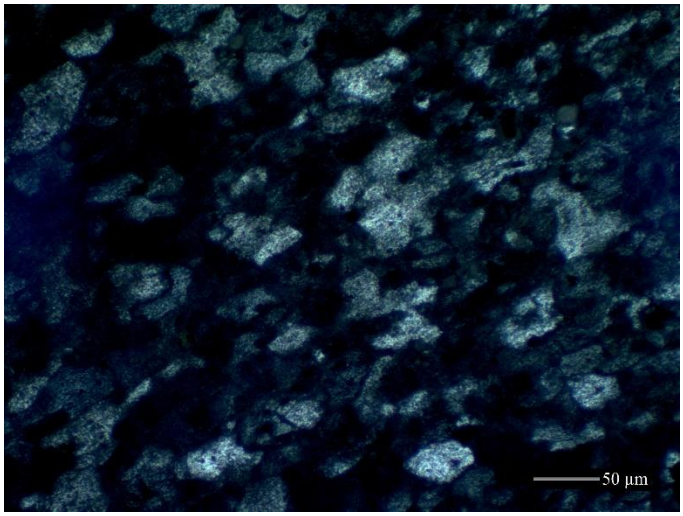

Figure 56: Grain Structure of Al 5456-H116 Sensitized

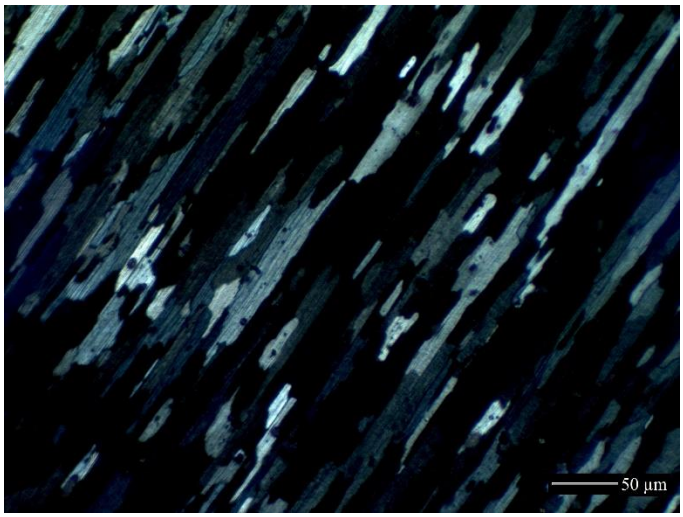

Figure 57: Grain Structure of Al 7075-T6

Each of the alloys has a lower-magnification image (Figure 58 through Figure 61) to illustrate the concentration and distribution of precipitates, and higher-magnification image (Figure 62 through Figure 65) with corresponding EDXA data (Table 14 through Table 17 below).

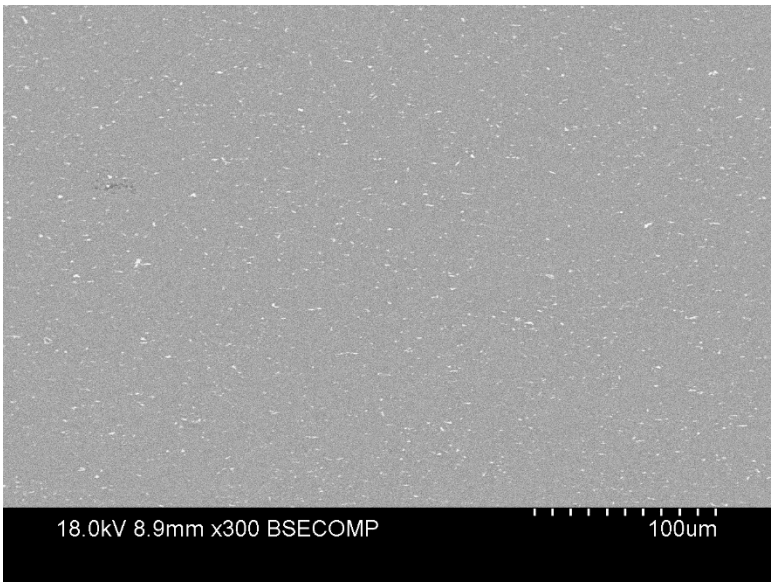

Figure 58: SEM Image of Al 1100-H14

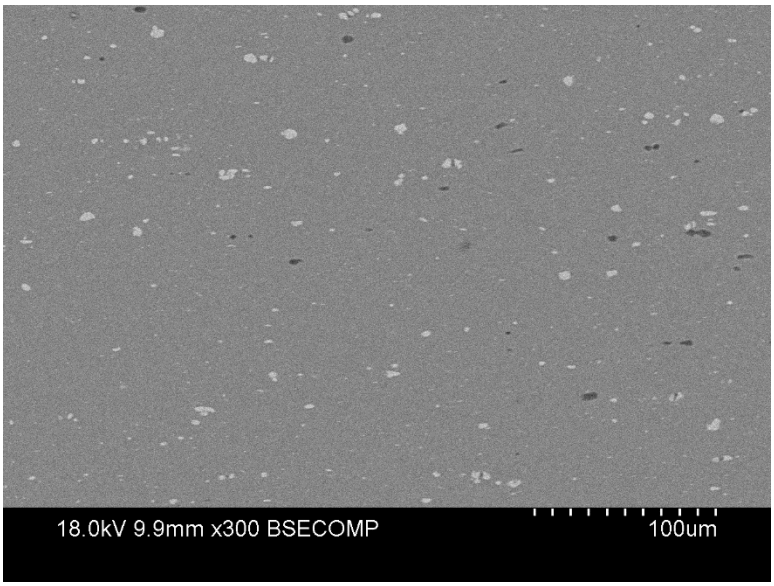

Figure 59: SEM Image of Al 5456-H116 Non-sensitized

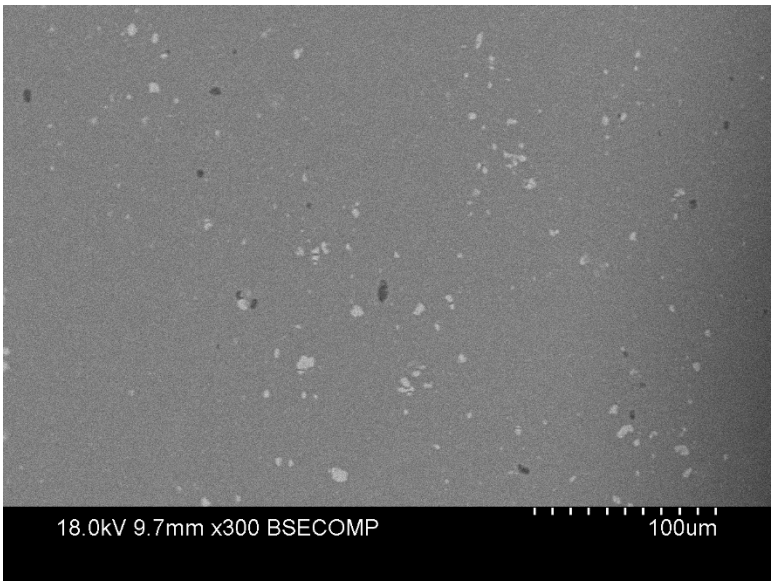

Figure 60: SEM Image of Al 5456-H116 Sensitized

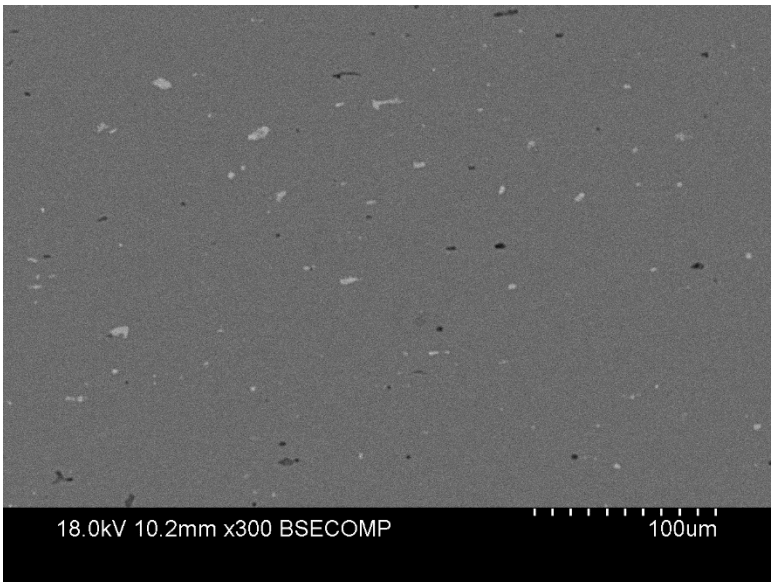

Figure 61: SEM Image of Al 7075-T6

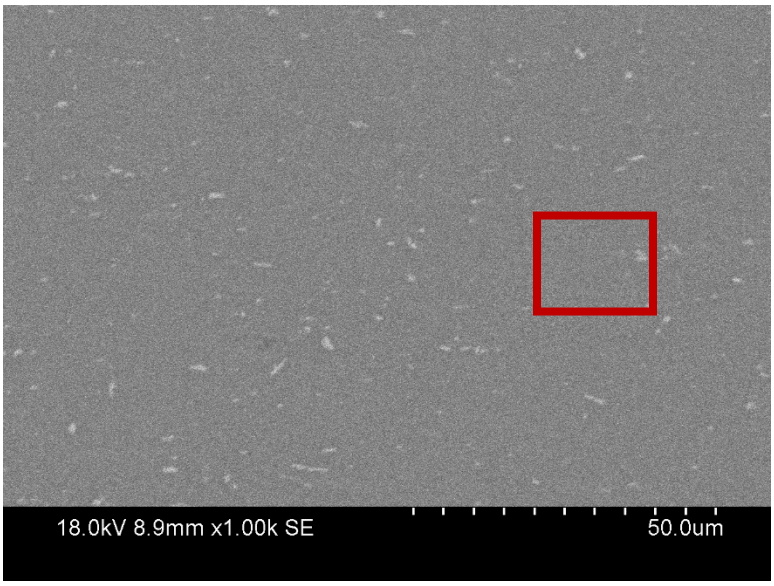

Figure 62: SEM Image of Al 1100-H14 (red box indicates EDX analysis area)

Table 14: Elemental Make-up of Al 1100-H14

Element	Atomic %
Iron (Fe)	0.97
Aluminum (Al)	99.03

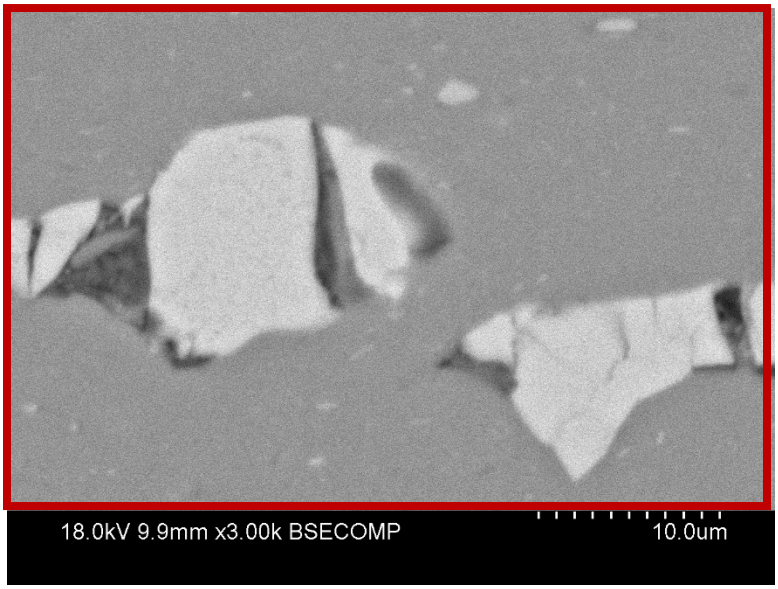

Figure 63: SEM Image of Al 5456-H116 Non-sensitized (red box indicates EDX analysis area)

Table 15: Elemental Make-up of Al 5456-H116 Non-sensitized

Element	Atomic %
Iron (Fe)	1.30
Manganese (Mn)	1.57
Magnesium (Mg)	5.62
Aluminum (Al)	91.51

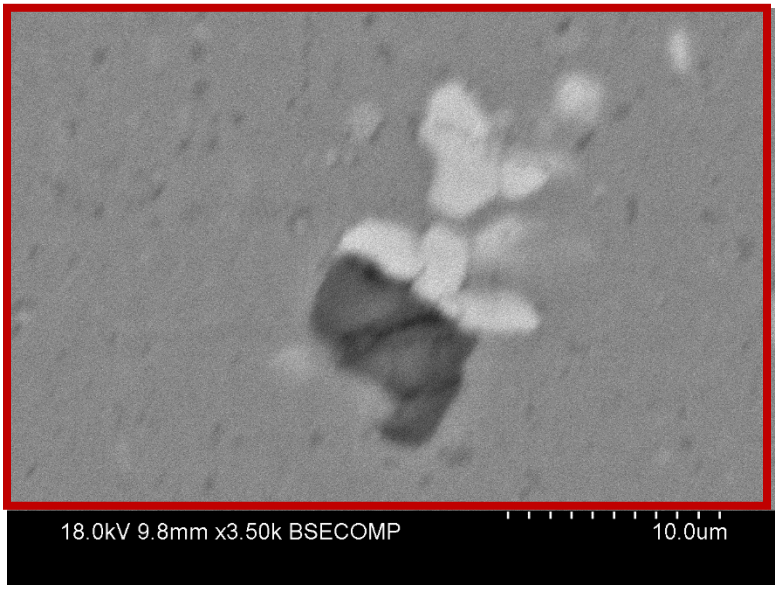

Figure 64: SEM Image of Al 5456-H116 Sensitized (red box indicates EDX analysis area)

Table 16: Elemental Make-up of Al 5456-H116 Sensitized

Element	Atomic %
Silicon (Si)	2.22
Oxygen (O)	5.38
Magnesium (Mg)	5.80
Aluminum (Al)	86.59

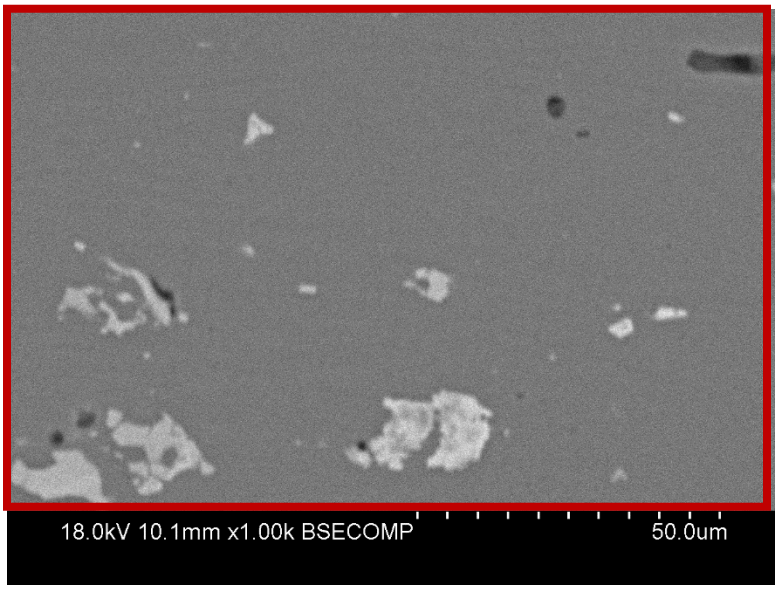

Figure 65: SEM Image of Al 7075-T6 (red box indicates EDX analysis area)

Table 17: Elemental Make-up of Al 7075-T6

Element	Atomic %
Copper (Cu)	1.49
Zinc (Zn)	2.38
Magnesium (Mg)	3.48
Aluminum (Al)	92.65

5.6 Polarization Experiment

5.6.1 Results

Cathodic Polarization diagrams for each of the alloys [Al 1100-H14, Al 5456-H116 (non-sensitized), Al 5456-H116 (sensitized), and Al 7075-T6] and the anodic polarization for Al 5456-H116 (sensitized) can be found in Figure 66 through Figure 69 below.

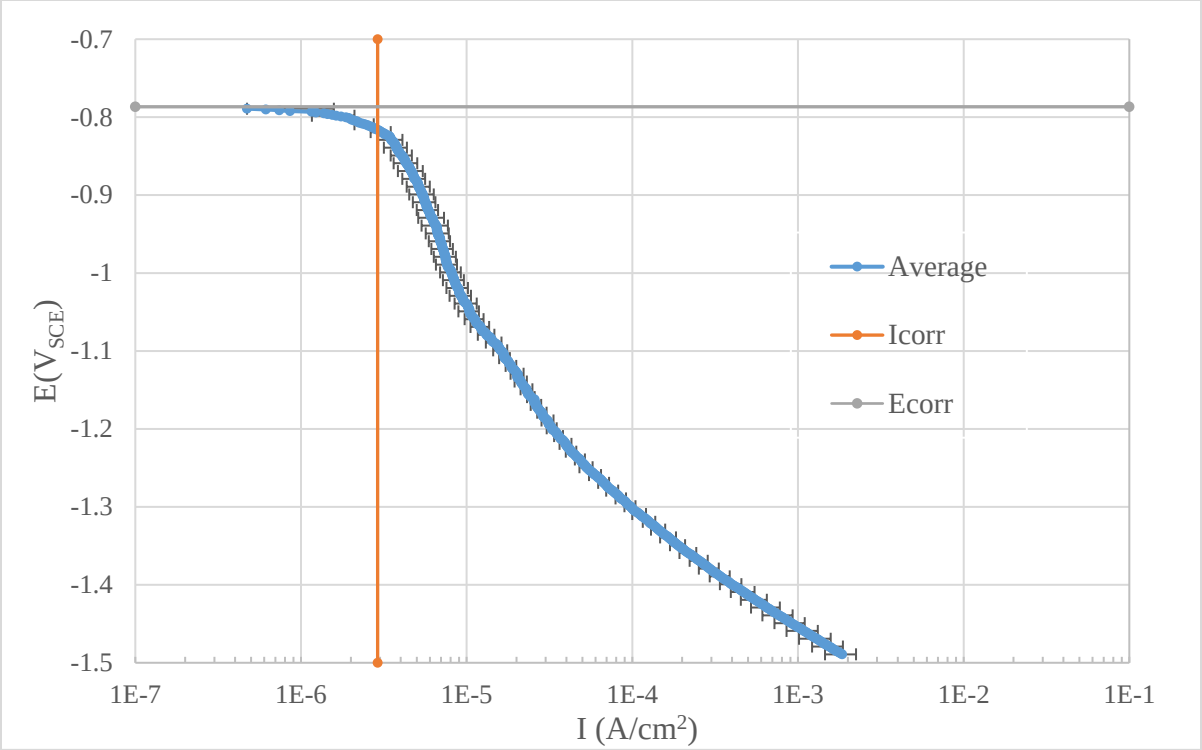

Figure 66: Cathodic Al 1100-H14 Polarization Diagram in Aerated 3.15 wt% NaCl solution at 30°C. Scan rate = 1 mV/s

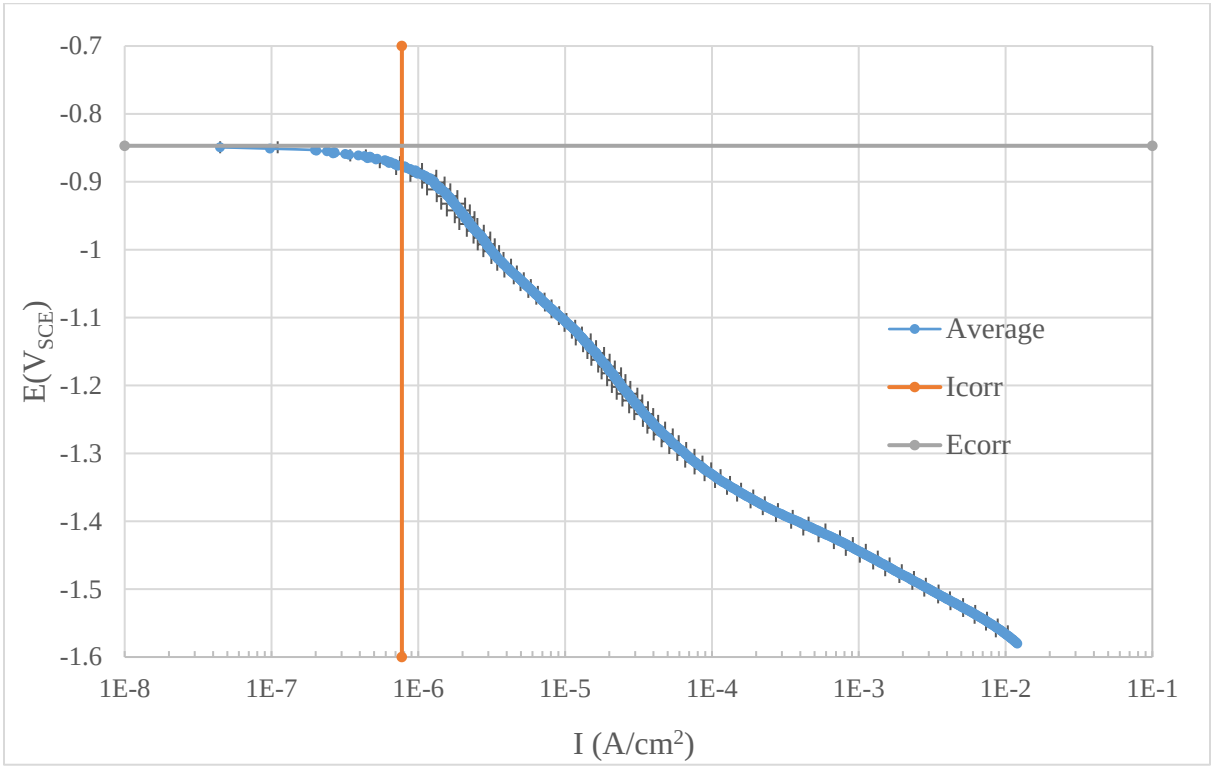

Figure 67: Cathodic Al 5456-H116 Non-sensitized Polarization Diagram in Aerated 3.15 wt% NaCl solution at 30°C. Scan rate = 1 mV/s

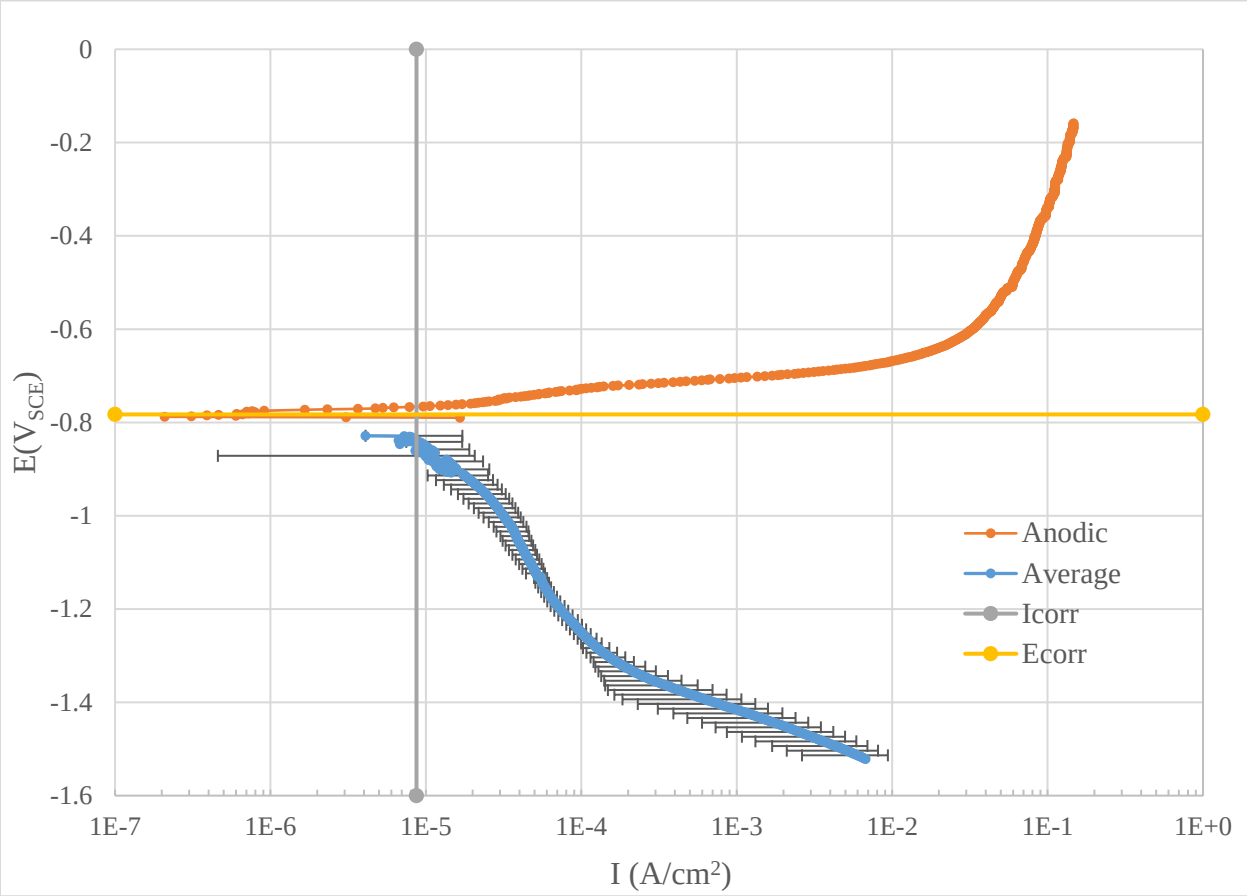

Figure 68: Cathodic and Anodic Al 5456-H116 Sensitized Polarization Diagram in Aerated 3.15 wt% NaCl solution at 30°C. Scan rate = 1 mV/s

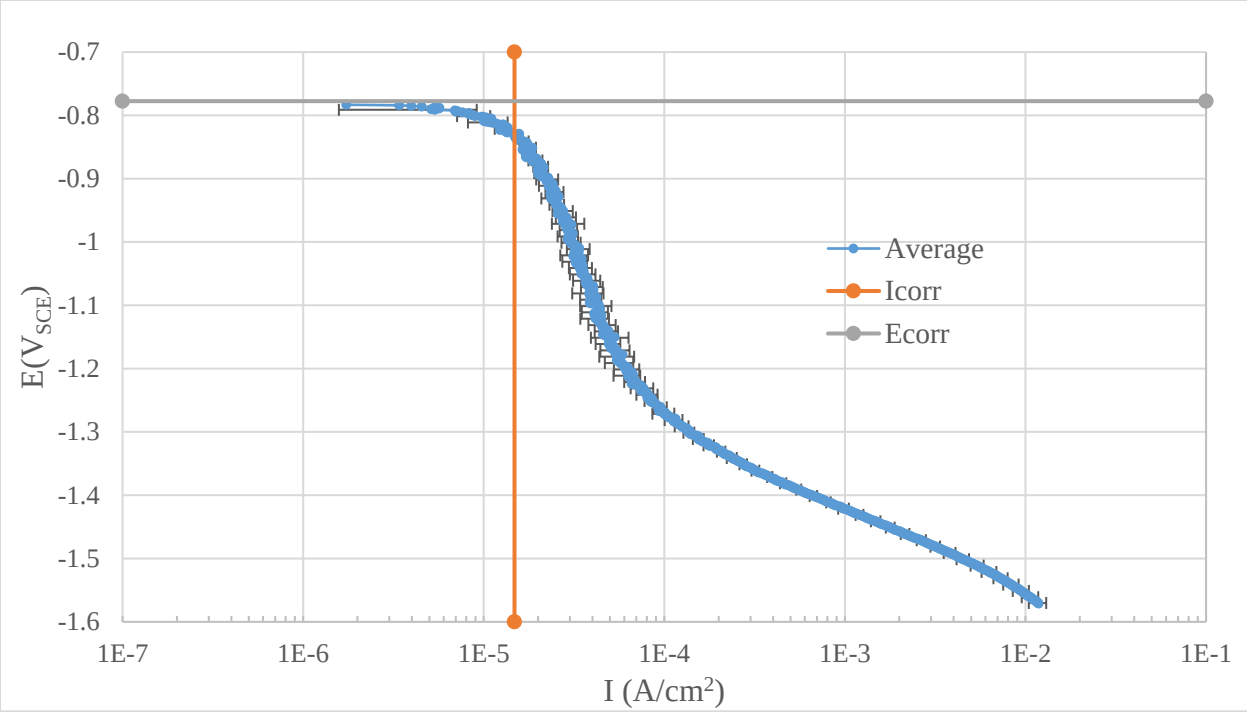

Figure 69: Cathodic Al 7075-T6 Polarization Diagram in Aerated 3.15 wt% NaCl solution at 30°C. Scan rate = 1 mV/s

Zero Resistance Ammeter tests conducted by Daniel Jensen in his thesis "*Corrosion of Aluminum Alloys-Polymer Matrix Composite Interfaces*" [6] are presented in Table 18 below.

Table 18: Galvanic Current & Potential of Al Alloys in Aerated 3.15 wt% NaCl at 30° C [6]

CF PMC Coupled to Al Alloy	Galvanic Current (mA)		Galvanic Potential (mV vs. SCE)	
	Average	Standard Deviation	Average	Standard Deviation
Al 1100-H14	0.18	0.02	-730	15
Al 5456-H116 Non-sensitized	0.17	0.02	-728	11
Al 5456-H116 Sensitized	0.14	0.03	-767	4
Al 7075-T6	0.16	0.02	-762	4

The potentiodynamic polarization test I_{corr} and E_{corr} values are presented in Table 19 below.

Table 19: Potentiodynamic Current & Potential of Al Alloys in Aerated 3.15 wt% NaCl at 30° C

CF PMC Coupled to Al Alloy	I_{corr} (µA)		E_{corr} (mV vs. SCE)	
	Average	Standard Deviation	Average	Standard Deviation
Al 1100-H14	2.90	0.484	-787	5.87
Al 5456-H116 Non-sensitized	0.773	0.174	-847	13.87
Al 5456-H116 Sensitized	8.70	4.00	-783	2.60
Al 7075-T6	14.8	1.31	-778	6.97

Chapter 6

DISCUSSION

6.1 Overall Experiment Discussion

When starting the analysis on each of the composite laminated aluminum samples, it is prudent to compare the elemental makeup, grain structure, and precipitate density of each alloy of aluminum. The aluminum alloys studied [Al 1100-H14, Al 5456-H116 (non-sensitized), Al 5456-H116 (sensitized), and Al 7075-T6] were either cold worked / strain hardened (H14 and H116 temper) or heat treated and artificially aged (T6 temper). An elongated grain structure is the hallmark of a cold worked alloy and that grain structure is clearly illustrated in Figure 55 for Al 5456-H116 non-sensitized. The Al 1100-H14 alloy in Figure 54 shows a slightly less elongated grain structure due to its partial anneal after cold working. During the sensitization procedure, the Al 5456 –H116 alloy likely recrystallized and formed equiaxed grains as illustrated in Figure 56 for Al 5456-H116 sensitized. The Al 7075-T6 alloy in Figure 57 shows an elongated grain pattern as well, due to its thermomechanical processing to endow additional strength to the material.

A lower magnification study (300x) was conducted in the SEM to illustrate the size and distribution of the larger precipitates within each alloy. Figure 58 indicates a very even distribution of the precipitates within the substrate for the Al 1100-H14 alloy. Both the Al 5456-H116 non-sensitized alloy in Figure 59 and the Al 5456-H116 sensitized alloy in Figure 60 show much larger precipitates compared to the Al 1100-H14 alloy. The sensitized alloy also showed slightly less uniformity of distribution of the precipitates than the non-sensitized alloy. The Al7075-T6 alloy in Figure 61

showed larger precipitate size and lower density when compared to Al 5456-H116 or Al 1100-H14 as well as a mostly uniform distribution.

A higher magnification study (between 1000x and 3500x) was conducted on each of the alloys in order to show the shape and elemental makeup of precipitates within the substrate. The elemental species (Table 14 through Table 17) identified in the precipitates and matrix of each of the alloys were in accordance with those expected for each alloy in Table 1.

For the composite laminated aluminum alloy samples that underwent testing in the CCTC, a modification to the GM-9540P test procedure was made. The last 8 hours of the test cycle (the heated drying phase) was eliminated in order to compare the adhesion strength between samples that were continuously wet versus those that were allowed to periodically dry. Daniel Jensen performed an unmodified GM-9540P test on the samples in his thesis "*Corrosion of Aluminum Alloys-Polymer Matrix Composite Interfaces*" [6]. The results between the modified and unmodified test are fairly similar for both the 7 and 14 cycle tests. It was determined that the 21 cycle test data for the modified test was not useable due to a clogged spray nozzle and lack of corrosion product on the control steel coupons.

The GFRP laminated aluminum alloy samples in the modified GM-9540P in Figure 31 (and Table 20) did not demonstrate a major loss in adhesion strength (ranged from -5% - 10%) throughout the entire test, but the loss of adhesion strength varied wildly (ranged from 17% - 75%) among the CFRP laminated aluminum alloy samples. The adhesion loss for the CFRP-laminated Al alloys was a

function of the substrate alloy type. The ordering from highest to lowest adhesion loss (Table 20) based on the substrate was 7075-T6 > 1100-H14 > 5456-H116 > 5456-H116 sensitized.

When comparing the unmodified GM-9540P (with the heated drying periods) to the modified GM-9540P (continuously wet) results from 0 up to 14 cycles, the heated drying periods were generally beneficial and lead to a lower decrease in adhesion strength. In fact, for the GFRP-laminated samples, the adhesion strength increased with exposure which was likely due to enhanced curing of the epoxy matrix during the heating cycles. The benefits of the heating cycle was not clear cut for the CFRP-laminated samples as the reduction in adhesion strength sometimes increased for the heated cases. This could potentially be caused by the competing factors of de-lamination due to corrosion at the laminate-aluminum interface and enhanced bonding due to curing of the epoxy. Corrosion rates can increase during the heated cycle before the electrolyte dries out. For both the heated and non-heated cases, the degradation of the adhesion strength was greatest for the Al 7075-T6, followed by that of Al 1100-H14, and then Al 5456-H116 (with the non-sensitized and sensitized cases flip flopping). This strongly indicated that the alloying elements in the Al alloys had a significant role in the degradation of the adhesion strength. Some variation in the adhesion strength could also be due to several other factors including spray nozzle placement, adhesion strength test epoxy used, and adhesion strength test material preparation. Table 20 below illustrates.

Table 20: Percentage Reduction in Strength for CCTC 0-14 Cycle Adhesion Test

Alloy	Laminate	Full GM-9540P % Reduction	Modified GM-9540P % Reduction
1100-H14	CFRP	59.72	70.98
5456-H116 Non-sensitized	CFRP	10.36	60.22
5456-H116 Sensitized	CFRP	19.50	16.62
7075-T6	CFRP	87.33	74.65
CFRP Average		**44.23**	**55.62**
CFRP Standard Deviation		**35.85**	**26.71**
1100-H14	GFRP	-26.18	-0.09
5456-H116 Non-sensitized	GFRP	-10.32	10.35
5456-H116 Sensitized	GFRP	-12.20	-4.49
7075-T6	GFRP	-26.28	0.94
GFRP Average		**-18.75**	**1.68**
GFRP Standard Deviation		**8.68**	**6.24**

When exposed to the 5 test locations, the composite-laminated aluminum samples produced similar outcomes to the CCTC tests, just with flatter trend lines overall. With the exception of the Mauna Loa test site where almost no corrosion was noted for all exposures and samples, the CFRP laminated aluminum samples fared the worst in adhesion strength as referenced in Figure 32 through Figure 36. As with the CCTC results, the CFRP-laminated Al 7075-T6 showed the highest adhesion strength loss with 1100-H14 coming in second. The CFRP-laminated Al 5456-H116 sensitized had, on average, the third highest adhesion strength loss and the Al 5456-H116 non-sensitized retained the most adhesion strength among the CFRP-laminated alloys at each test location. The GFRP laminated aluminum alloys had minor adhesion strength losses, but there was not a consistent or clear "worst performer" among any of the alloys.

Each of the 5 test locations produced varying results when compared against the composite laminated alloys. Pyramid Rock was by far the most corrosive to all samples due to its high concentration of salt spray due to its proximity to the ocean as well as the high wave action on the beach. Pyramid

Rock test results most closely mimic those of the CCTC of any of the test locations. The CFRP laminated aluminum alloy samples that were placed at Pyramid Rock actually had to be brought back significantly earlier than any other test site (0.63 months, 2.67 months, and 3.63 months versus 1, 6, and 12 months) due to their rapid degradation. The GFRP laminated aluminum alloy samples at Pyramid Rock also lost more adhesion strength than any other test site. Coconut Island, Lyon Arboretum, and Kilauea volcano all had very similar effects on the adhesion strength loss with CFRP laminated samples performing much worse overall when compared to GFRP laminated samples. The least corrosive environment was Mauna Loa; most likely due to its high elevation, dry climate and cool temperatures which caused very little adhesion loss in either CFRP or GFRP laminated samples. Figure 37 through Figure 40 illustrate the effect of location on each of the test samples.

Once the adhesion tests were completed, 1 relief area was selected on 17 samples that represented a solid delineation between uncorroded and corroded regions to get the maximum working value for the SEM and EDX. Only 1 of the 17 samples tested was laminated with GFRP due to the fact that almost no corrosion appeared under the laminate for any exposure duration or location. All of the samples chosen with the exception of Pyramid Rock due to its extremely thick corrosion layer would prevent the EDX from detecting corrosion species directly on the substrate surface. Each sample that was chosen is listed in Table 5.

The results from the SEM and EDX correlated well with the results from previous tests and showed that the CFRP-laminated alloy samples were subjected to crevice corrosion and eventual delamination of the composite, resulting from galvanic coupling between the Al substrate anode and carbon fiber which served as the cathode. The SEM and EDX results also correlated well with the

previous test results for the GFRP laminated alloy samples in that the composite insulated and protected the substrate alloy.

When aluminum corrodes Al^{3+} ions and free electrons are produced. The free electrons migrate to the surface of the substrate and bond with oxygen (O_2) and water molecules (H_2O) to form hydroxide ions (OH^-) [20]. The OH^- ions and/or H_2O react with the Al^{3+} ions to create aluminum hydroxide [$Al(OH)_3$] [20]. $Al(OH)_3$ is a gel and unstable corrosion product which eventually crystalizes into the much more stable aluminum oxide (Al_2O_3) in a process known as "ageing" [20].

The first reaction that occurs is anodic and is presented in Equation 1.

$$Al \rightarrow Al^{3+} + 3e^- \quad \text{(Eq. 1)}$$

The second reaction that occurs is cathodic and is presented in Equation 2.

$$O_2 + 2H_2O + 4e^- \rightarrow 4OH^- \quad \text{(Eq. 2)}$$

The anodic and cathodic reactions can be added together to yield the net reaction in Equation 3.

$$3O_2 + 6H_2O + 4Al \rightarrow 4Al^{3+} + 12OH^- \quad \text{(Eq. 3)}$$

The resultant products from Equation 3 combine to form aluminum hydroxide (Bayerite) as shown in Equation 4.

$$Al^{3+} + 3OH^- \rightarrow Al(OH)_3 \quad \text{(Eq. 4)}$$

This unstable gel then produces the more stable aluminum oxide (alumina) as shown in Equation 5.

$$2Al(OH)_3 \rightarrow Al_2O_3 + 3H_2O \quad \text{(Eq. 5)}$$

This entire process can be simplified as presented in Equation 6.

$$2Al^{3+} + 3H_2O \rightarrow Al_2O_3 + 3H_2O \quad \text{(Eq. 6)}$$

When the aluminum substrate is bonded to the electrically conductive CFRP laminate, accelerated galvanic corrosion can take place between the Al substrate and CFRP relief. Oxygen reduction and the generation of OH^- (Eq. 2) will take place on the bare carbon fibers on the perimeter of the CFRP relief, and Al^{3+} (Eq. 1) will be produced in the crevice between the CFRP laminate and Al substrate (Figure 70). In addition, within the crevice, Al^{3+} will react with $3H_2O$ and form $Al(OH)_3$ and $3H^+$. If the Al alloy does not have a significant amount of effective cathodic sites (e.g., copper-containing precipitates), the cathodic reaction will primarily take place on the perimeter of the CFRP laminate and not on the alloy substrate, which corresponds to the case for CFRP laminated Al 5456-H116 sensitized and non-sensitized (Figure 70). Hence, within the crevice, very little OH^- will be generated and the accumulation of Al^{3+} and H^+ will electrostatically attract anions such as Cl^- and repel cations such as Na^+ to maintain charge neutrality (Figure 73). If the substrate aluminum has a significant amount of precipitates that are effective cathodic sites (e.g., copper-containing precipitates), oxygen reduction and the generation of OH^- can also occur in the crevice to some degree (Figure 71), which corresponds to the case of CFRP laminated 7075-T6 and somewhat to the case of CFRP laminated 1100-H16. In these cases then, the generation of OH^- within the crevice will reduce the excess positive charge from the Al^{3+} and H^+ generation, and the propensity to repel other cations may be attenuated. As a result, other cations (e.g., Na^+) have a greater chance to be found in the crevice (Figure 74). The Al 1100-H14 and Al 5456-H116 sensitized and non-sensitized substrates showed a lower inward migration of sodium under the CFRP laminate than the Al 7075-T6. Sodium ingress illustrated in Figure 74 was more strongly seen in the unmodified CCTC experiments performed by Daniel Jensen [6] than in the outdoor environmental experiments.

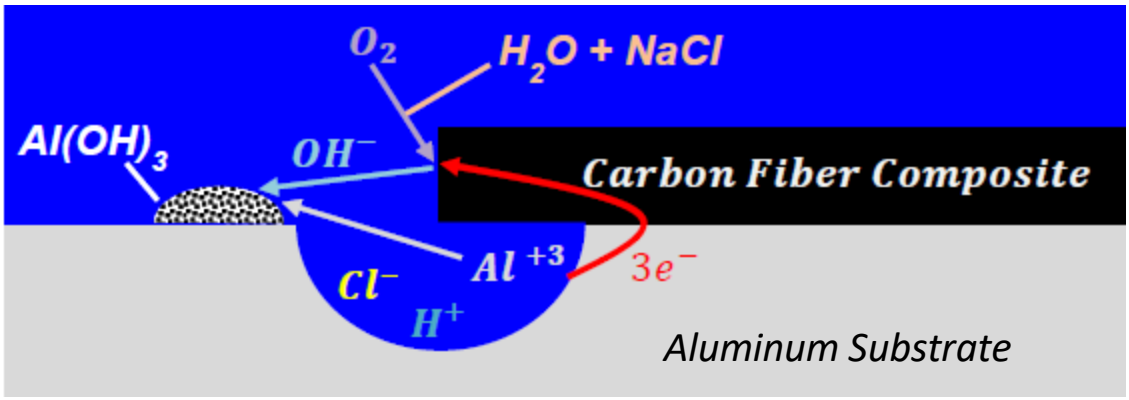

Figure 70: CFRP Laminated Al (e.g., 1100-H14, 5456-H116) in Alkaline Solution [6]

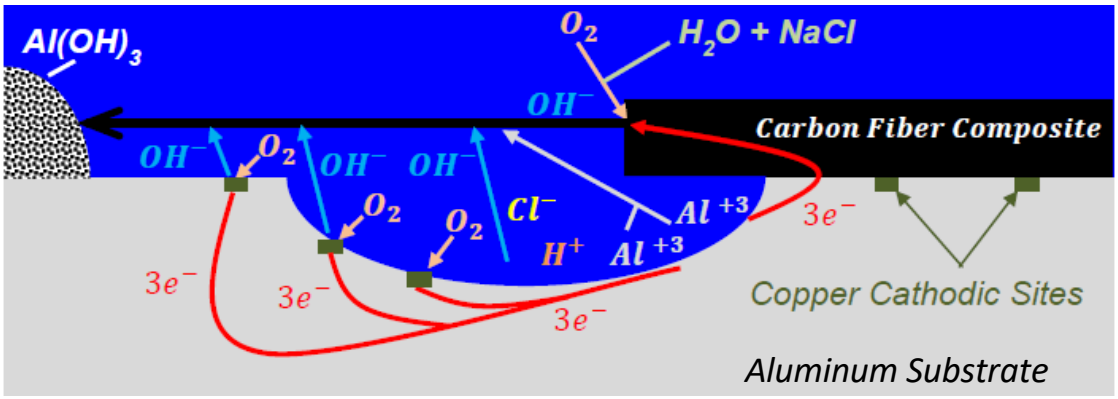

Figure 71: CFRP Laminated Al (e.g., 7075-T6) in Alkaline Solution [6]

All of the GFRP laminated aluminum samples were not subjected to galvanic coupling between the GFRP and the substrate, since GFRP is electrically insulative. The only corrosion process that occurred on the GRFP-laminated samples was due to local cathodic sites (e.g., copper-rich regions) and is illustrated in Figure 72 below.

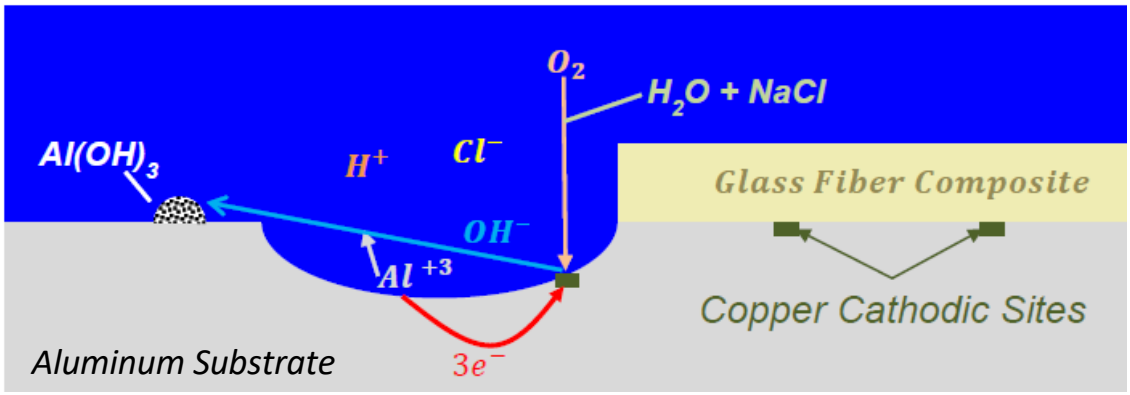

Figure 72 GFRP Laminated Al (e.g., 1100-H14, 5456-H116, 7075-T6) in Alkaline Solution [6]

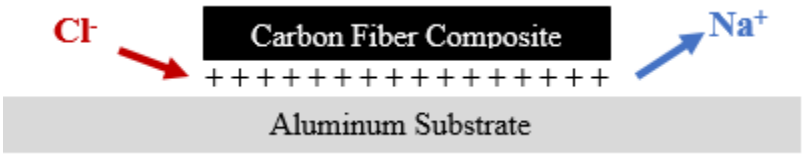

Figure 73: Laminate and Substrate Interface with Few Cathodic Sites

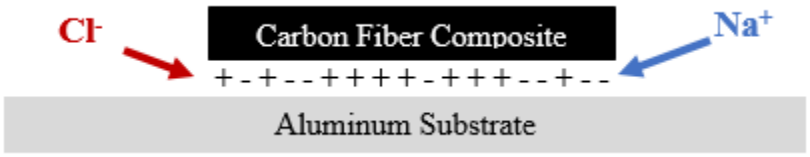

Figure 74: Laminate and Substrate Interface with Many Cathodic Sites

Of the 17 SEM and EDX analysis samples, 8 were chosen for profile analysis. All samples that were chosen were laminated with CFRP due to the higher corrosion rate under the laminate. Coconut Island was chosen to represent all 4 aluminum alloy substrates due to its more even corrosion products and that it represented a mild marine environment. Al 5456-H116 sensitized and non-sensitized samples were chosen for Kilauea volcano and Lyon Arboretum mostly due to budget and time constraints and that the follow on test (nitric acid mass loss test) is only designed to effect 5xxx series alloys.

The first analysis conducted on each sample was a pitting depth analysis that ran along a specified chord of each sample. The image on the left side of Figure 44 through Figure 51 shows the chord chosen along the surface of each test sample, while the right side of Figure 44 through Figure 51 shows the pit depth along that chord. Since most of the corrosion occurred at the outer edges of the relief, the deepest pits occur toward the ends of each chord or the outer edge of the relief. Pit depths between 75 µm to 175 µm can be seen on the outside edge of the reliefs. Towards the center of the chords a gradual decrease in corrosion is seen with the exception of square looking pits that are especially prevalent in the Coconut Island Al 5456-H116 non-sensitized sample (Figure 45) and the Kilauea volcano Al 5456-H116 sensitized sample (Figure 49). In certain areas the aluminum alloy substrate was left exposed in an area about equal to a pinhole due to gaps in the bi-weave structure of the carbon fiber fabric. Figure 75 below illustrates.

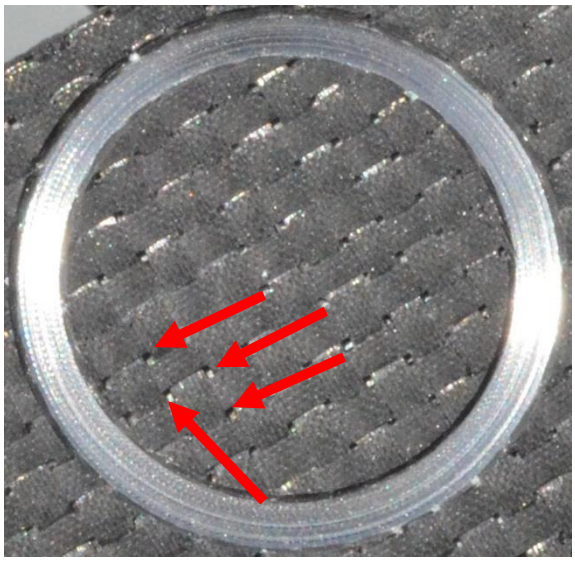

Figure 75: Exposed Aluminum Substrate (arrows)

The volume of the pits on the surface, as well as the surface area those pits cover for each of the samples can be found in Table 11. An example of the area of interest for calculating volume and

surface area for pitting is shown in Figure 52. The highest volume loss due to pitting for the samples tested were Lyon Arboretum Al 5456-H116 non-sensitized and sensitized, followed by Coconut Island Al 1100-H14 and Al 7075-T6. The surface area of the pits within the relief section showed Coconut Island 7075-T6 with the largest pitting surface area followed by Lyon Arboretum Al 5456-H116 non-sensitized, Coconut Island Al 1100-H14, and Lyon Arboretum Al 5456-H116 sensitized. These results are mostly unsurprising due to the extra cathodic sites created by copper and zinc in the Al 7075-T6 and the extra iron in Al 1100-H14. By dividing the volume into the area, the average pit depth can be calculated with both Lyon Arboretum and Coconut Island Al 5456-H116 sensitized samples showing the deepest pits. This is most likely due to the Mg_2Al_3 particles that precipitate on the alloy grain boundaries and corrode much more quickly than the substrate aluminum. Overall, across all of the alloys, the average pit depth remained relatively constant even as the amount of corroded surface area increased (Figure 52), indicating that the corrosion propagated laterally under the laminate rather than bored deep into the substrate.

Following the profile testing, the 8 test samples along with 2 control samples (unexposed CFRP Al 5456-H116 sensitized and non-sensitized) for a total of 10 samples were subjected to a nitric acid mass loss test. The unexposed samples used in this test served as a baseline to see if any additional sensitization had occurred in each of the exposed samples. The results in Table 13 do show that the sensitized Al 5456-H116 samples had a little more than twice the mass loss than the Al 5456-H116 non-sensitized samples regardless of exposure location. This is due to the increased Mg_2Al_3 particles that precipitate along the grain boundary and corrode preferentially to the alloy matrix. There does not appear to be a significant increase in mass loss in the Al 5456-H116 sensitized samples due to exposure when compared to an unexposed sample, but there is a slight increase in mass loss in the

Al 5456-H116 non-sensitized samples due to exposure. Unsurprisingly, the Al 1100-H14 and Al 7075-T6 alloys had very little mass loss, due to their low magnesium content.

A decohesion model was created in conjunction with the polarization test results to compare predicted to actual decohesion rates for the composite-laminated aluminum samples. The derivation for the model is discussed below. Figure 76 below is used as a reference for the following derivation.

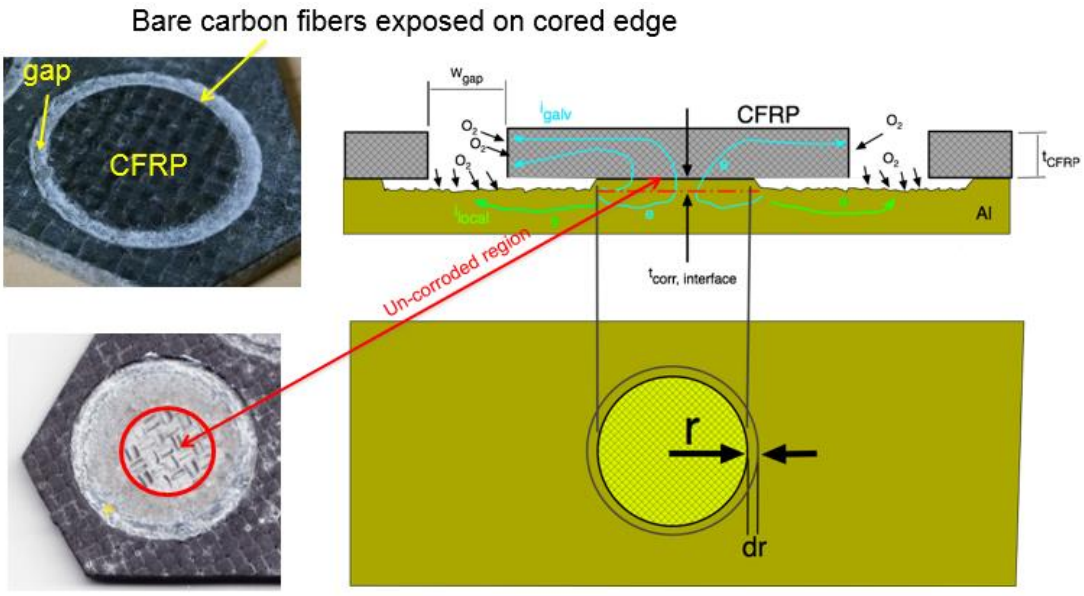

Figure 76: Decohesion Model Illustration

To start, the assumption is made that the total cathodic current is equal to the total anodic current in the system in Equation 7.

$$I_C = I_A \qquad \text{(Eq. 7)}$$

Where I_C is the total cathodic current, and I_A is the total anodic current. The I_C can then be equated to the galvanic current created on the CFRP laminate plus the local current produced by cathodic sites on the aluminum substrate. Equation 8 refers.

$$I_C = I_{galv} + I_{local} = I_{C,CFRP} + I_{C,alloy} \qquad \text{(Eq.8)}$$

Where I_{galv} corresponds to $I_{C,\,CFRP}$ which is the galvanic current induced by the CFRP laminate, and I_{local} corresponds to $I_{C,\,alloy}$ which is the local cathodic current on the aluminum substrate. The galvanic and local currents can be found by multiplying the current density by the surface area as shown in Equation 9 and 10.

$$I_{C,CFRP} = i_{C,CFRP} \cdot 2\pi R t_{CFRP} \quad \text{(Eq. 9)}$$

$$I_{C,alloy} = i_{C,alloy} \cdot 2\pi R W_{gap} \quad \text{(Eq. 10)}$$

Where $i_{C,CFRP}$ and $i_{C,alloy}$ are galvanic and local current densities, respectively, R is the radius of the CFRP patch, t_{CFRP} is the thickness of the CFRP patch, and W_{gap} is the width of the bare exposed aluminum substrate. Figure 76 above illustrates.

In order to determine the mass loss from the aluminum substrate, Faraday's Law is used as demonstrated in Equation 11.

$$m = \frac{I \cdot t \cdot A_m}{nF} \quad \text{(Eq. 11)}$$

Where m is the mass loss of the substrate, I is the current (equal to Eq. 9 + Eq. 10), t is the time of exposure, A_m is the atomic mass of the substrate, n is the number of valence electrons, and F is Faraday's constant.

When taking the derivative to find the change in mass from start to end exposure, it is assumed that the current (I) is constant while the specimen is corroding and yields Equation 12.

$$\partial m = \frac{I \cdot A_m}{nF}\partial t + \frac{t \cdot A_m}{nF}\partial I = \frac{I \cdot A_m}{nF} dt \quad \text{(Eq. 12)}$$

The change in mass can also be found based on the geometric volume loss and density with Equation 13.

$$\partial m = \rho t_{corr,interface} \cdot 2\pi r dr \quad \text{(Eq. 13)}$$

Where ρ is the density of the substrate, $t_{corr,interface}$ is the thickness of the corroded region under the CFRP patch (Figure 76 refers), and *r* is the radius of the uncorroded substrate region. Equation 12 and Equation 13 can be set equal to each other and yield Equation 14.

$$\frac{I \cdot A_m}{nF\rho t_{corr,interface} \cdot 2\pi} \partial t = r \partial r \quad \text{(Eq. 14)}$$

All of the constants before ∂t can be combined into one variable (*B*) for ease of calculation. The integral with respect to time is taken and is presented in Equation 15.

$$B \int_0^t \partial t = \int_R^r r \, \partial r \quad \text{(Eq. 15)}$$

Solving the integral yields Equation 16.

$$Bt = \frac{r^2}{2}\Big|_R^r = \frac{r^2}{2} - \frac{R^2}{2} \quad \text{(Eq. 16)}$$

Rearranging Equation 16 yields Equation 17.

$$r^2 = R^2 + 2Bt \quad \text{(Eq. 17)}$$

Where B is equal to $B_1\left(B_2 i_{C,CFRP} + B_3 i_{C,alloy}\right)$ and yields Equation 18.

$$r^2 = R^2 + 2B_1\left(B_2 i_{C,CFRP} + B_3 i_{C,alloy}\right)t \quad \text{(Eq. 18)}$$

The adhesive force (Adh) of the CFRP laminate is then calculated by multiplying the adhesion strength by the surface area of the uncorroded region of the CFRP patch as shown in Equation 19.

$$Adh = \sigma_{interface}\pi\left[R^2 + 2B_1\left(B_2 i_{C,CFRP} + B_3 i_{C,alloy}\right)t\right] \quad \text{(Eq. 19)}$$

Where $\sigma_{interface}$ is the adhesion strength of the interface. Taking the derivative with respect to time yields Equation 20.

$$\frac{\partial(Adh)}{\partial t} = -\sigma_{interface}\pi 2B_1\left(B_2 i_{C,CFRP} + B_3 i_{C,alloy}\right) \quad \text{(Eq. 20)}$$

Simplifying this equation yields Equation 21.

$$\frac{\partial(Adh)}{\partial t} = -B_4 f\left(i_{C,CFRP}, i_{C,alloy}\right) \quad \text{(Eq. 21)}$$

The $i_{C,CFRP}$ term was relatively independent of the alloy, and was taken from zero-resistance ammeter (ZRA) galvanic corrosion tests shown in Table 18. The $i_{C,alloy}$ term was dependent on the alloy, and was taken from potentiodynamic polarization curves presented in Figure 66 through Figure 69. Hence, the model indicates that the decohesion rate will primarily be a function of $i_{C,alloy}$. Based on the values of $i_{C,alloy}$ (Table 19), the decohesion rates should be of the following order: Al 7075-T6 > Al 5456-H116 sensitized > Al 1100-H14 > Al 5456-H116 non-sensitized. The data in Figure 42 of the decohesion rate for the various alloys and test sites show similar trends albeit not exact, as the actual values of $i_{C,alloy}$ are not expected to be identical to those measured during the polarization tests.

Chapter 7

CONCLUSIONS

7.1 Summary of Composite Laminated Alloy Corrosion Resistance

Overall, the GFRP laminate on all aluminum alloy substrates was determined to have lost the least adhesion strength in addition to protecting the substrates from corrosion product growth at all testing locations. The CFRP laminate was found to have formed a galvanic couple with each of the alloys, causing a significant increase in the corrosion rate at the interface of the CFRP laminate and aluminum substrate. This phenomena was found to increase significantly when coupled to an alloy that had more cathodic sites; e.g., Al 7075-T6 with its high copper and zinc content and Al 1100-H14 with its iron content.

The CFRP laminated Al 5456-H116 sensitized showed a slightly lower corrosion resistance than Al 5456-H116 non-sensitized which supports the claim that the Mg_2Al_3 particles that precipitate on the alloy grain boundaries in the sensitized alloy play a role in corrosion resistance. The CFRP laminated Al 1100-H14 performed overall slightly worse than the Al 5456-H116 sensitized due to its additional iron content which created cathodic sites for corrosion to occur. The CFRP laminated Al 7075-T6 performed the worst overall due to its high copper and zinc content which also created cathodic sites for additional corrosion to occur. An R^2 value (excluding the Mauna Loa test site) of 0.89 for the adhesive force vs exposure time indicated that the decohesion behavior of the CFRP laminated alloys (listed in Figure 42) were in agreement to that of the decohesion model. The decohesion rates slope (listed in Table 4) were also a function of the substrate alloy and ranked from highest to lowest as Al 7075-T6 > Al 1100-H14 > Al 5456-H116 sensitized > Al 5456-H116 non-sensitized. The

ordering was somewhat similar to that of the normal corrosion rates for the uncoupled alloys: Al 7075-T6 > Al 5456-H116 sensitized > Al 1100-H14 > Al 5456-H116 non-sensitized, which is generally in agreement with the decohesion model.

The overall performance of the GFRP laminated alloys was significantly better than their CFRP laminated counterparts due to, as stated above, the laminate insulating the substrate alloy and preventing further corrosion underneath. An R^2 value (excluding the Mauna Loa test site) of 0.58 for the adhesive force vs exposure time indicated that the decohesion of the GFRP laminated alloys (listed in Figure 41) does not follow the decohesion model.

Looking at overall decohesion rates for all testing locations, Pyramid Rock caused the highest amount of corrosion on each of the samples, regardless of laminate type. This is consistent with literature that states that chloride-heavy environments increase corrosion rates. Lyon Arboretum was the next highest amount of corrosion, at least for the CFRP sample, most likely due to its extremely high humidity and rainfall which causes a more consistent salt bridge for the laminate and substrate alloy to galvanically couple. Coconut Island had the second highest corrosion rate for the GFRP laminated samples, mostly due to its much higher chloride content than Lyon Arboretum. Since there is no galvanic couple between the GFRP and the substrate alloy, the primary mechanism for corrosion is localized from chloride exposure. Kilauea volcano and Coconut Island produce very similar decohesion rates overall for CFRP laminated samples, where Lyon Arboretum and Kilauea volcano produce very similar decohesion rates for GFRP laminated samples. Mauna Loa samples retained the most adhesion strength due to the cold and dry environment of the test site.

Appendix A
Adhesion Test Bar Charts by Location

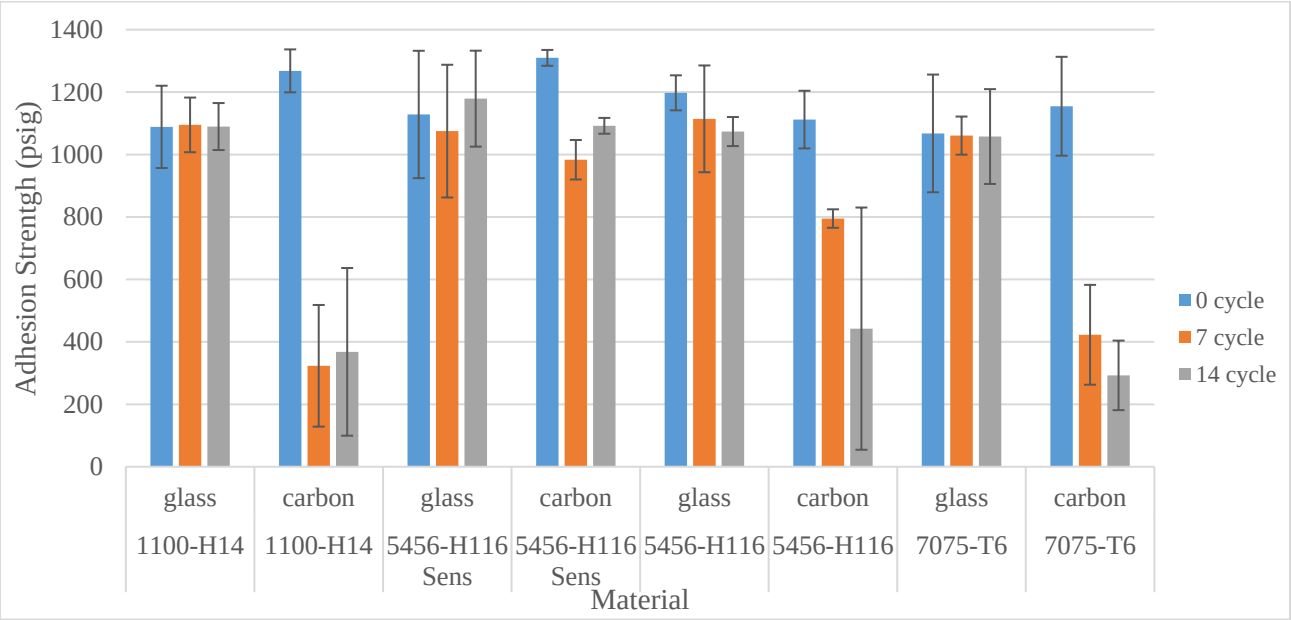

Figure 77: CCTC Adhesion Test Results

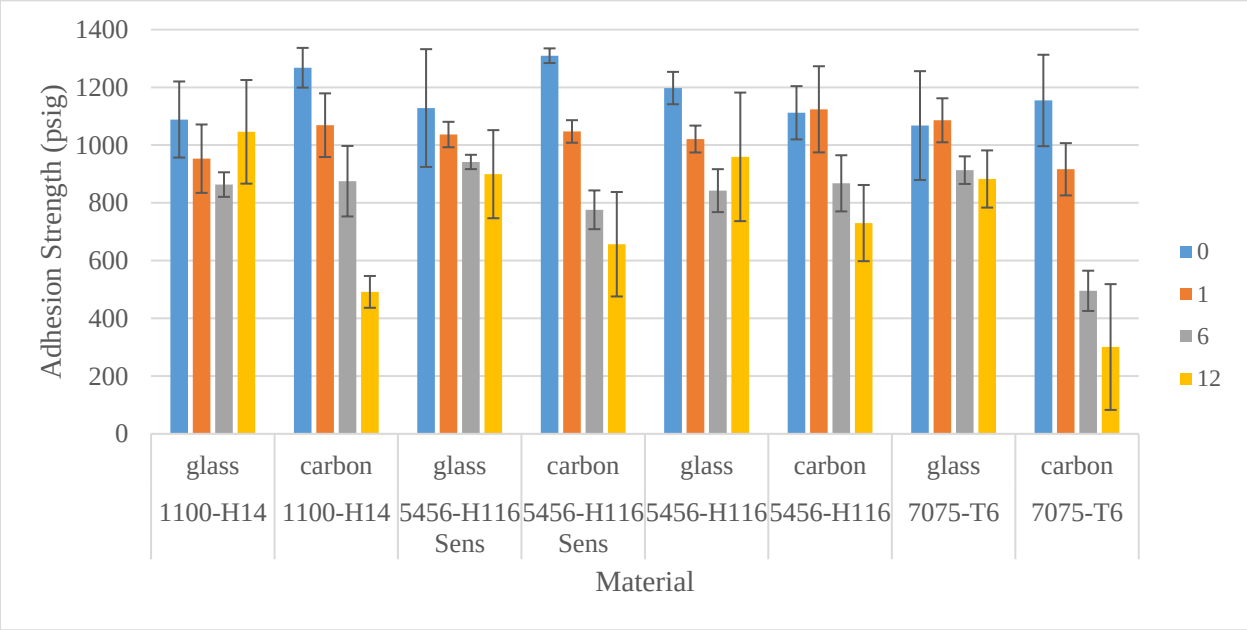

Figure 78: Lyon Arboretum Adhesion Test Results

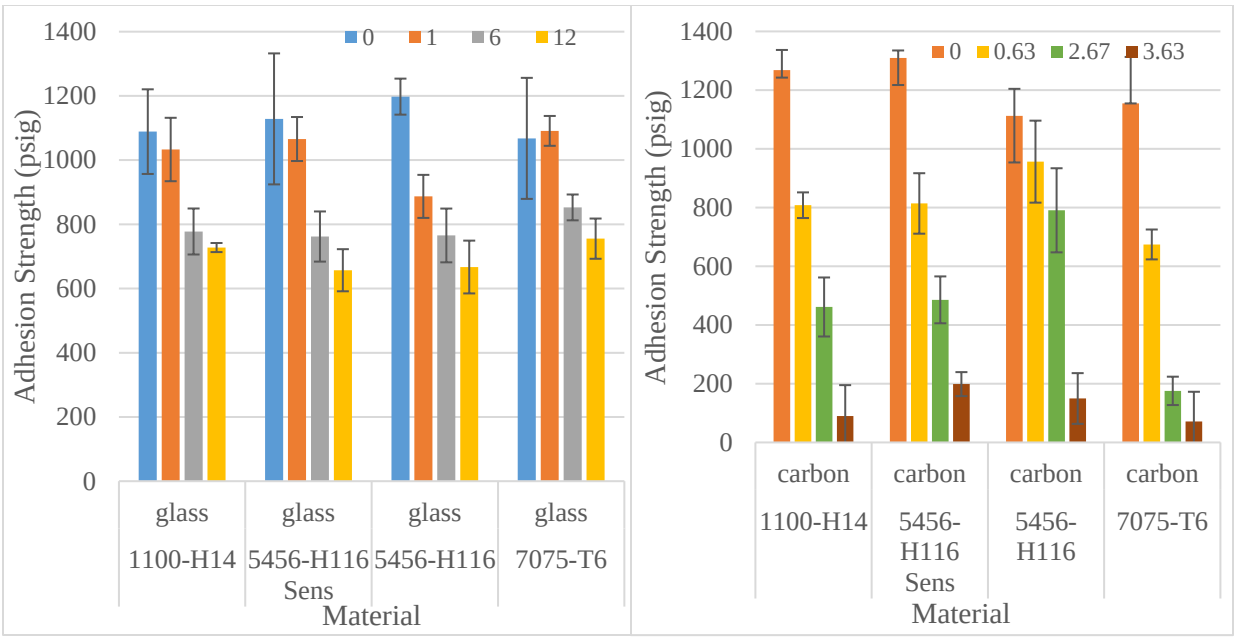

Figure 79: Pyramid Rock GFRP (left) and CFRP (right) Adhesion Test Results

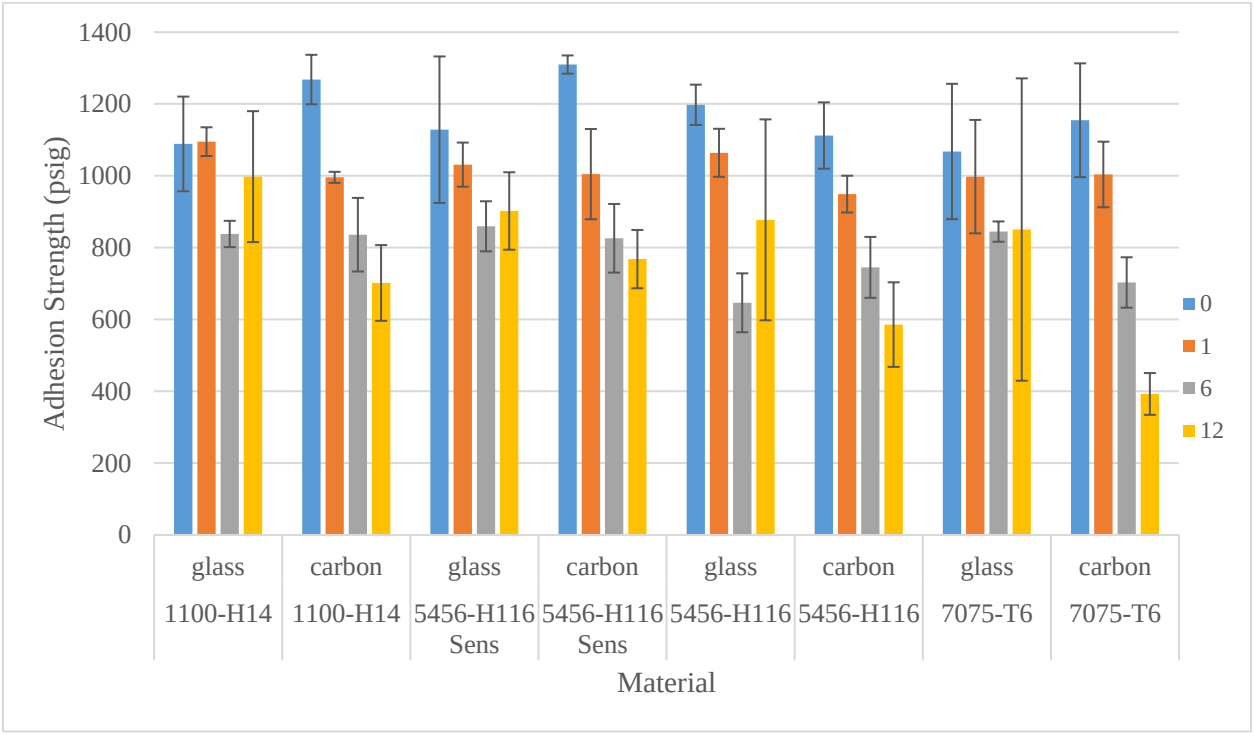

Figure 80: Coconut Island Adhesion Test Results

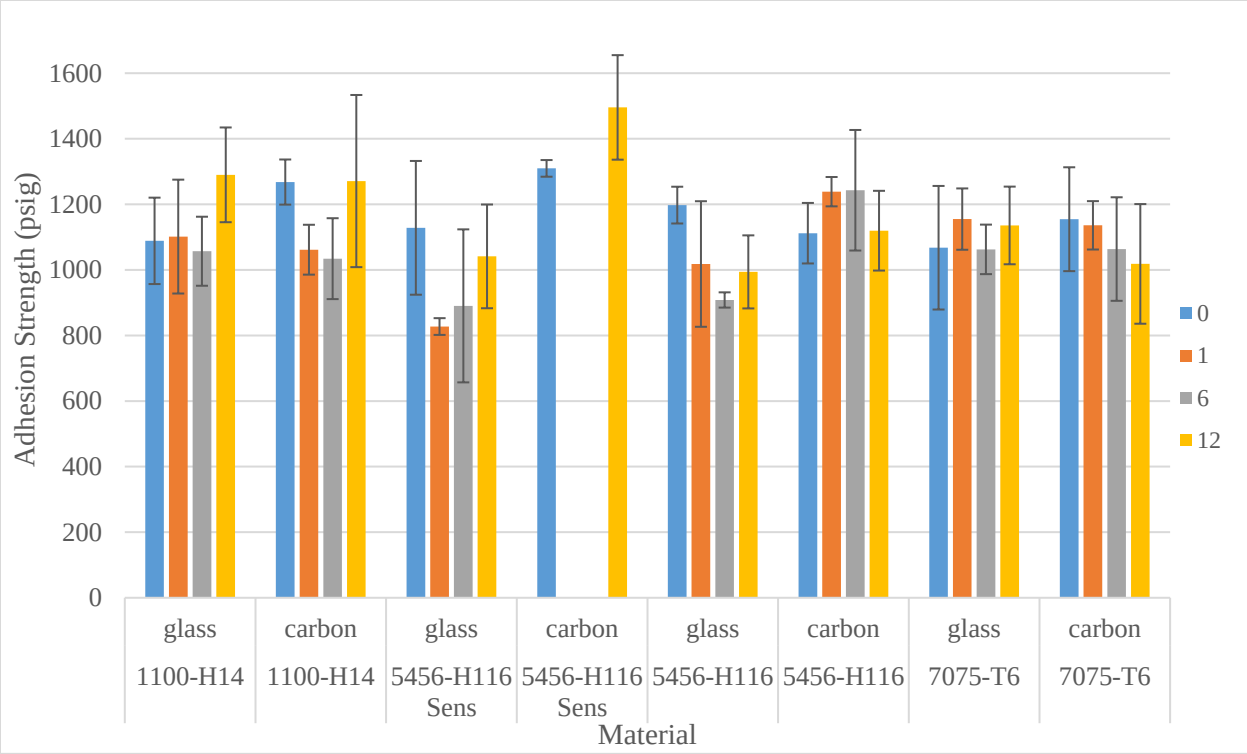

Figure 81: Mauna Loa Adhesion Test Results

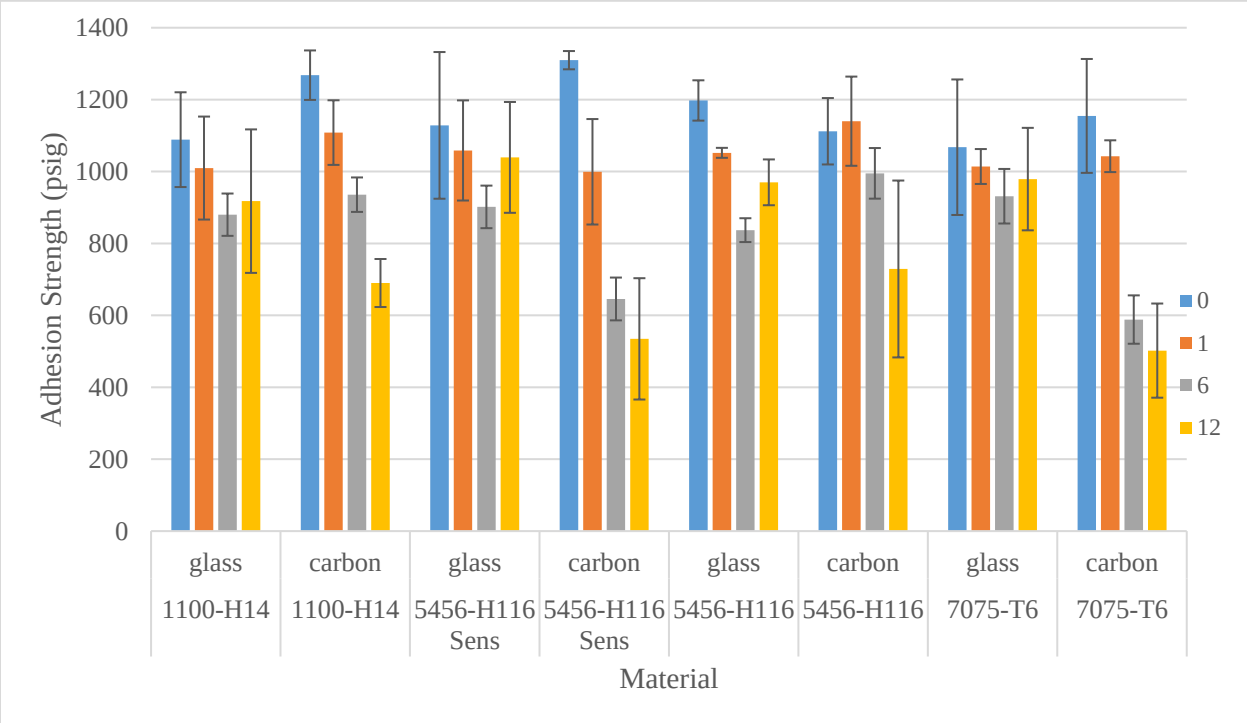

Figure 82: Kilauea Volcano Adhesion Test Results

Appendix B
Adhesion Test Bar Charts by Alloy

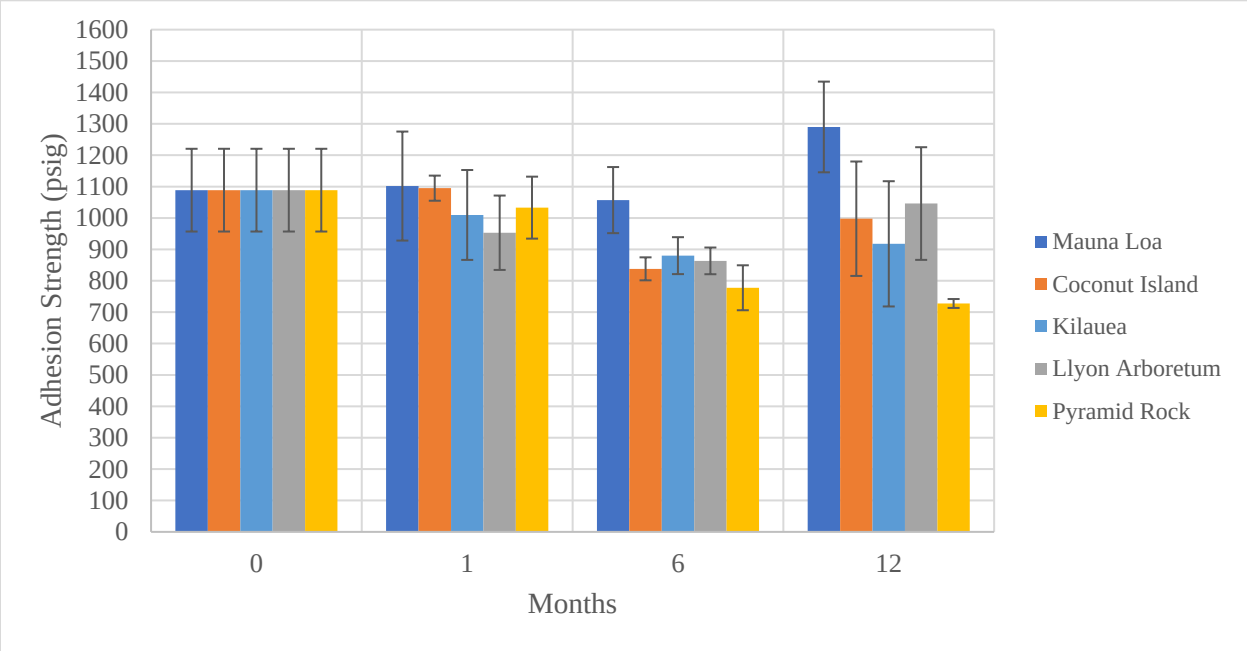

Figure 83: Al 1100-H14 GFRP Adhesion Test

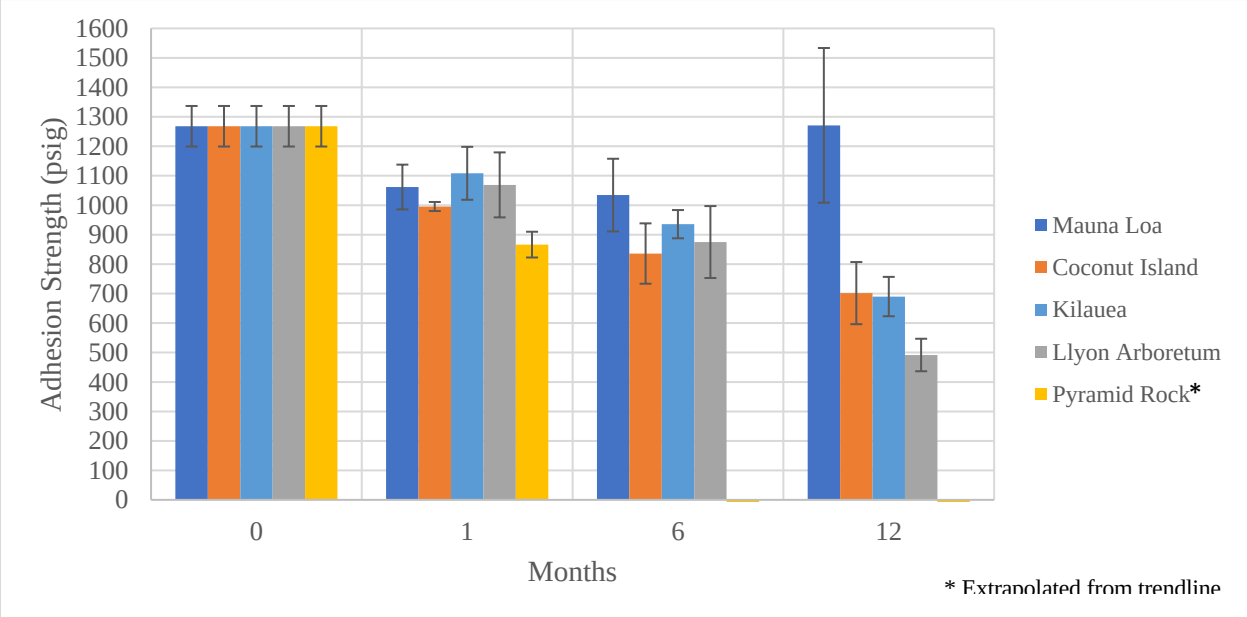

Figure 84: Al 1100-H14 CFRP Adhesion Test

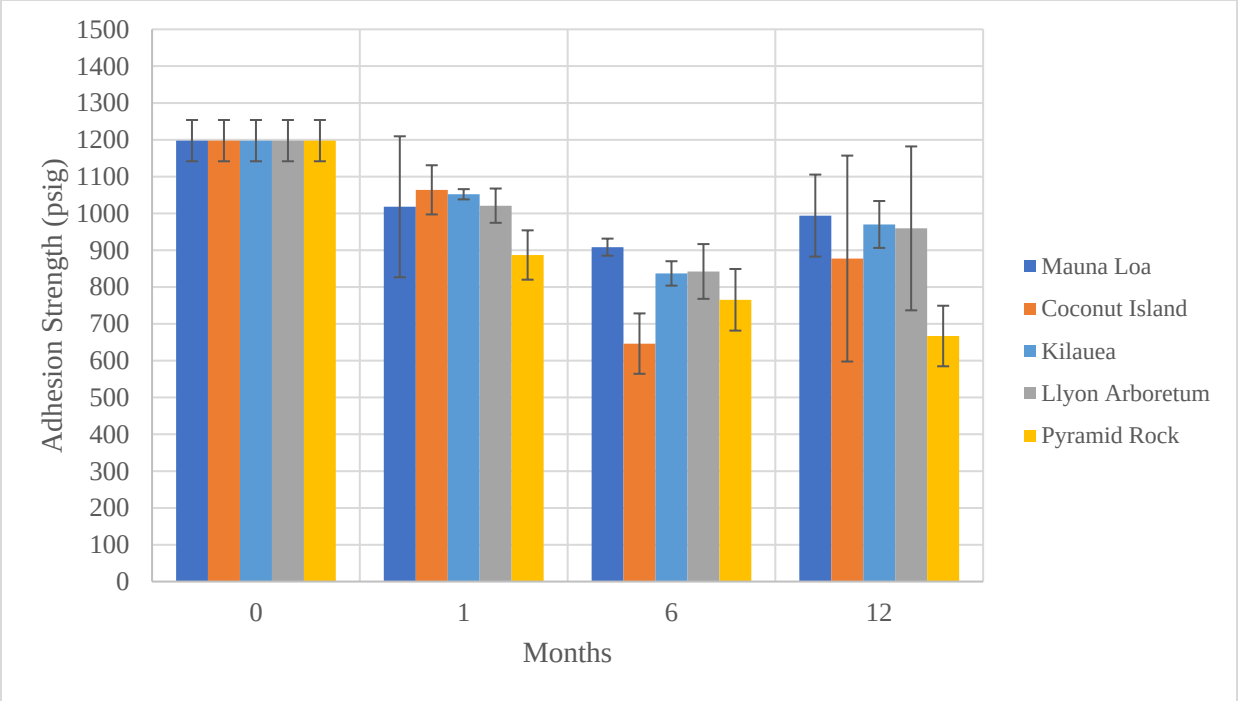

Figure 85: Al 5456-H116 Non-sensitized GFRP Adhesion Test

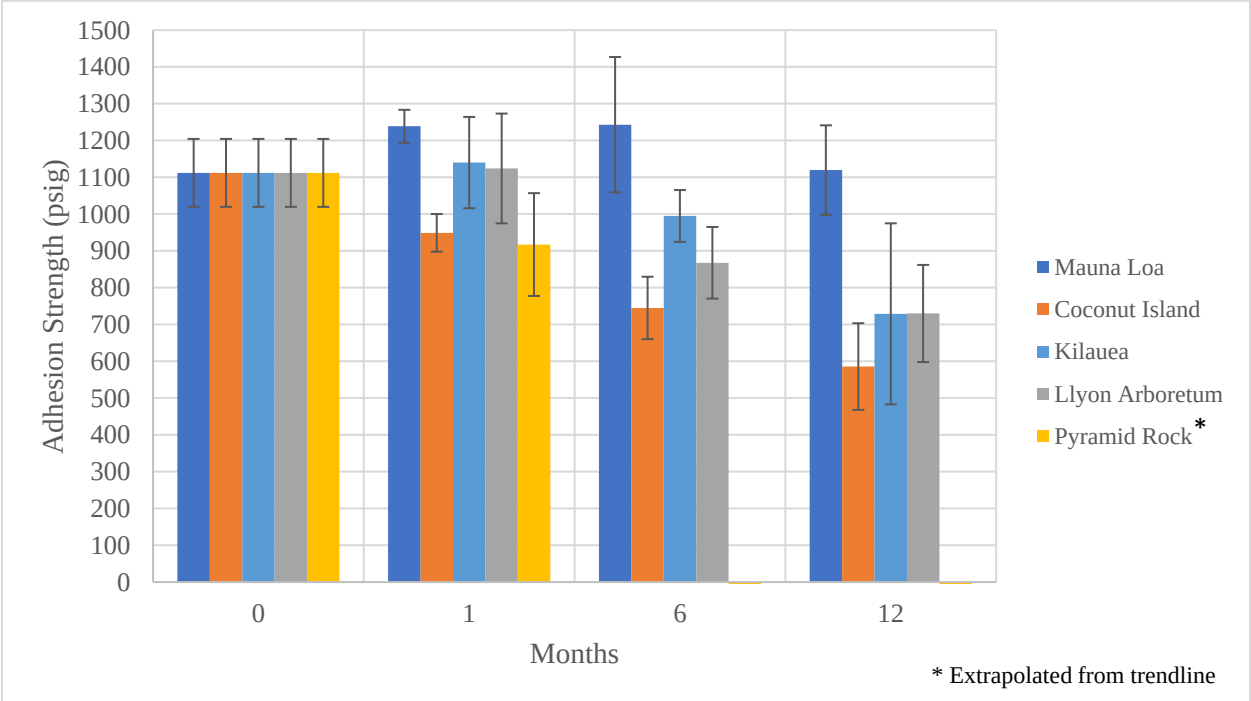

Figure 86: Al 5456-H116 Non-sensitized CFRP Adhesion Test

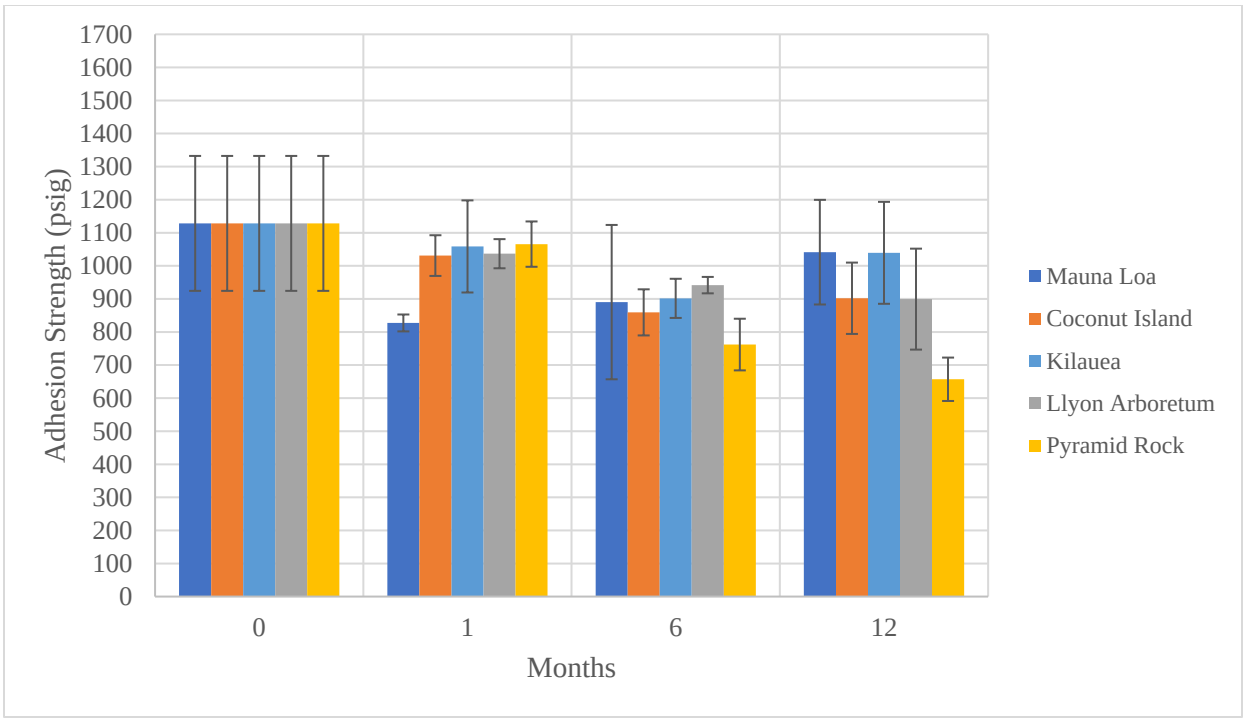

Figure 87: Al 5456-H116 Sensitized GFRP Adhesion Test

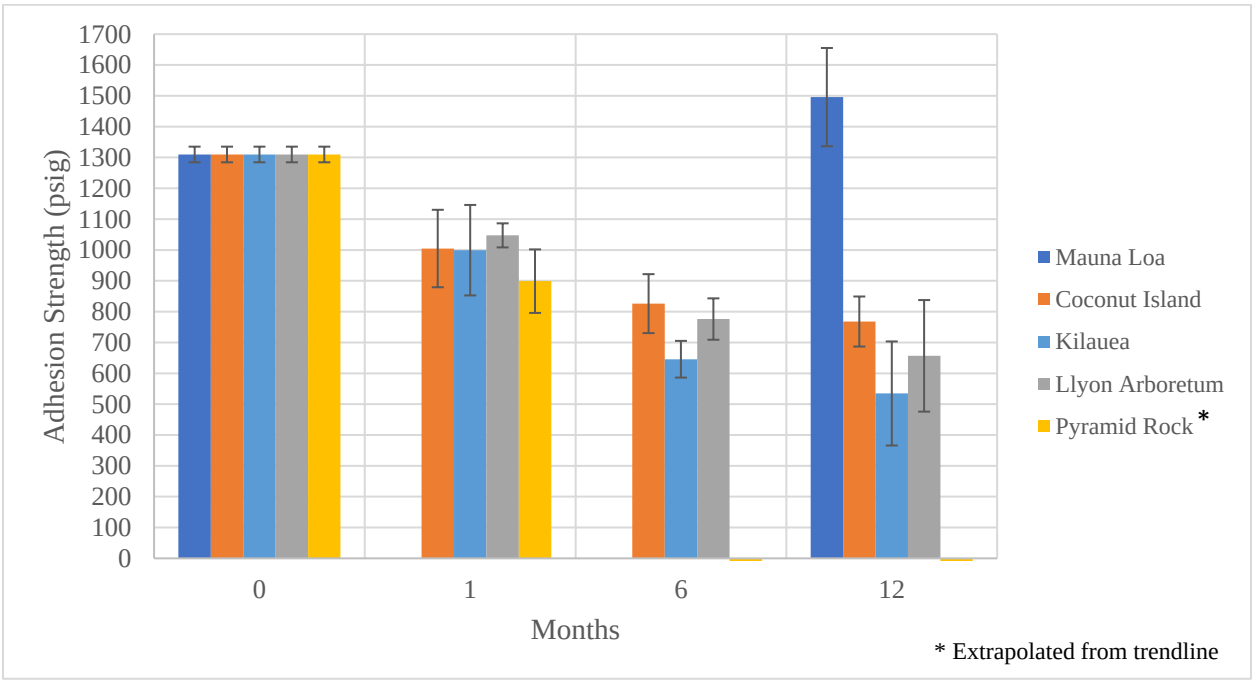

Figure 88: Al 5456-H116 Sensitized CFRP Adhesion Test

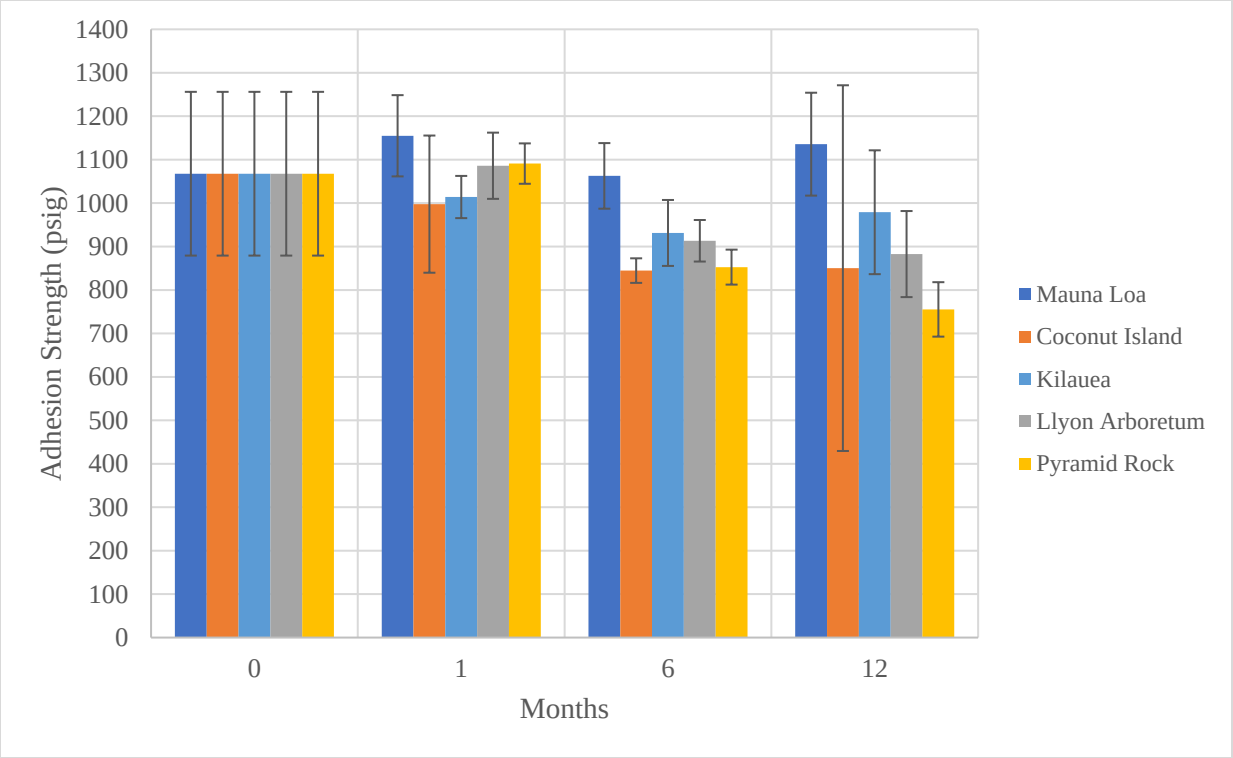

Figure 89: Al 7075-T6 GFRP Adhesion Test

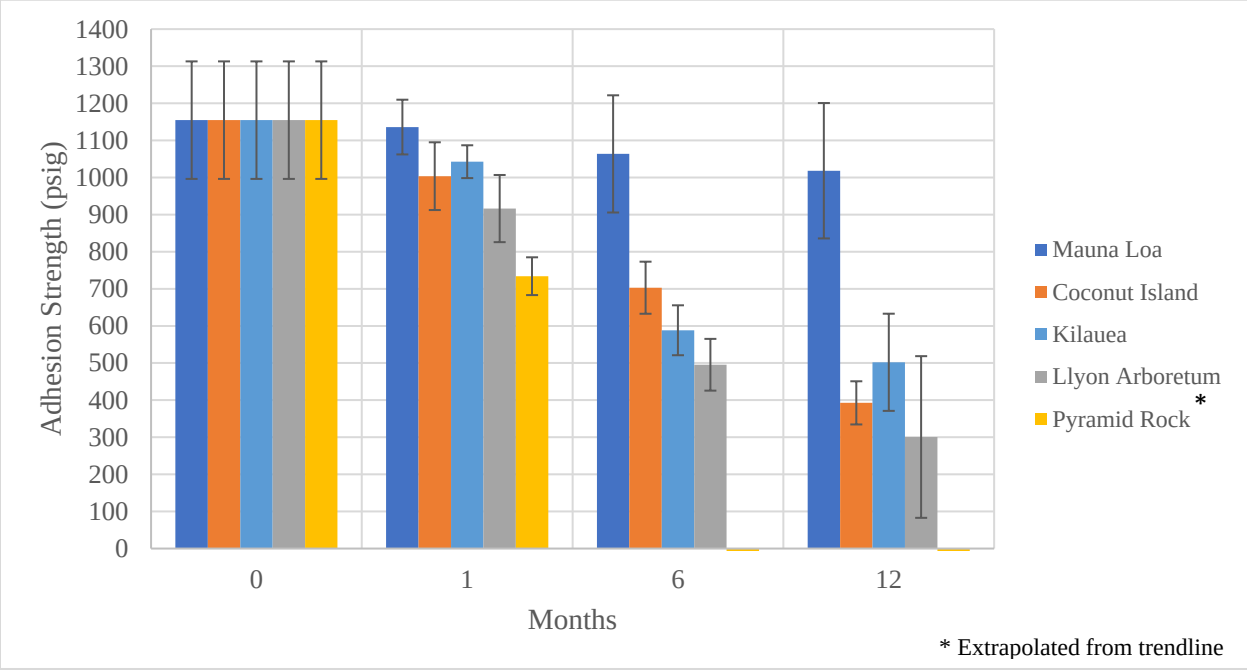

Figure 90: Al 7075-T6 CFRP Adhesion Test

Appendix C
EDX Analysis Charts

Table 21: Coconut Island 1100-H14 CFRP 1 year

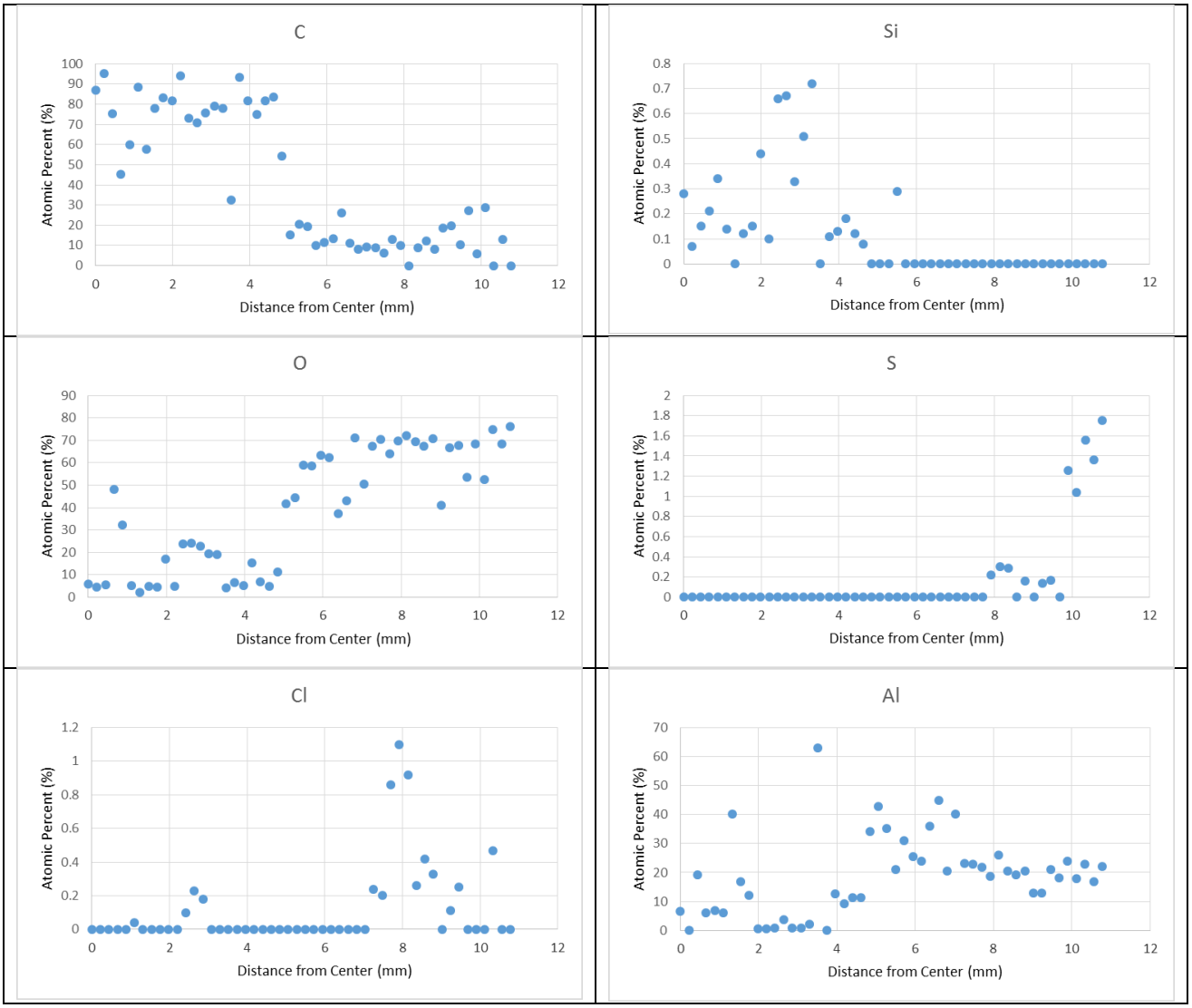

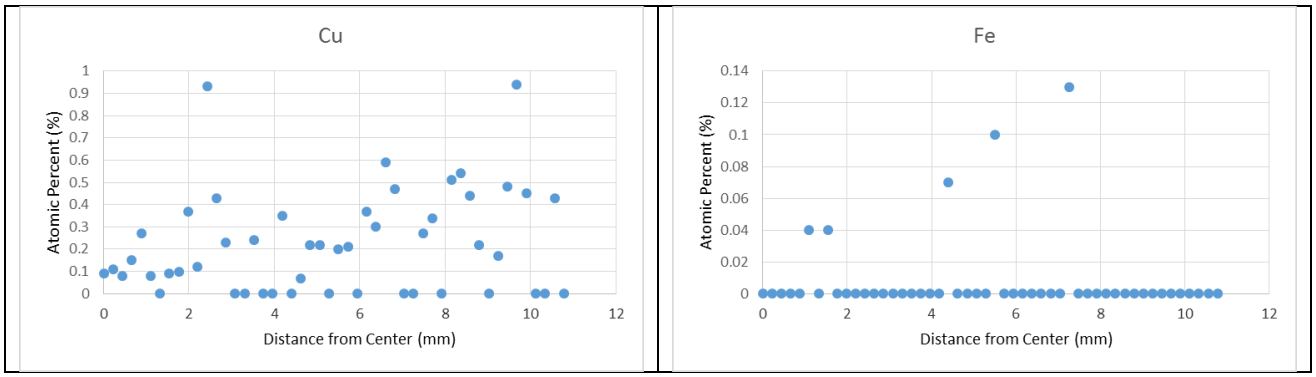

Table 22: Coconut Island 5456-H116 Non-sensitized CFRP 1 year

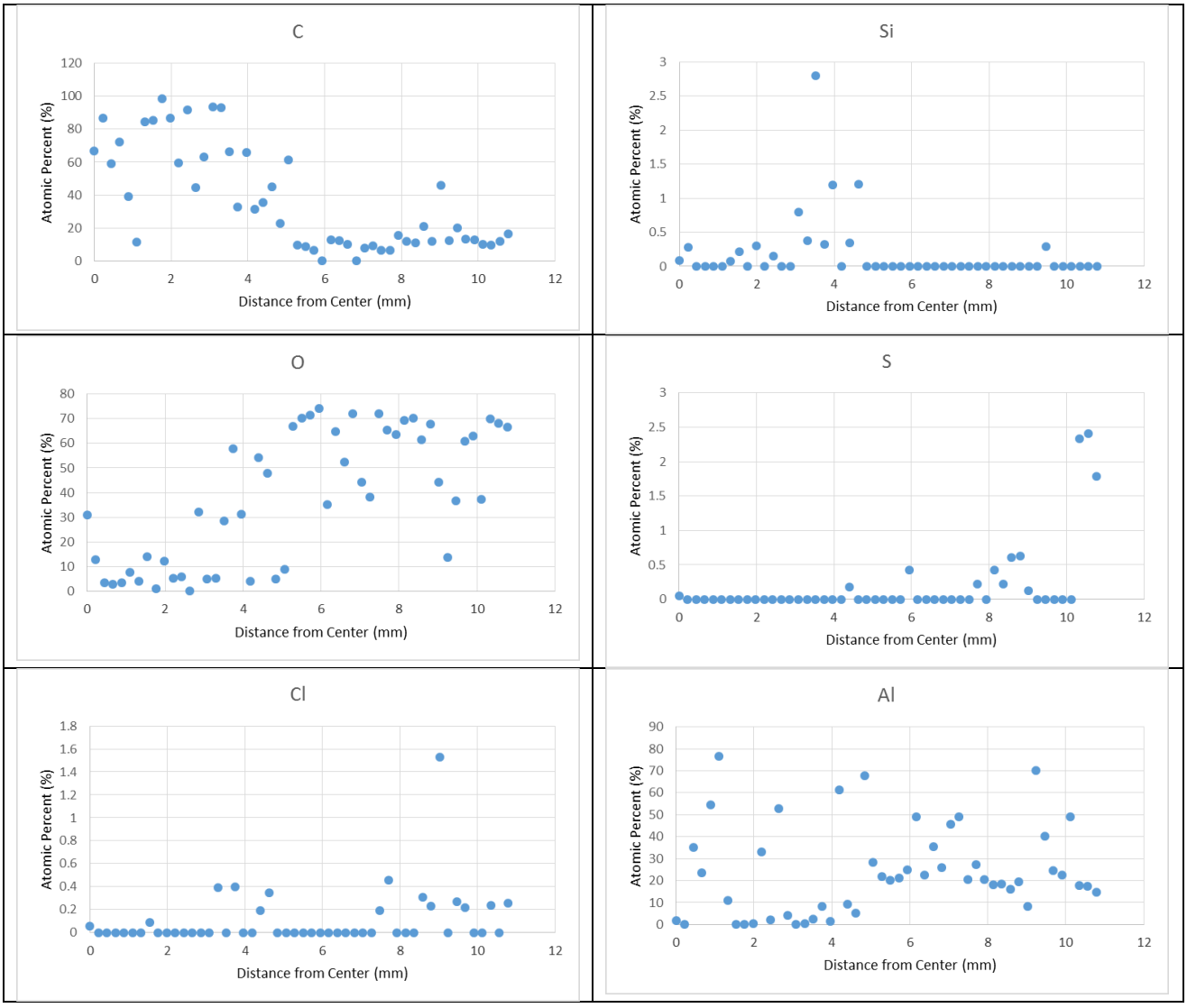

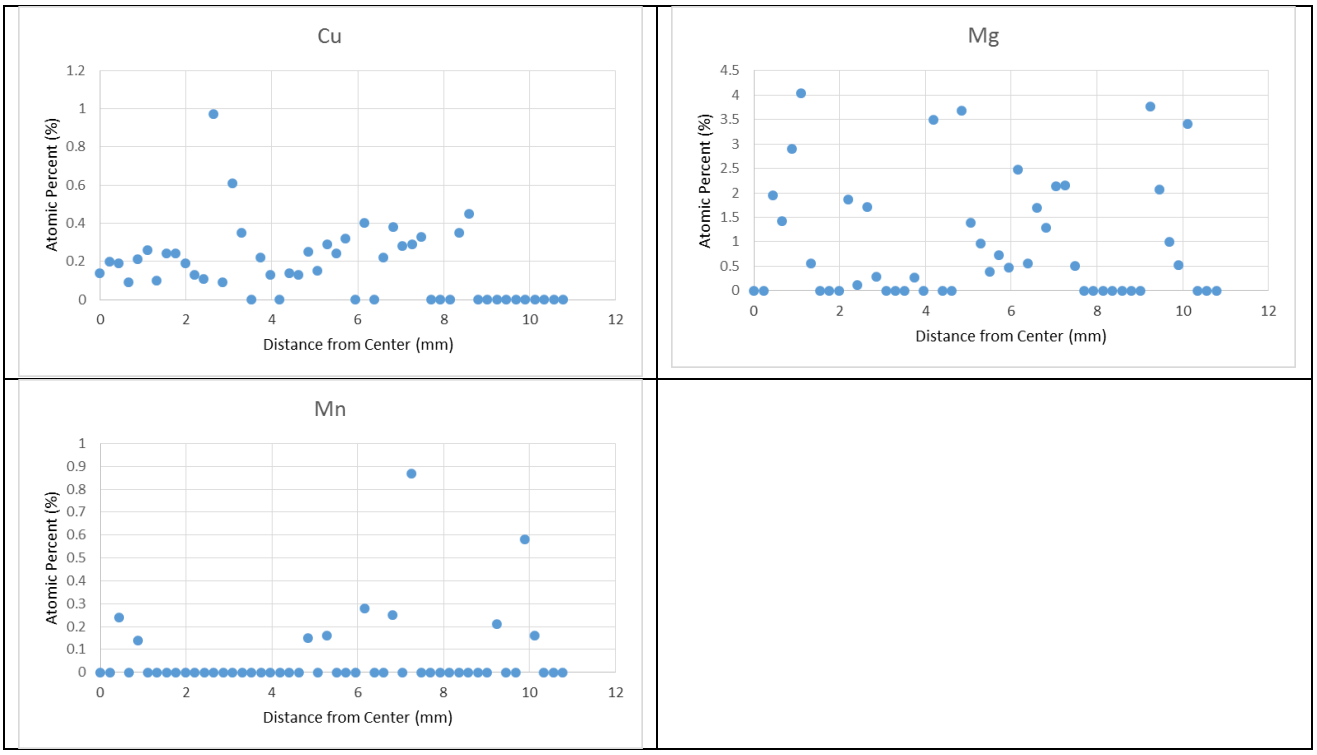

Table 23: Coconut Island 5456-H116 Sensitized CFRP 1 year

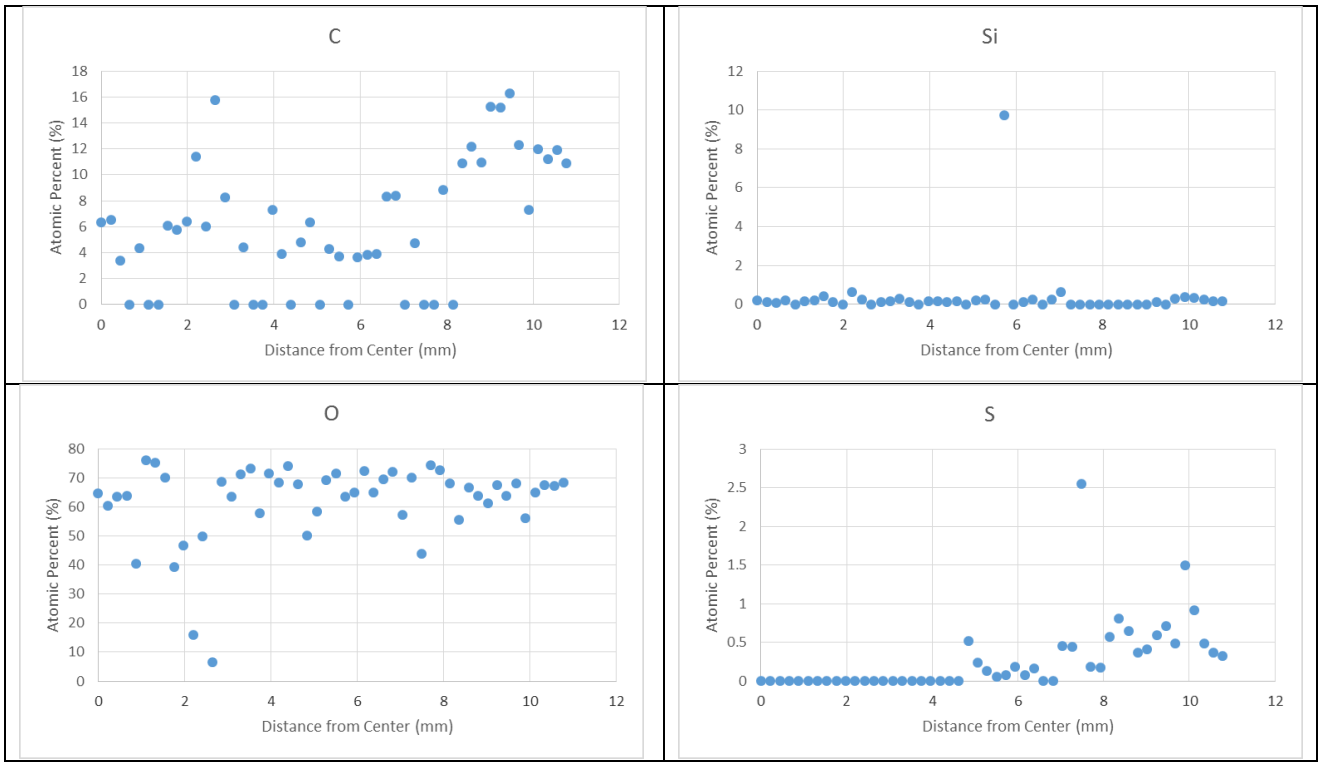

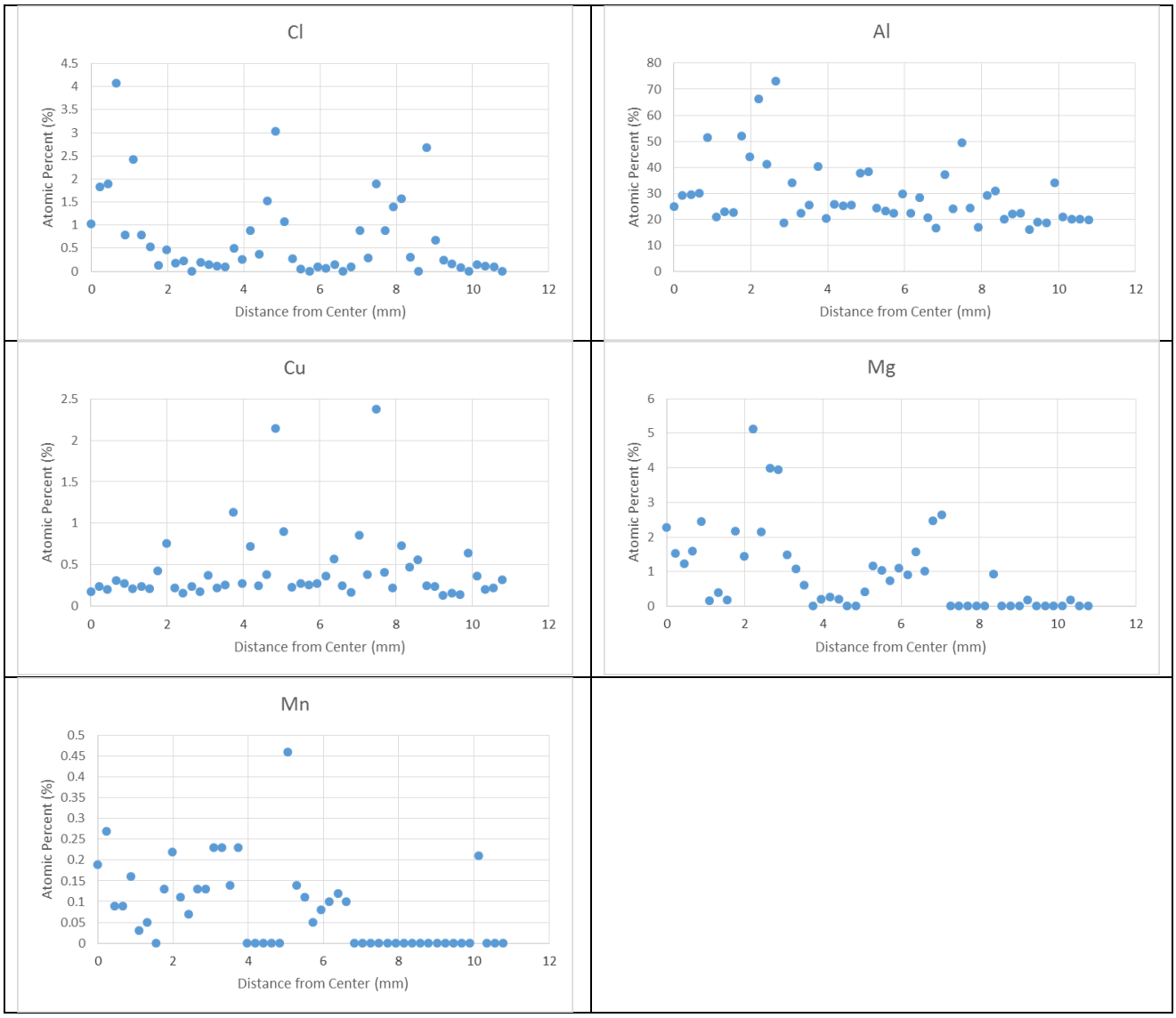

Table 24: Coconut Island 7075-T6 CFRP 1 year

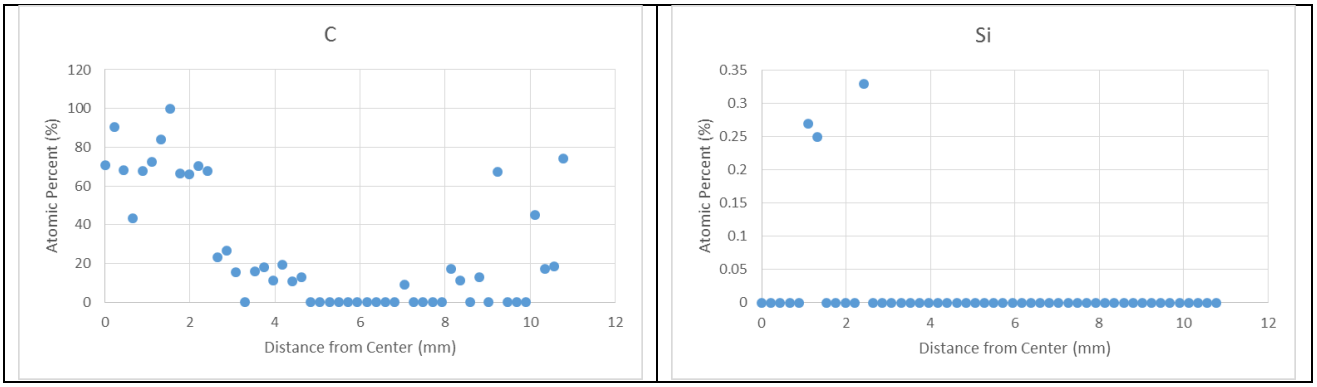


O
Atomic Percent (%)
Distance from Center (mm)
S
Atomic Percent (%)
Distance from Center (mm)
Cl
Atomic Percent (%)
Distance from Center (mm)
Al
Atomic Percent (%)
Distance from Center (mm)
Cu
Atomic Percent (%)
Distance from Center (mm)
Mg
Atomic Percent (%)
Distance from Center (mm)
Zn
Atomic Percent (%)
Distance from Center (mm)

Table 25: Kilauea Volcano 1100-H14 CFRP 1 year

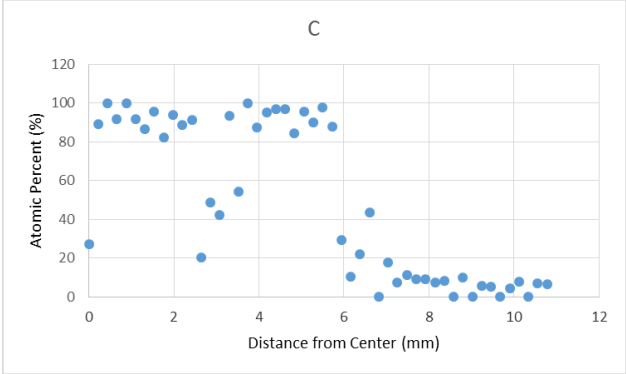

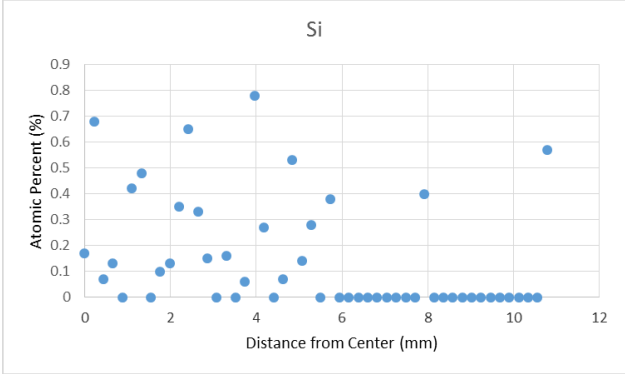

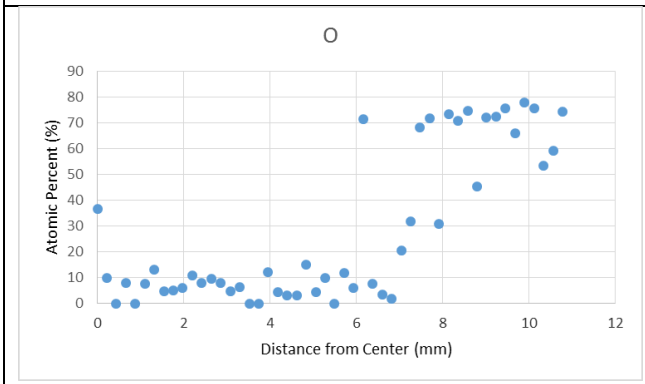

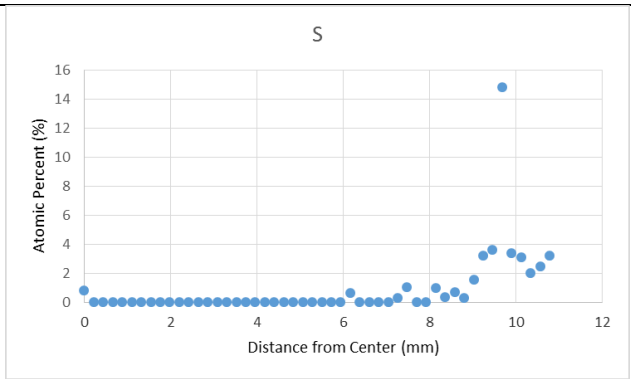

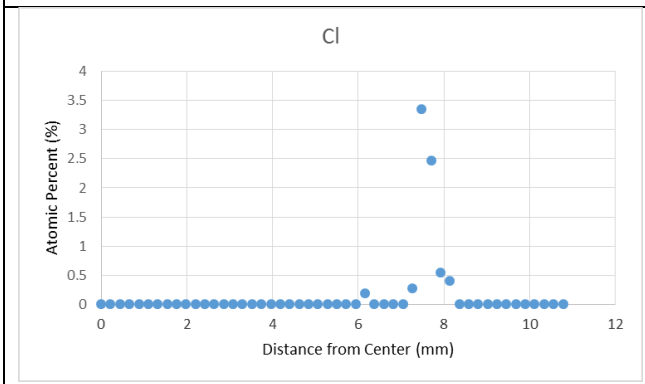

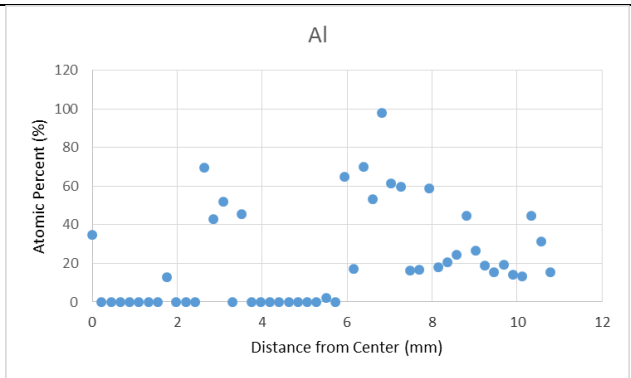

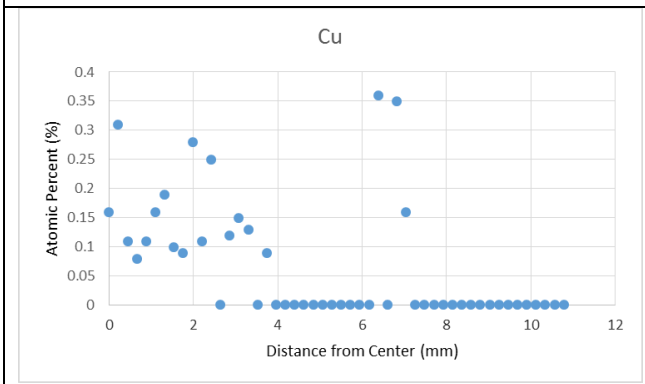

Table 26: Kilauea Volcano 5456-H116 Non-sensitized CFRP 1 year

Table 27: Kilauea Volcano 5456-H116 Sensitized CFRP 1 year

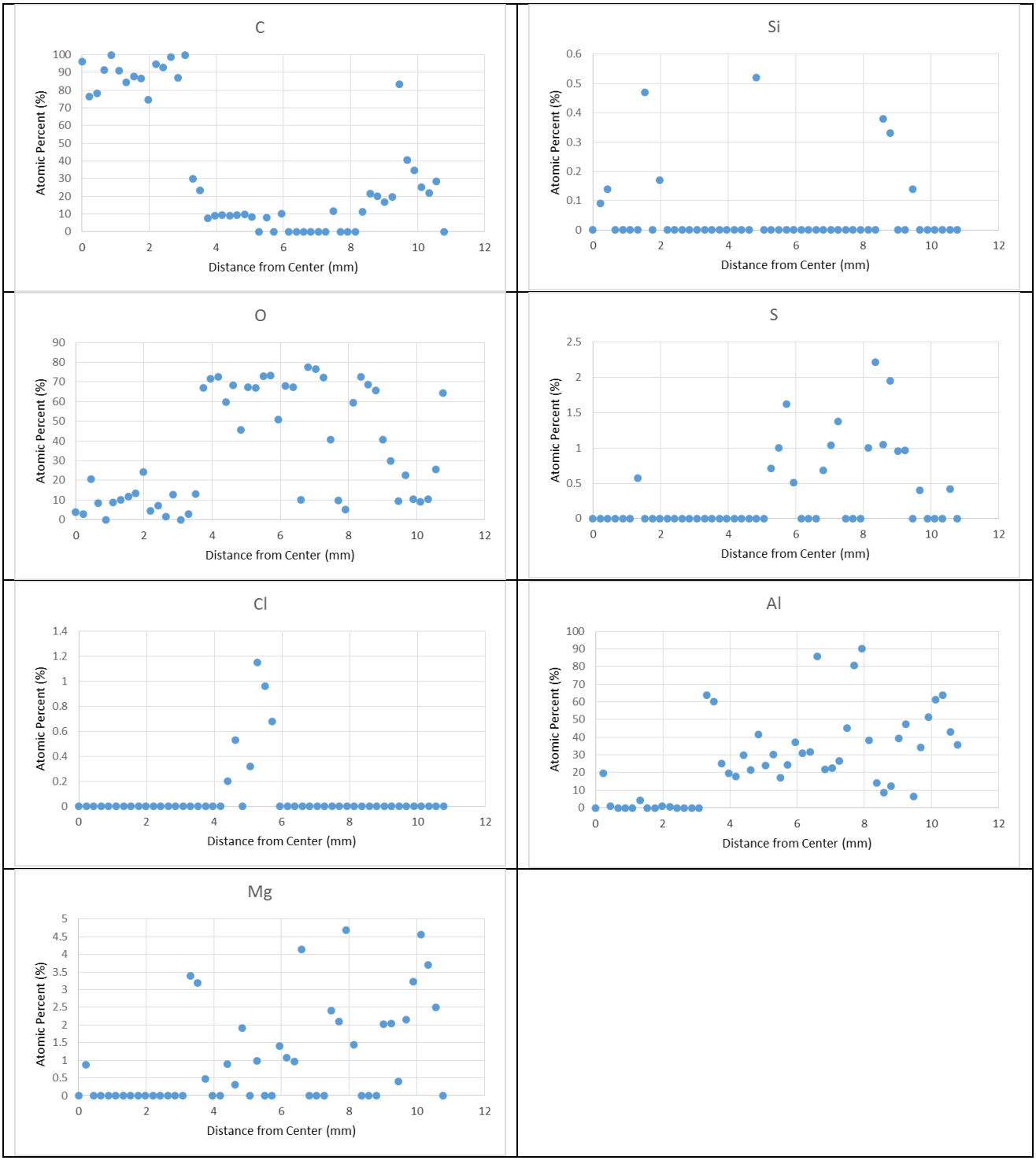

Table 28: Kilauea Volcano 7075-T6 CFRP 1 year

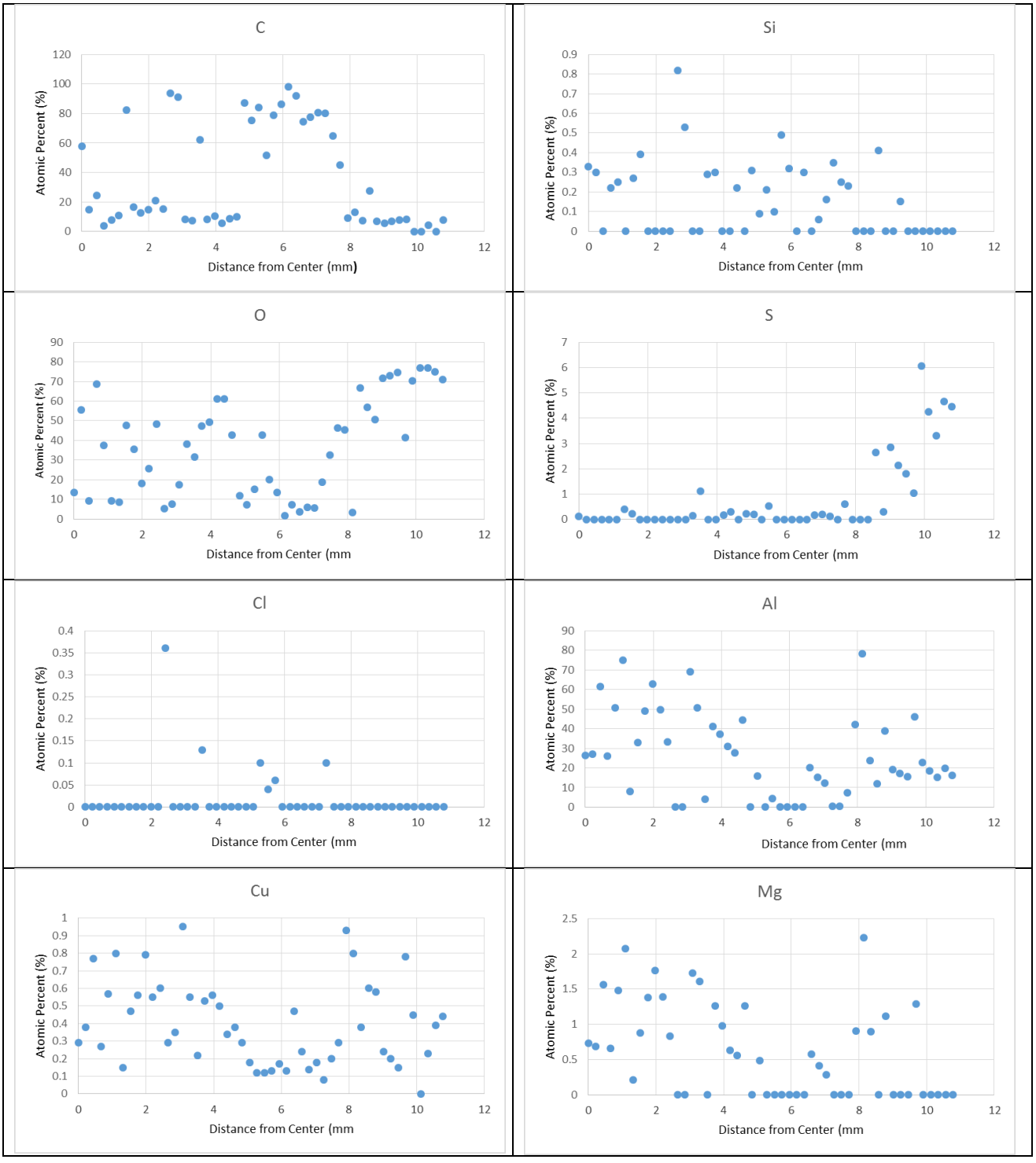

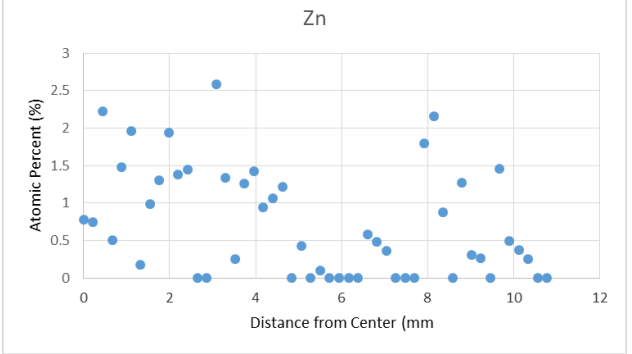

Table 29: Lyon Arboretum 1100-H14 CFRP 1 year

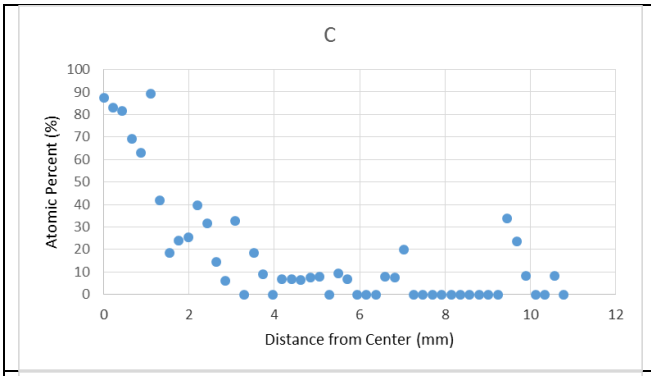

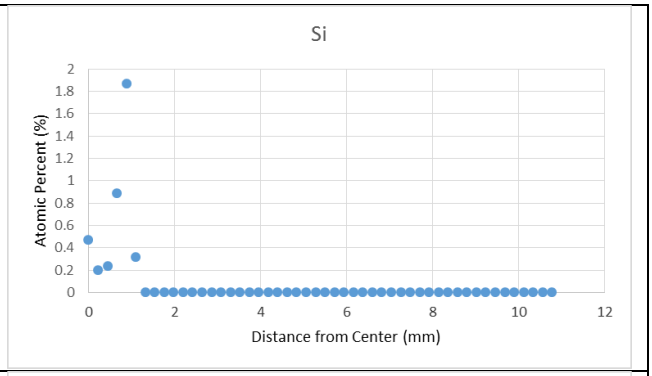

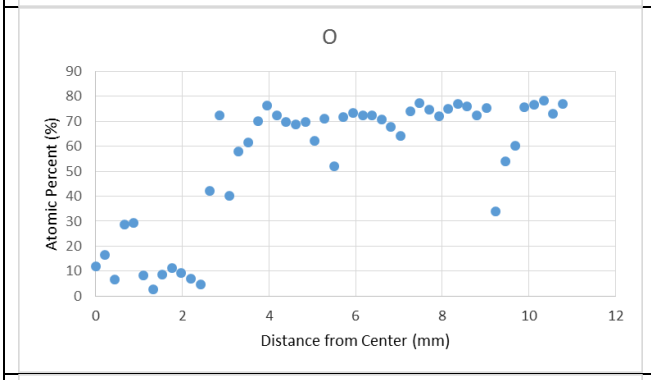

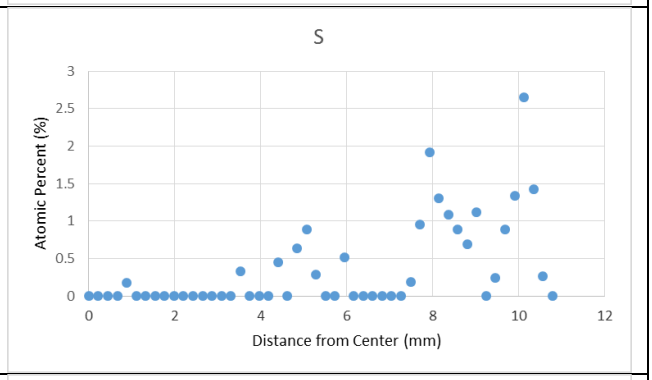

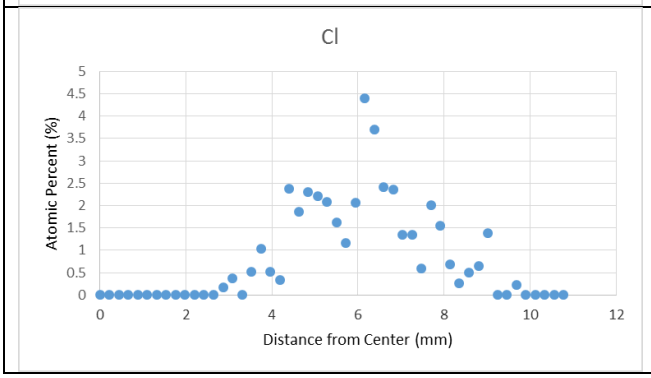

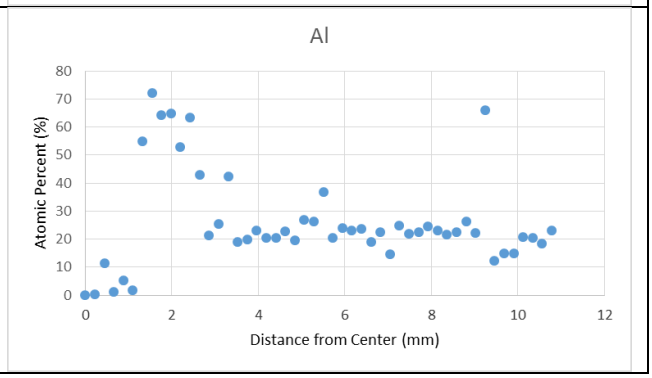

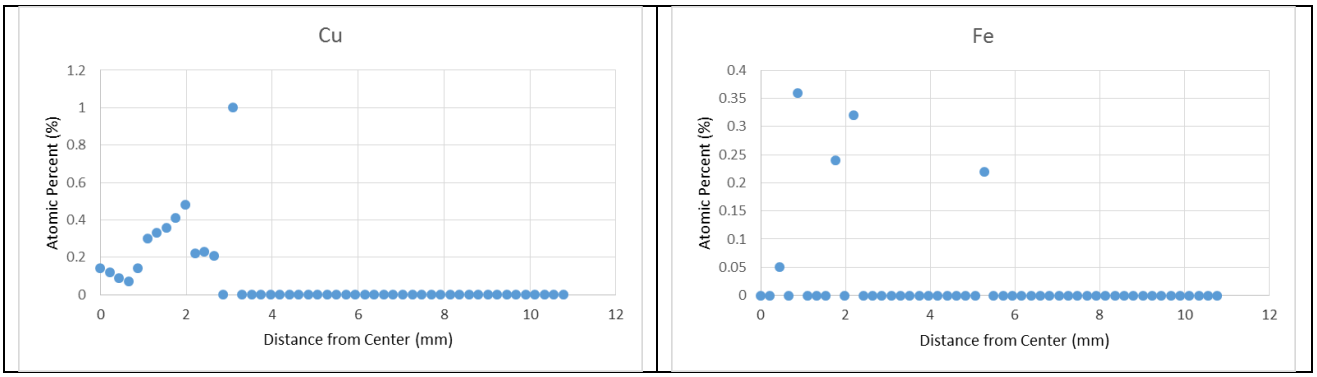

Table 30: Lyon Arboretum 5456-H116 Non-sensitized CFRP 1 year

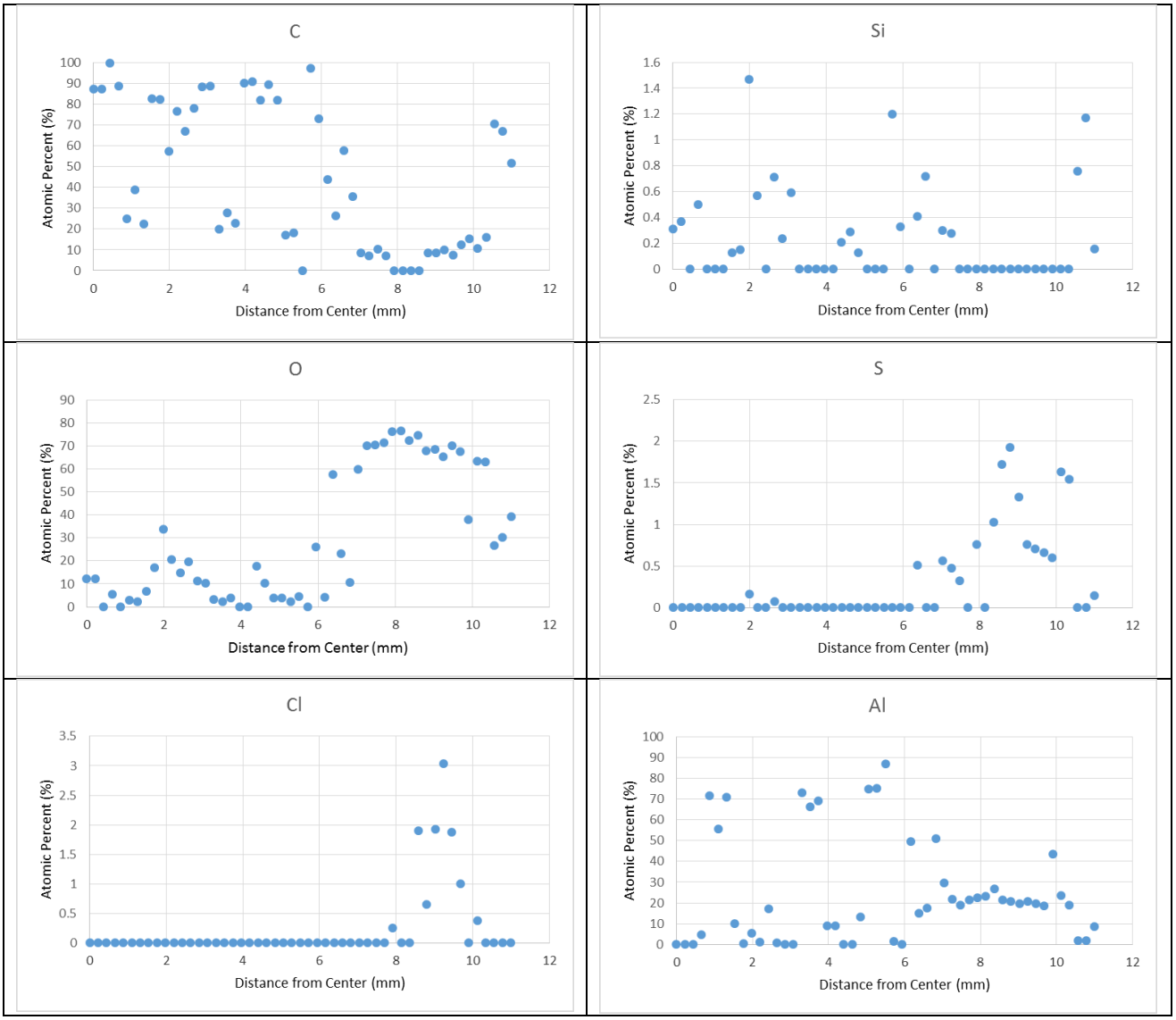

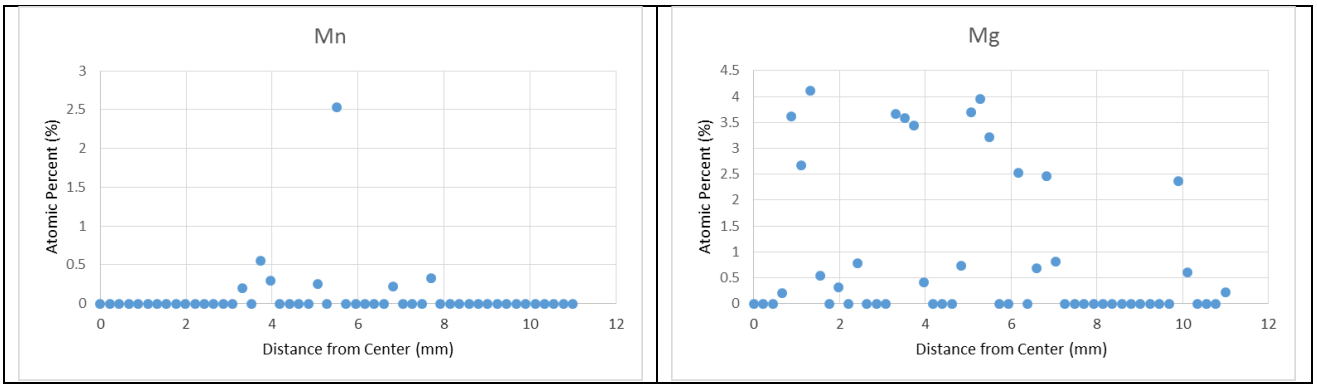

Table 31: Lyon Arboretum 5456-H116 Sensitized CFRP 1 year

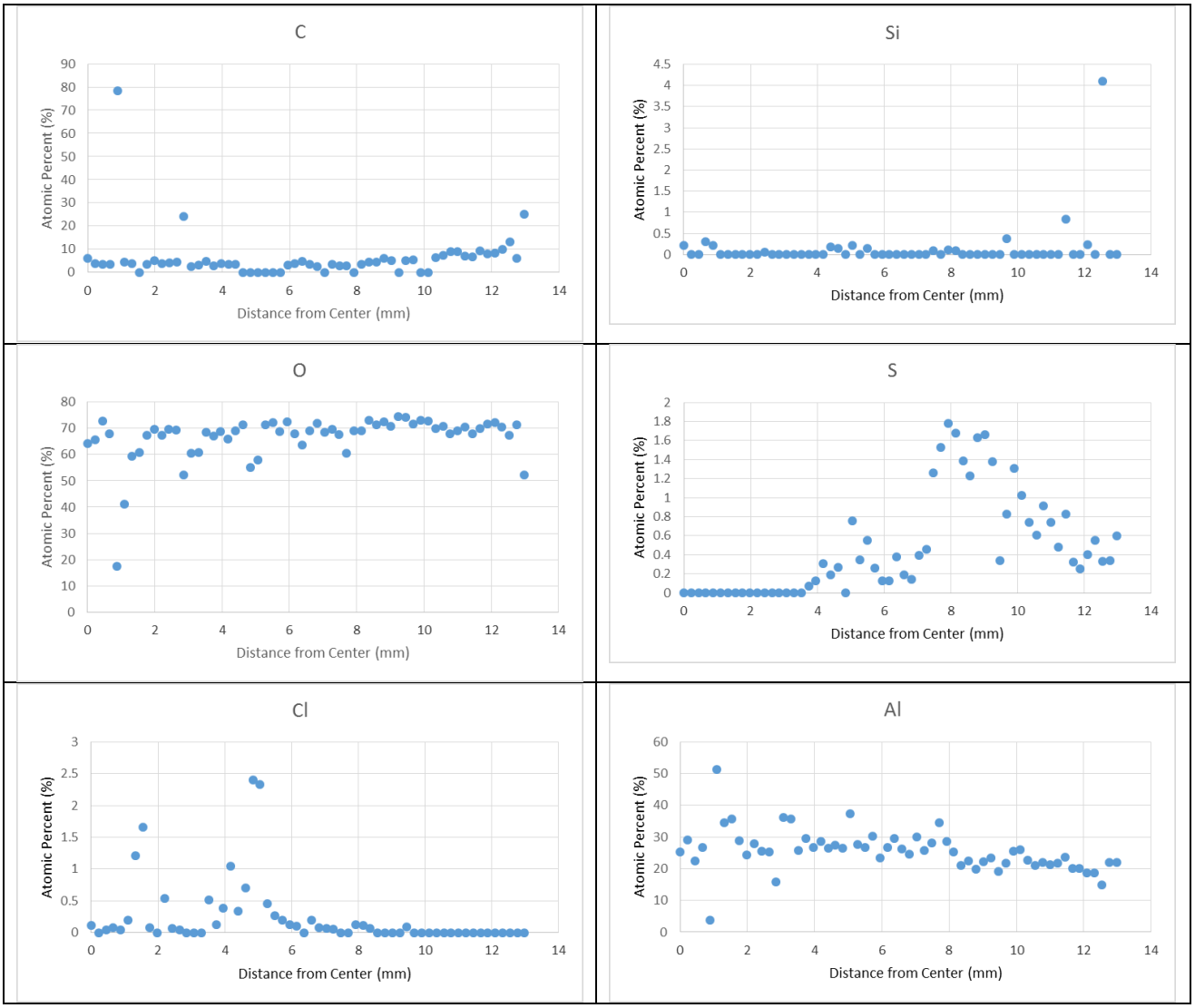

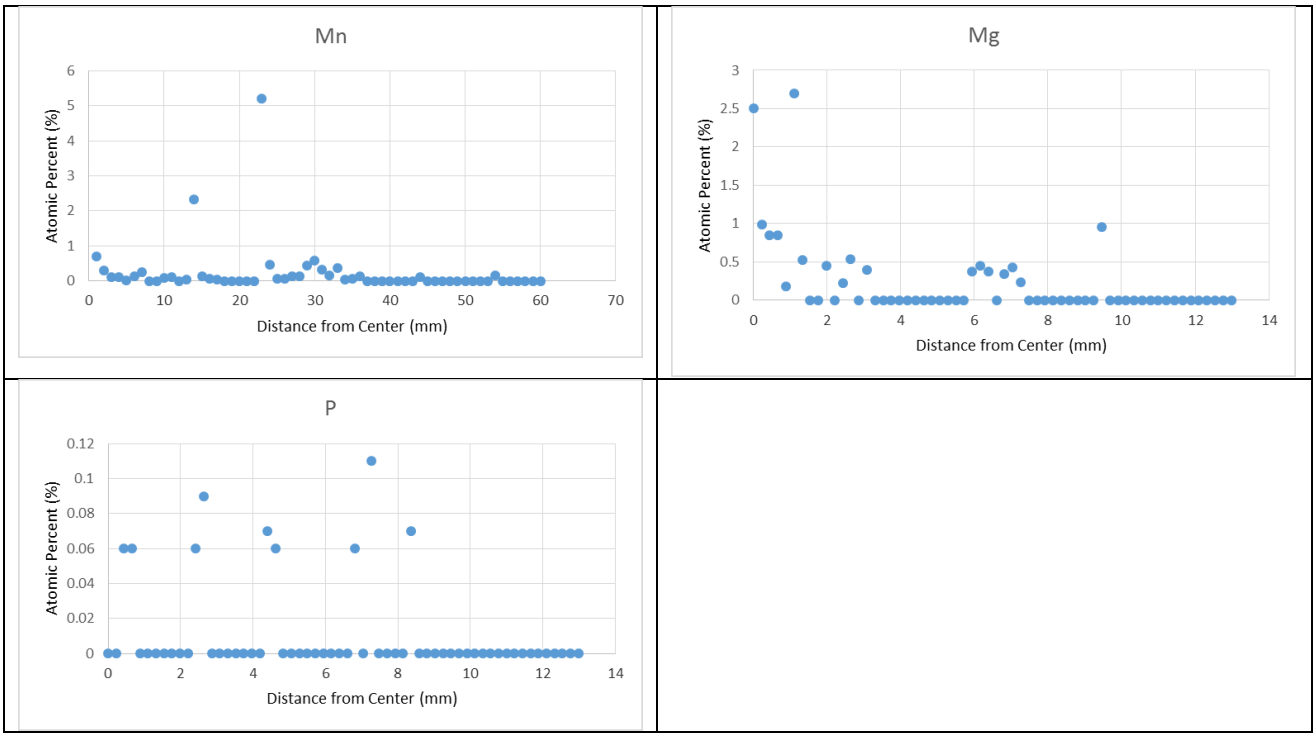

Table 32: Lyon Arboretum 7075-T6 CFRP 1 year

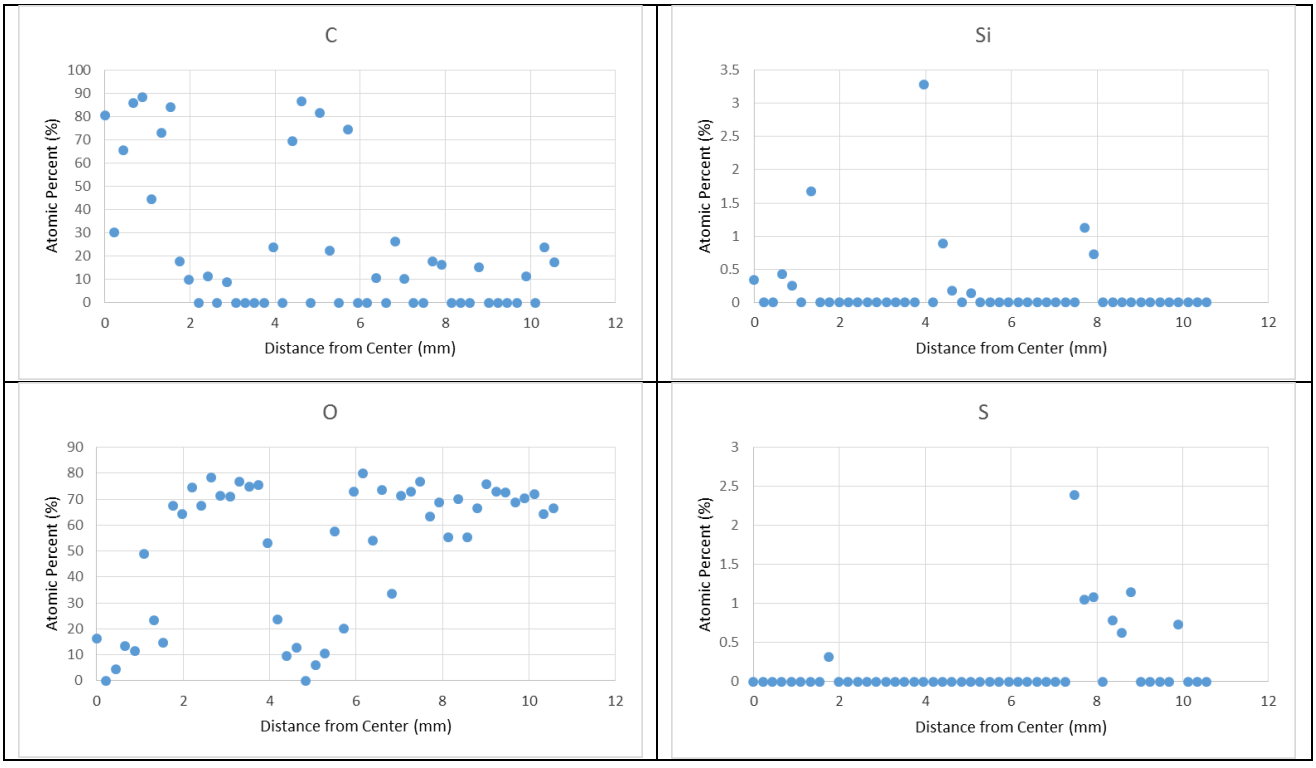

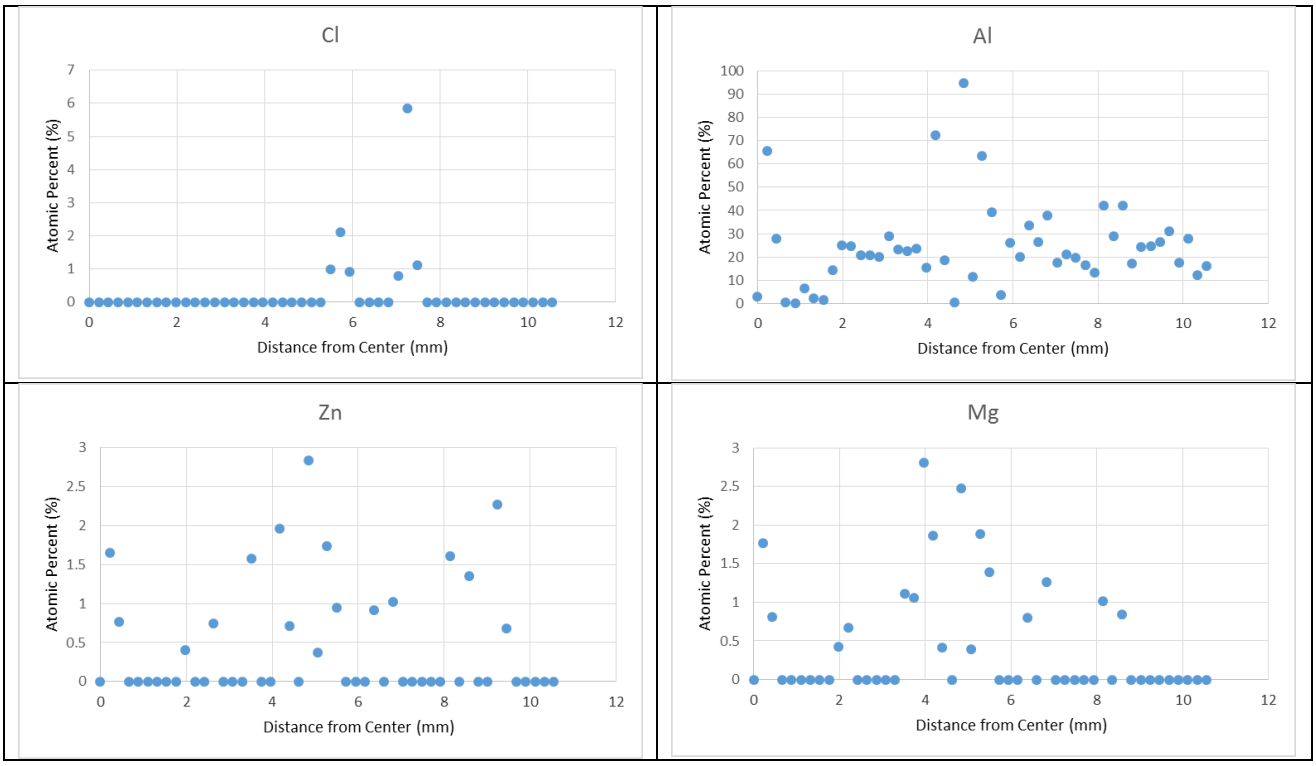

Table 33: Pyramid Rock 1100-H14 CFRP 2.67 months

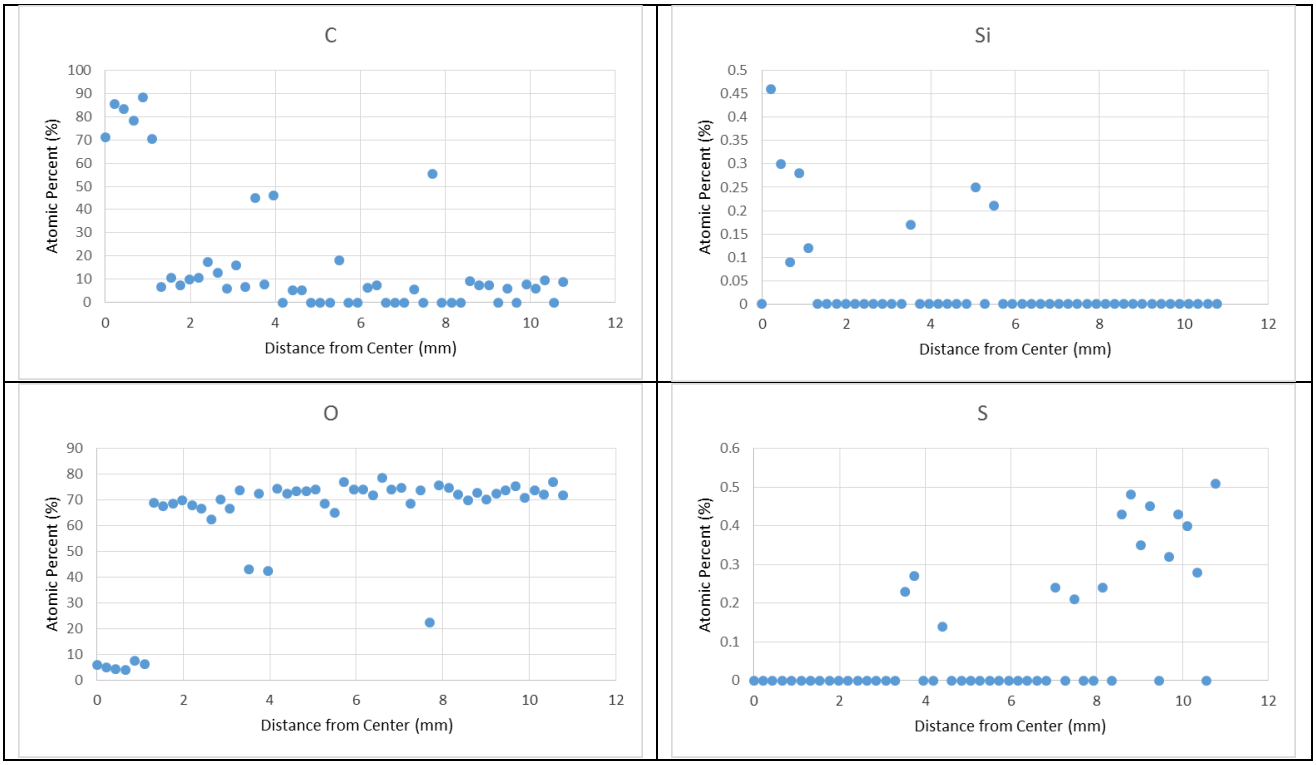

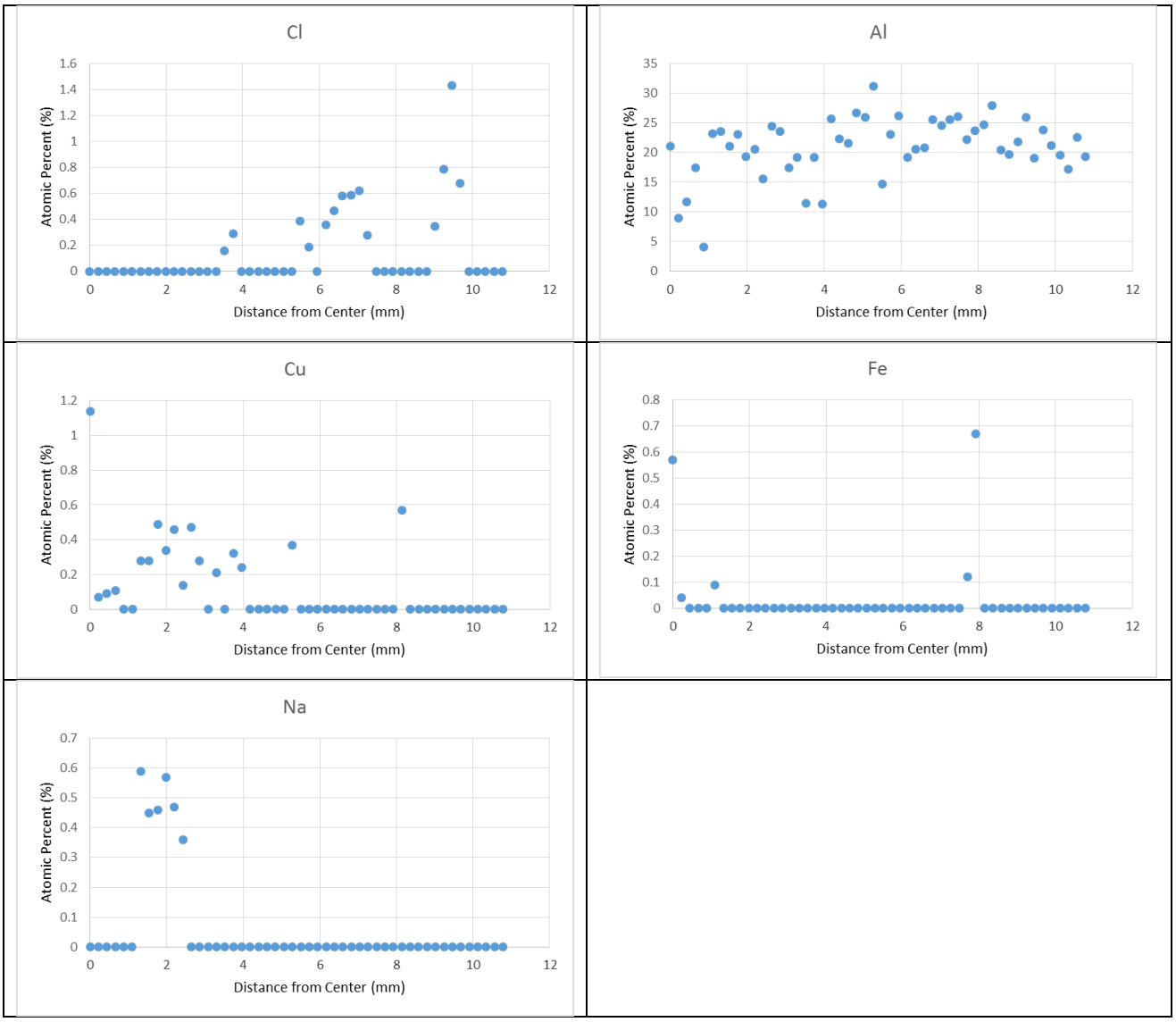

Table 34: Pyramid Rock 5456-H116 Non-sensitized CFRP 2.67 months

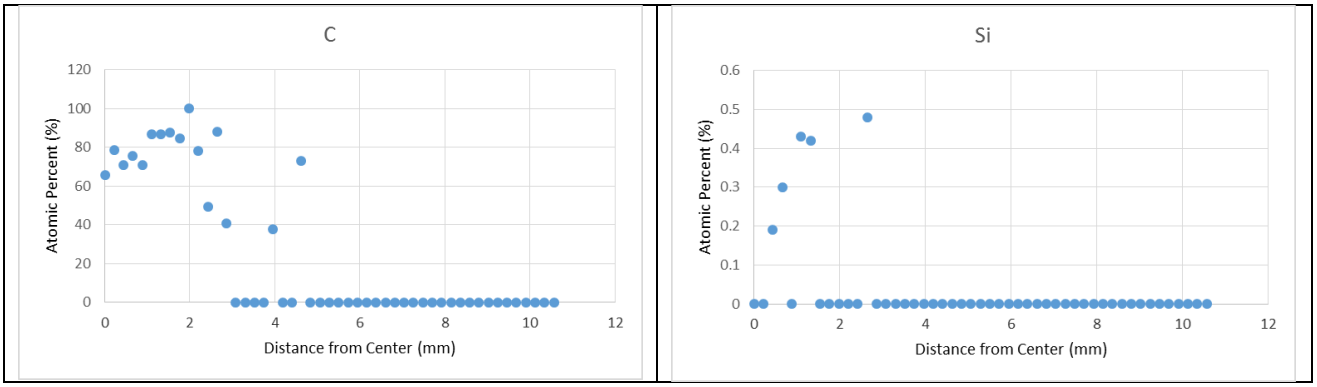

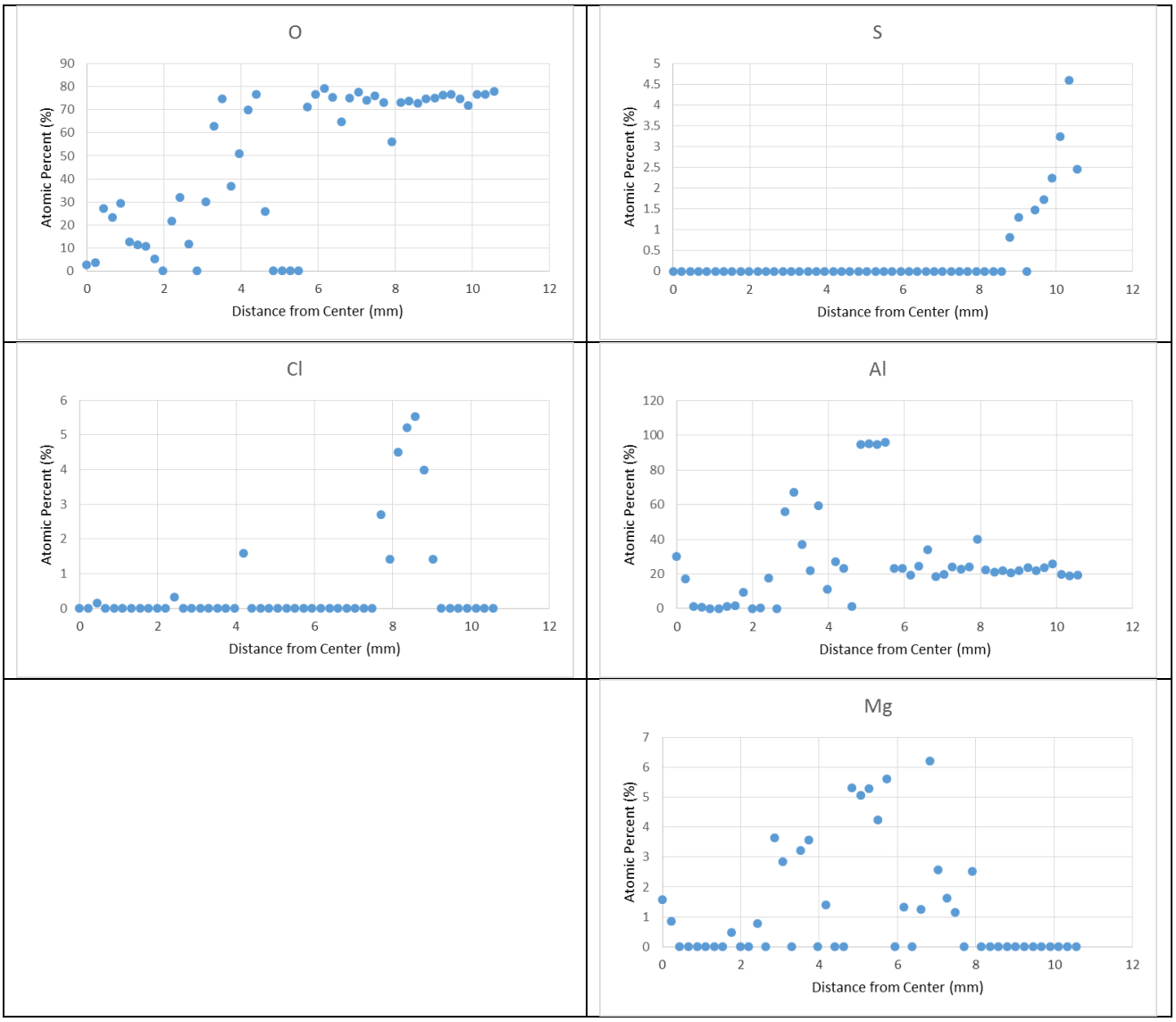

Table 35: Pyramid Rock 5456-H116 Sensitized CFRP 2.67 months

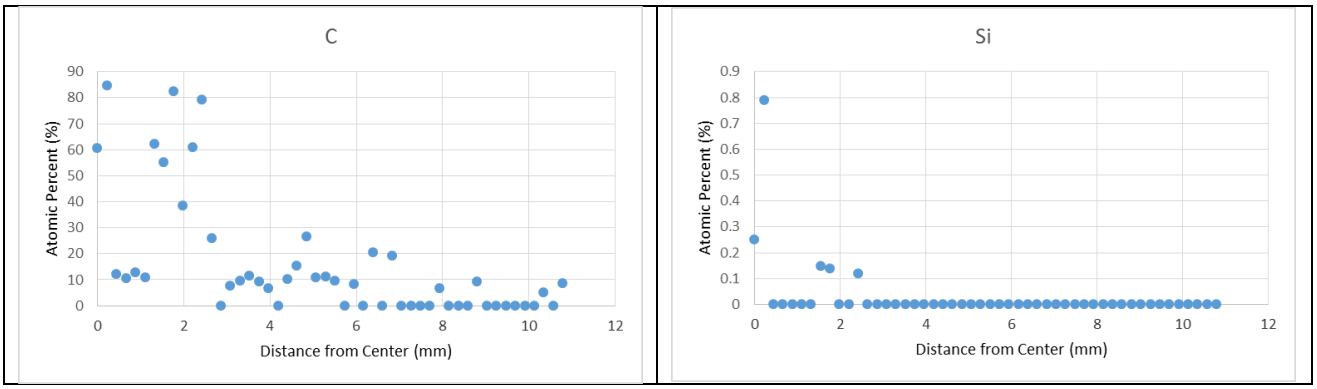


O
Atomic Percent (%)
Distance from Center (mm)
S
Atomic Percent (%)
Distance from Center (mm)
Cl
Atomic Percent (%)
Distance from Center (mm)
Al
Atomic Percent (%)
Distance from Center (mm)
Cu
Atomic Percent (%)
Distance from Center (mm)
Mg
Atomic Percent (%)
Distance from Center (mm)
Mn
Atomic Percent (%)
Distance from Center (mm)

Table 36: Pyramid Rock 70075-T6 CFRP 2.67 months

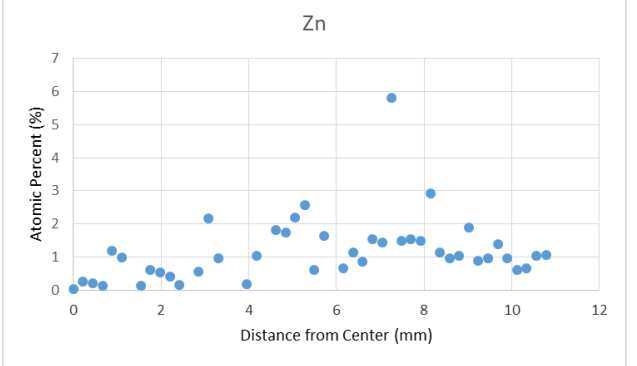

Table 37: Pyramid Rock 7075-T6 GFRP 1 year

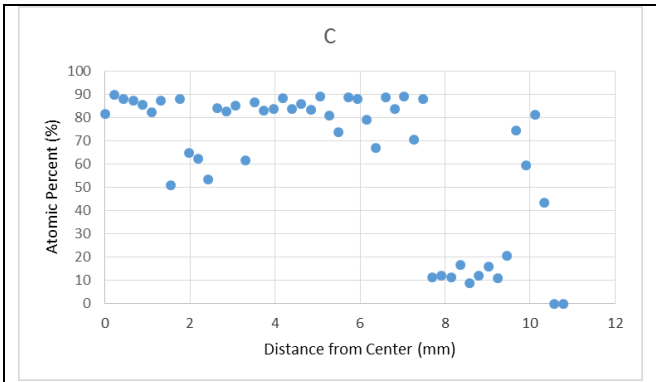

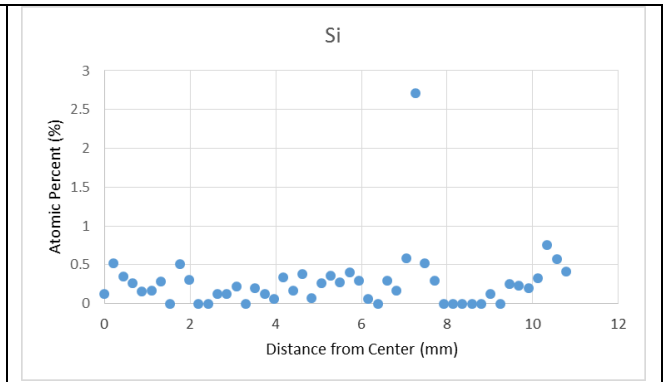

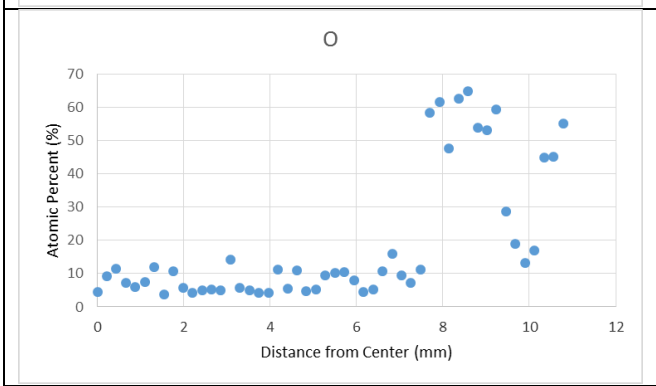

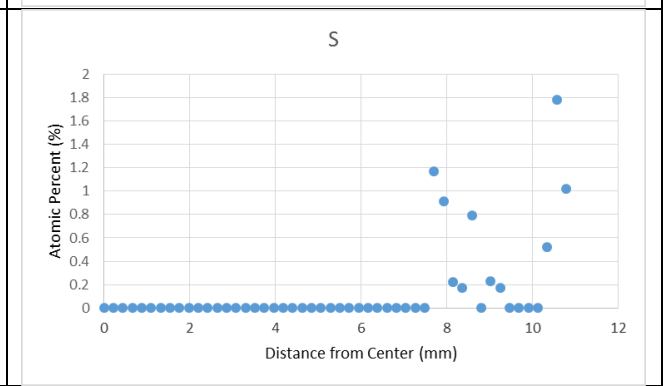

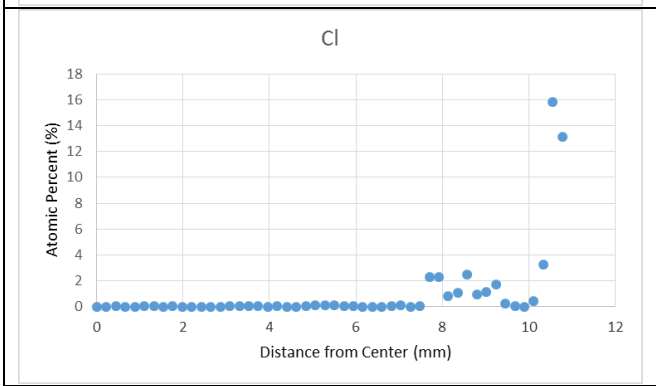

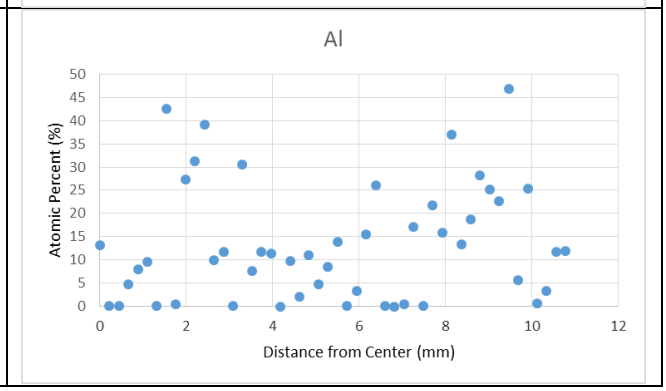

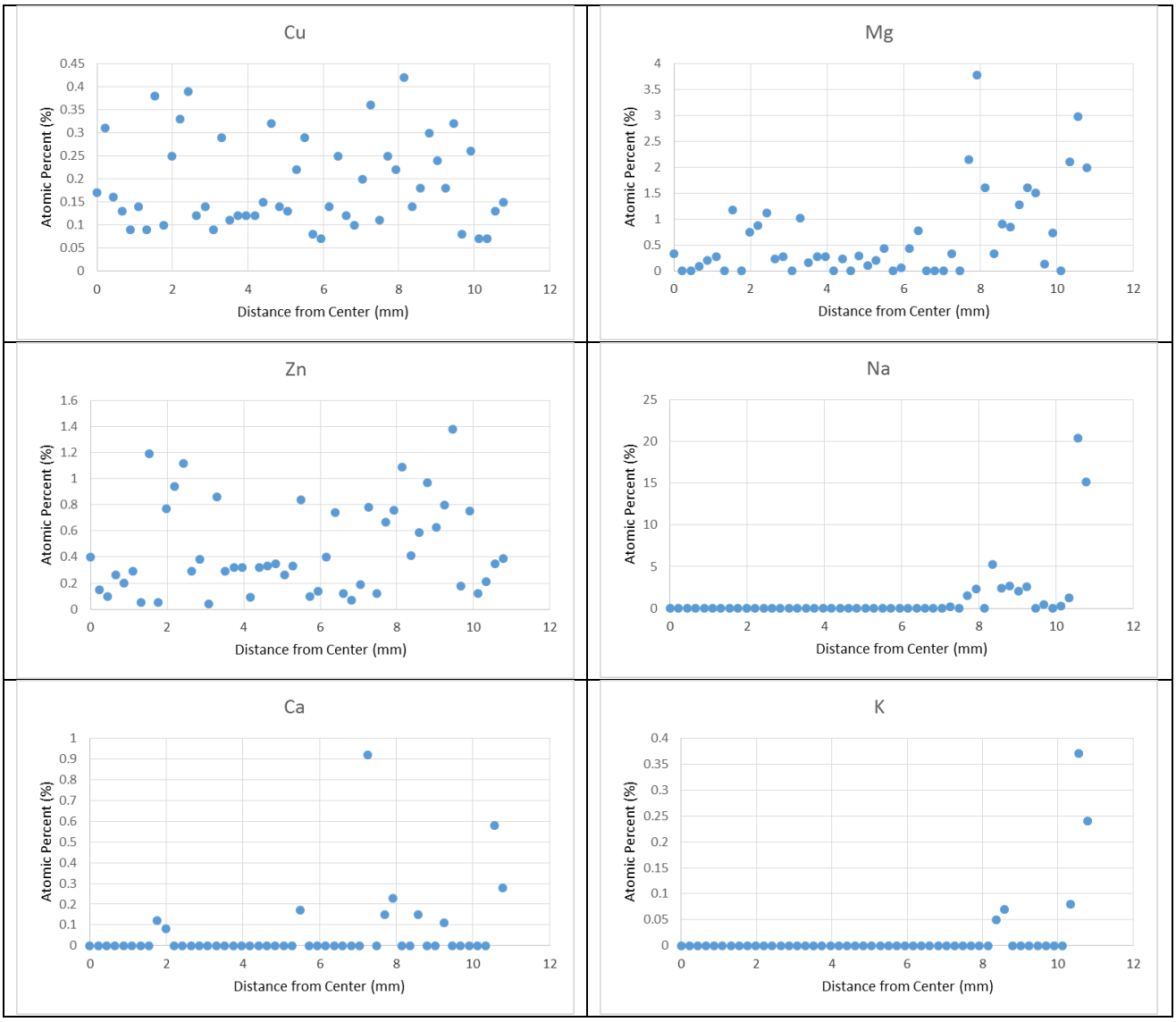
Cu
Atomic Percent (%)
Distance from Center (mm)
Mg
Atomic Percent (%)
Distance from Center (mm)
Zn
Atomic Percent (%)
Distance from Center (mm)
Na
Atomic Percent (%)
Distance from Center (mm)
Ca
Atomic Percent (%)
Distance from Center (mm)
K
Atomic Percent (%)
Distance from Center (mm)

Appendix D
Sample Pictures After Adhesion Testing

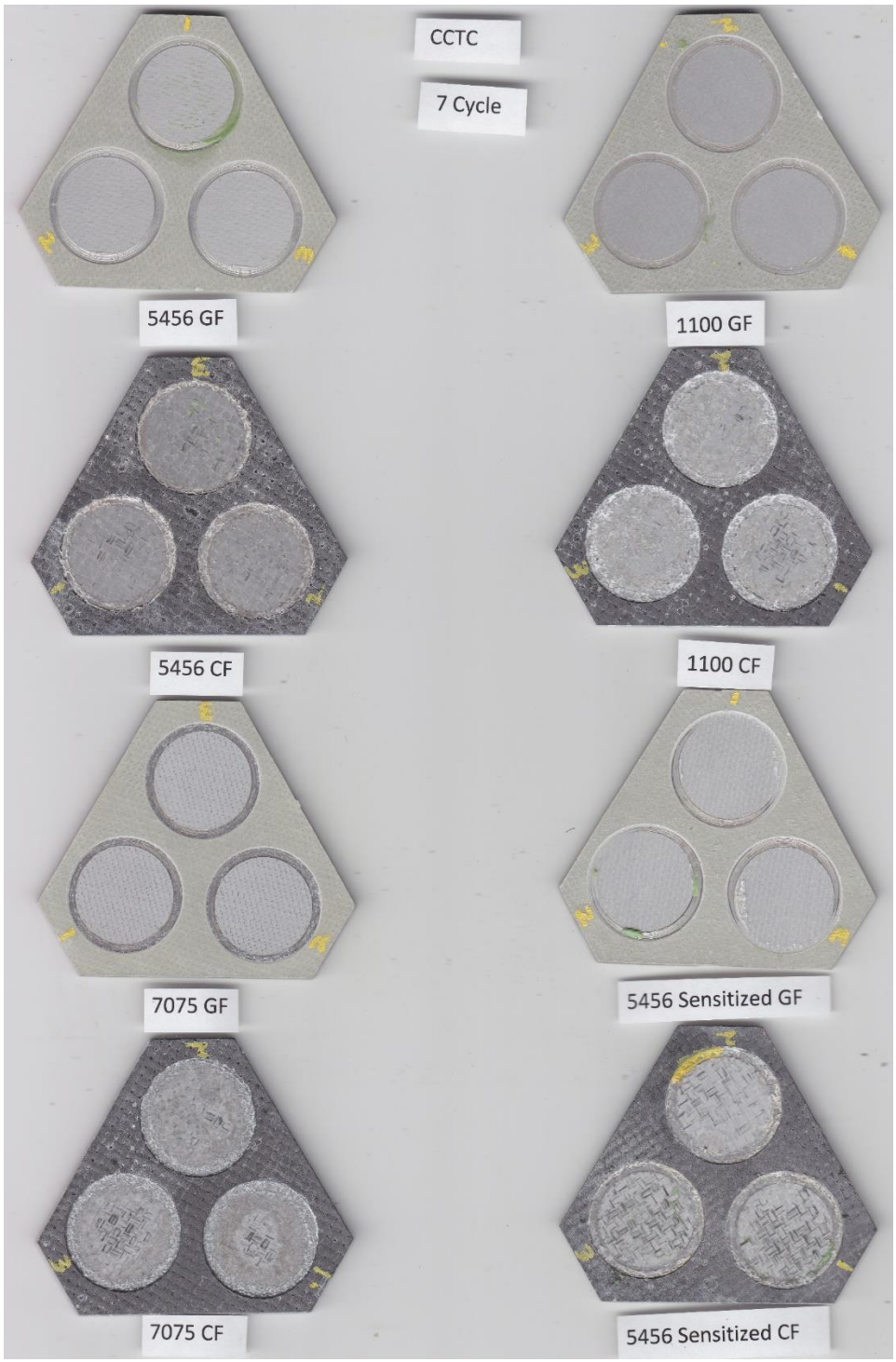

Figure 91: CCTC 7 Cycle Samples After Adhesion Testing

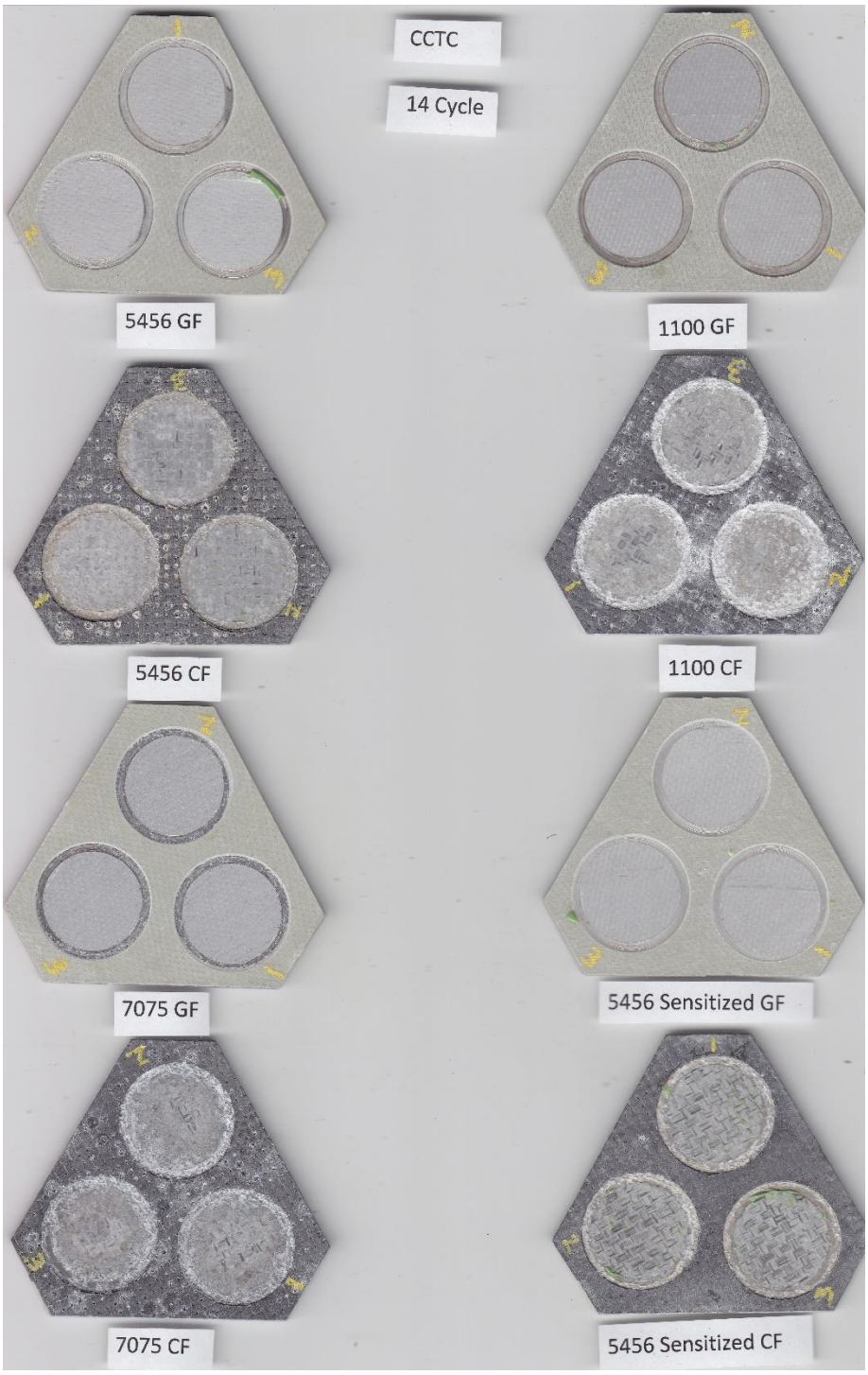

Figure 92: CCTC 14 Cycle Samples After Adhesion Testing

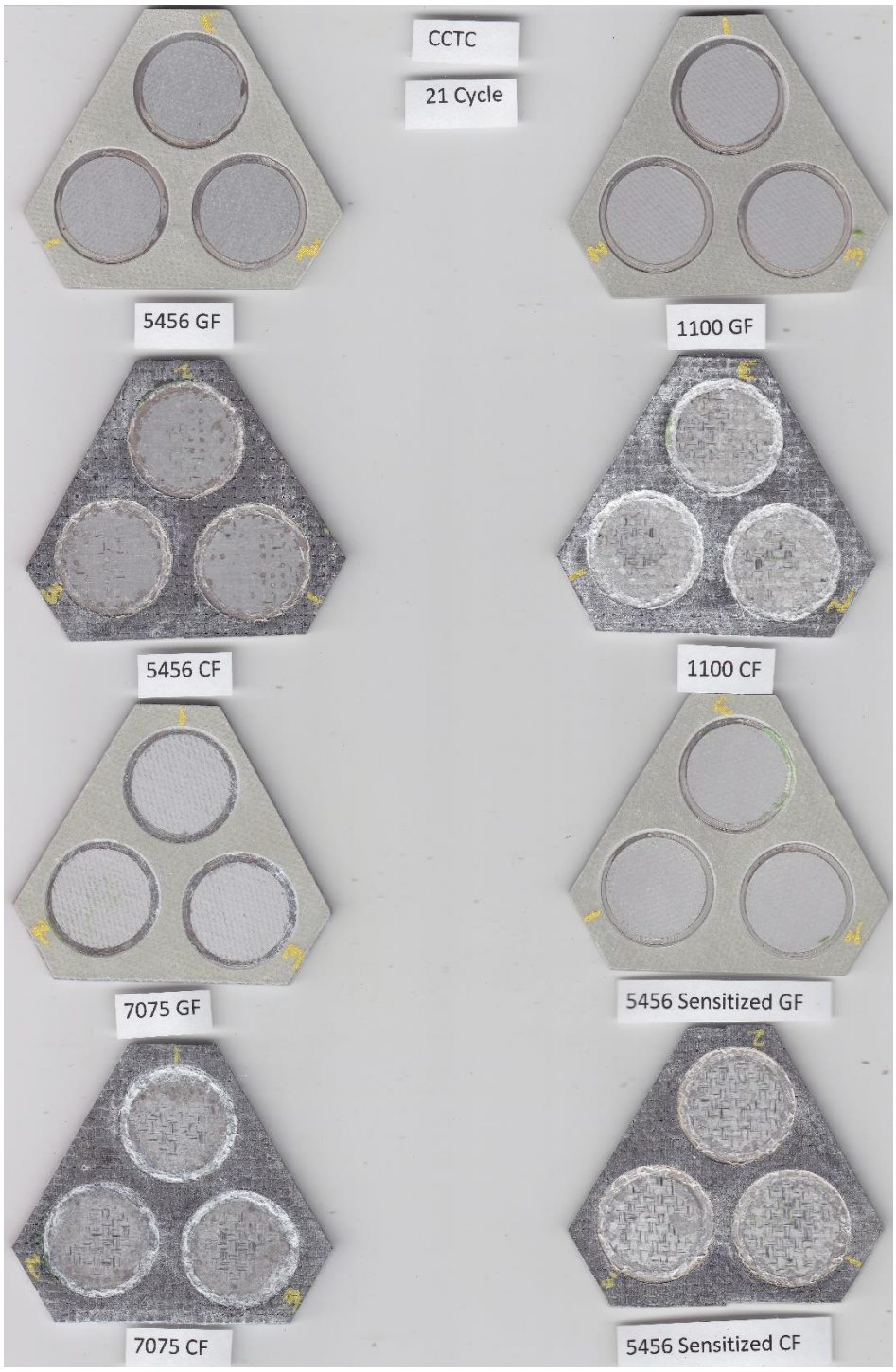

Figure 93: CCTC 14 Cycle Samples After Adhesion Testing

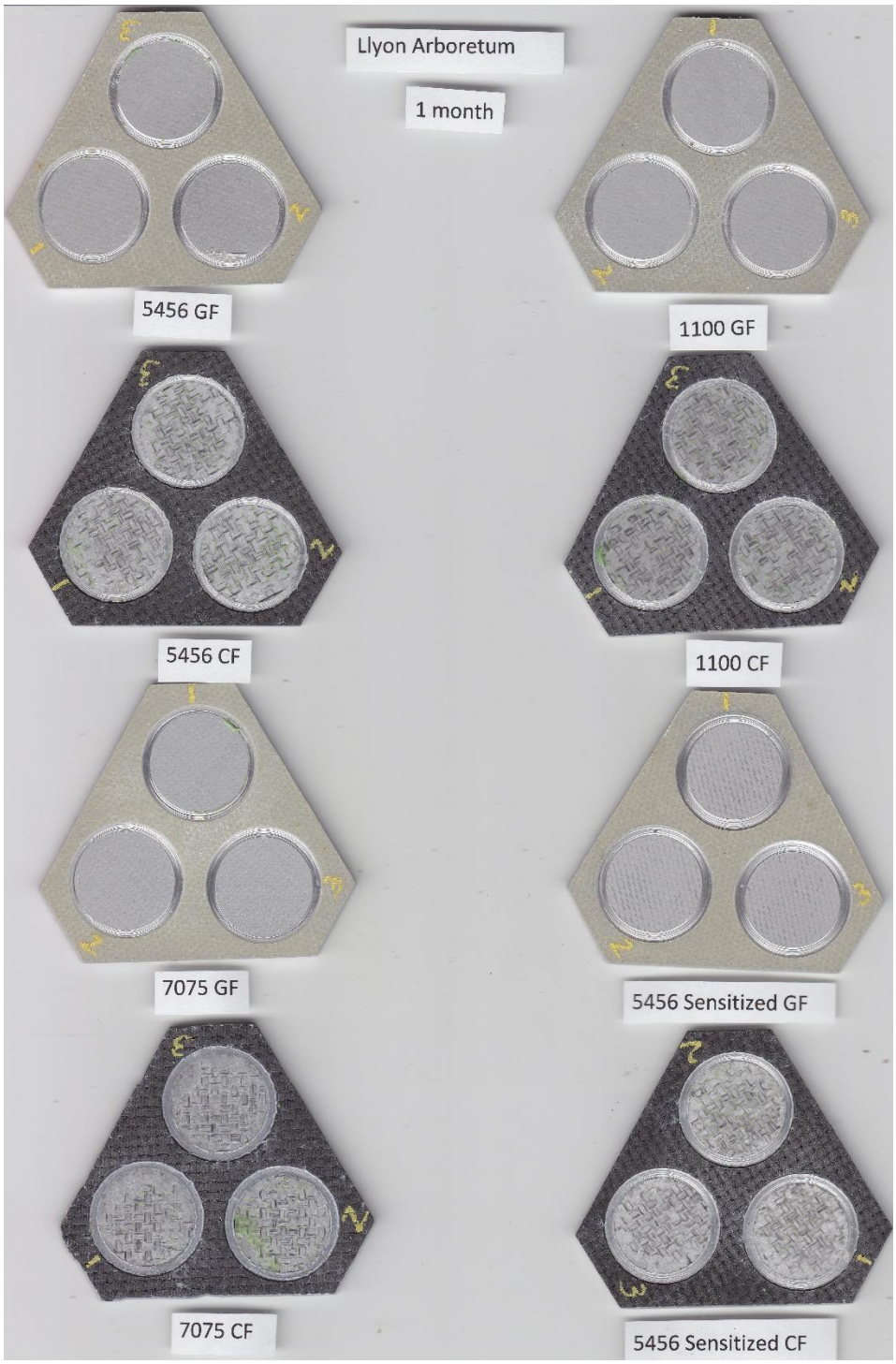

Figure 94: Lyon Arboretum 1 Month Samples After Adhesion Testing

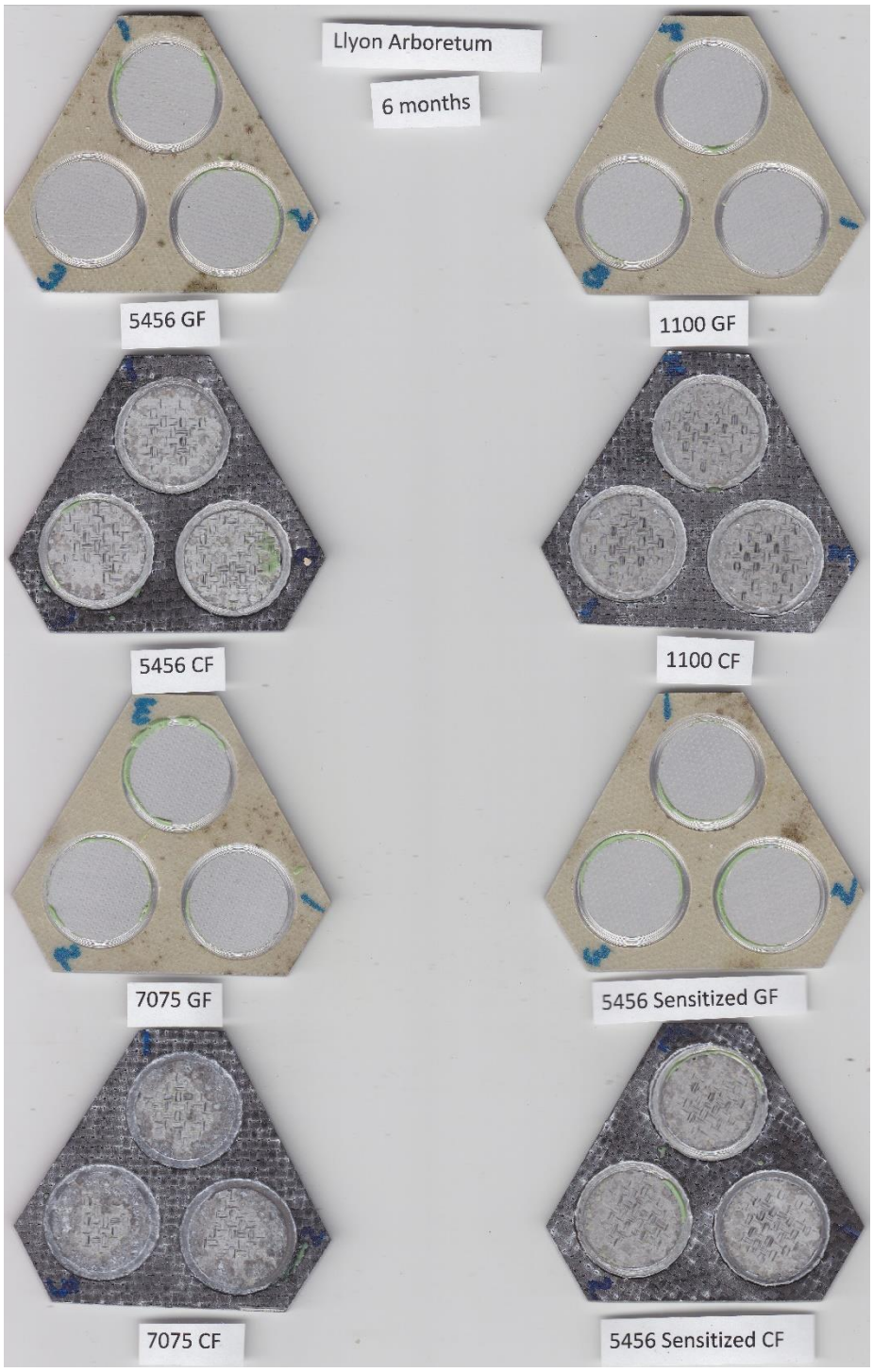

Figure 95: Lyon Arboretum 6 Month Samples After Adhesion Testing

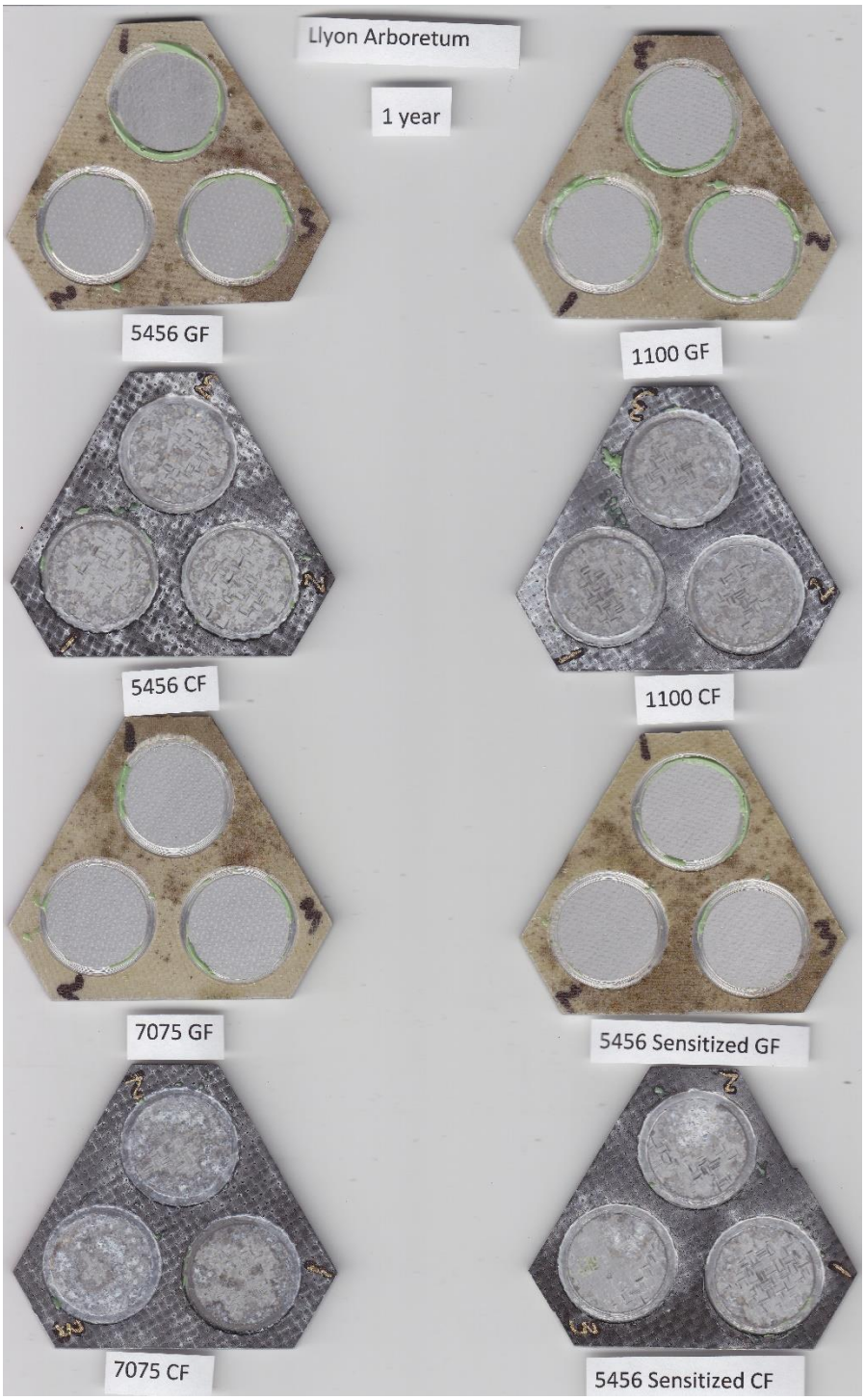

Figure 96: Lyon Arboretum 12 Month Samples After Adhesion Testing

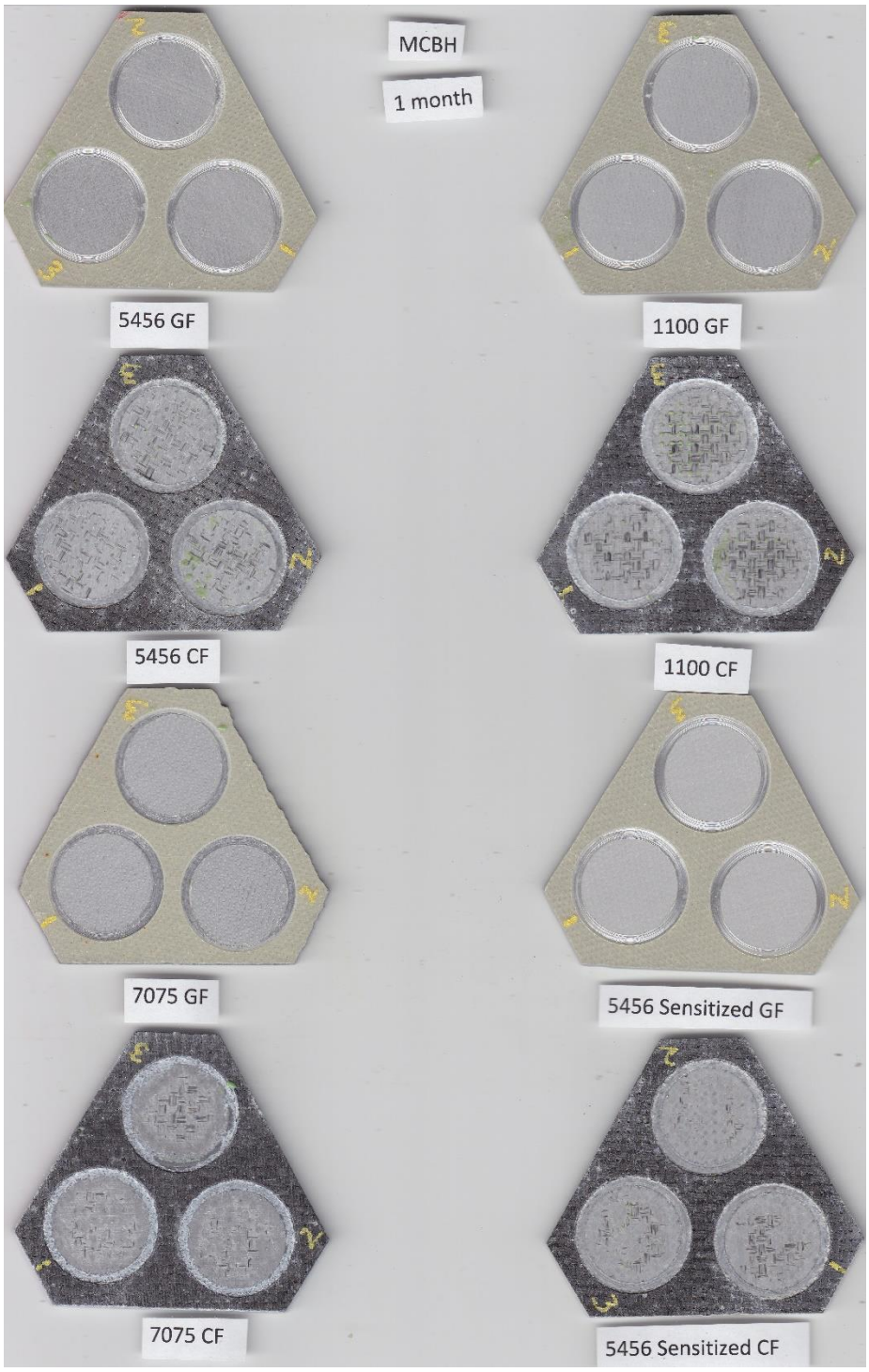

Figure 97: Pyramid Rock 0.63 Month (CFRP) and 1 Month (GFRP)Samples After Adhesion Testing

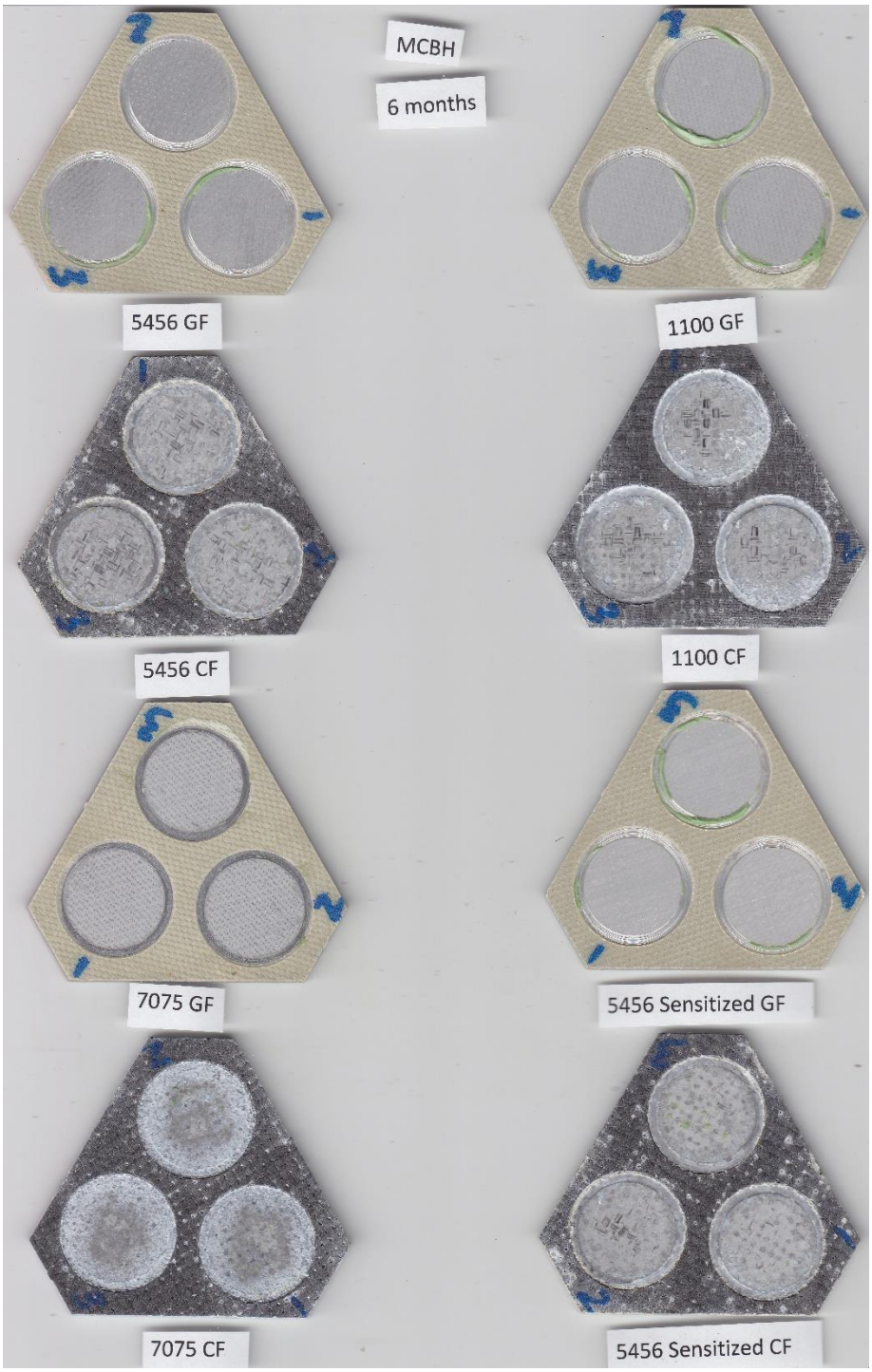

Figure 98: Pyramid Rock 2.67 Month (CFRP) and 6 Month (GFRP) Samples After Adhesion Testing

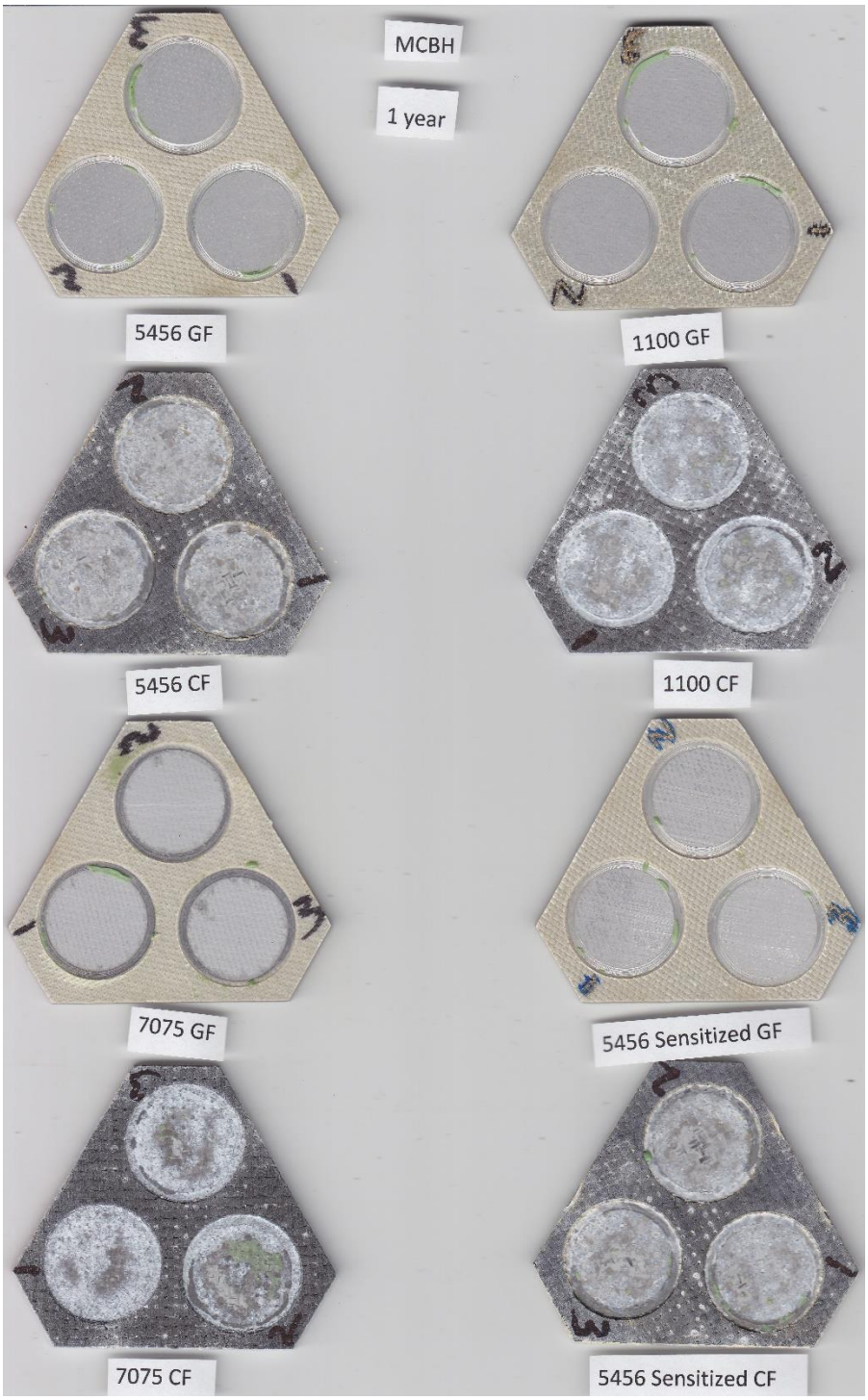

Figure 99: Pyramid Rock 3.63 Month (CFRP) and 12 Month (GFRP) Samples After Adhesion Testing

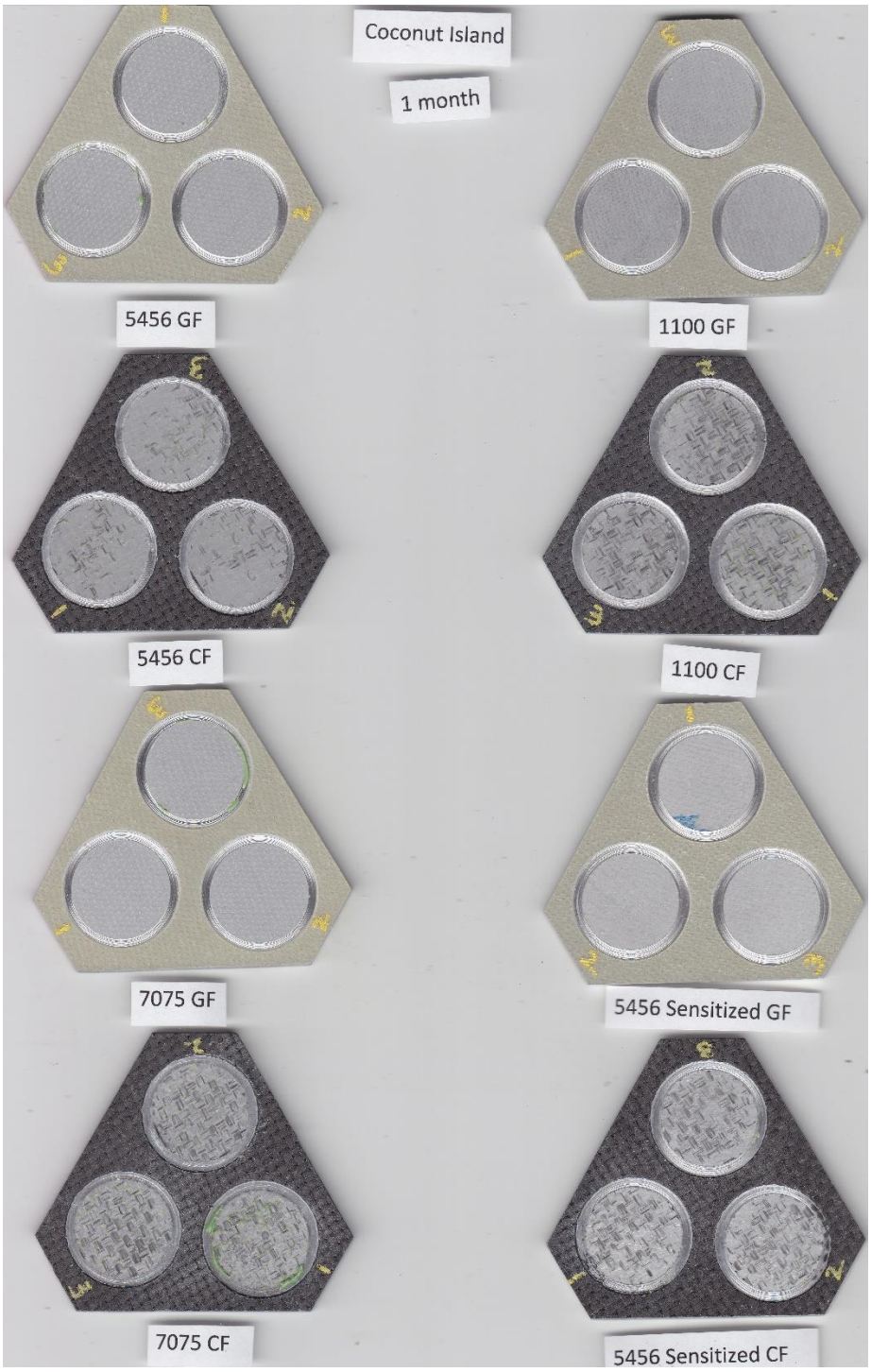

Figure 100: Coconut Island 12 Month Samples After Adhesion Testing

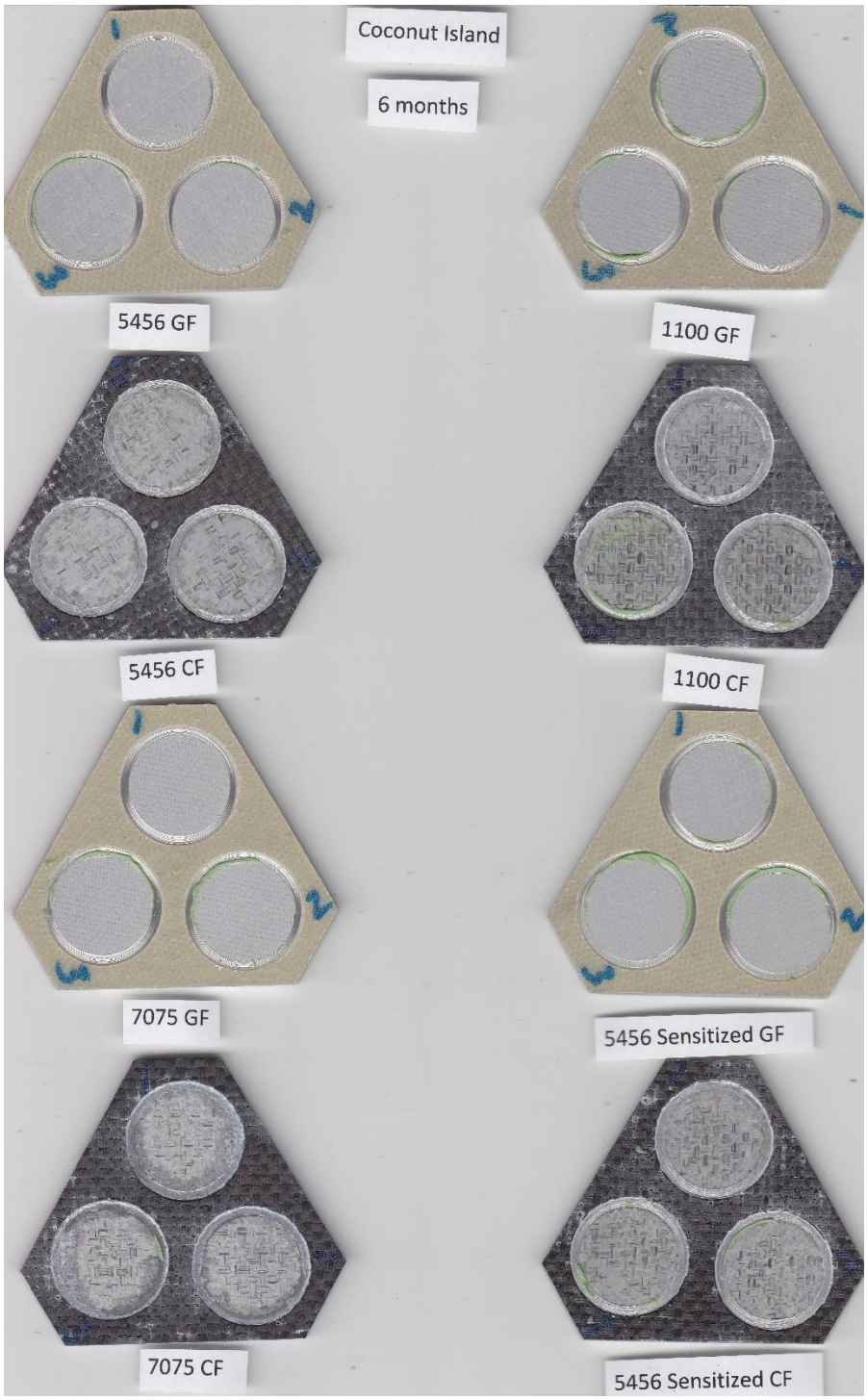

Figure 101: Coconut Island 12 Month Samples After Adhesion Testing

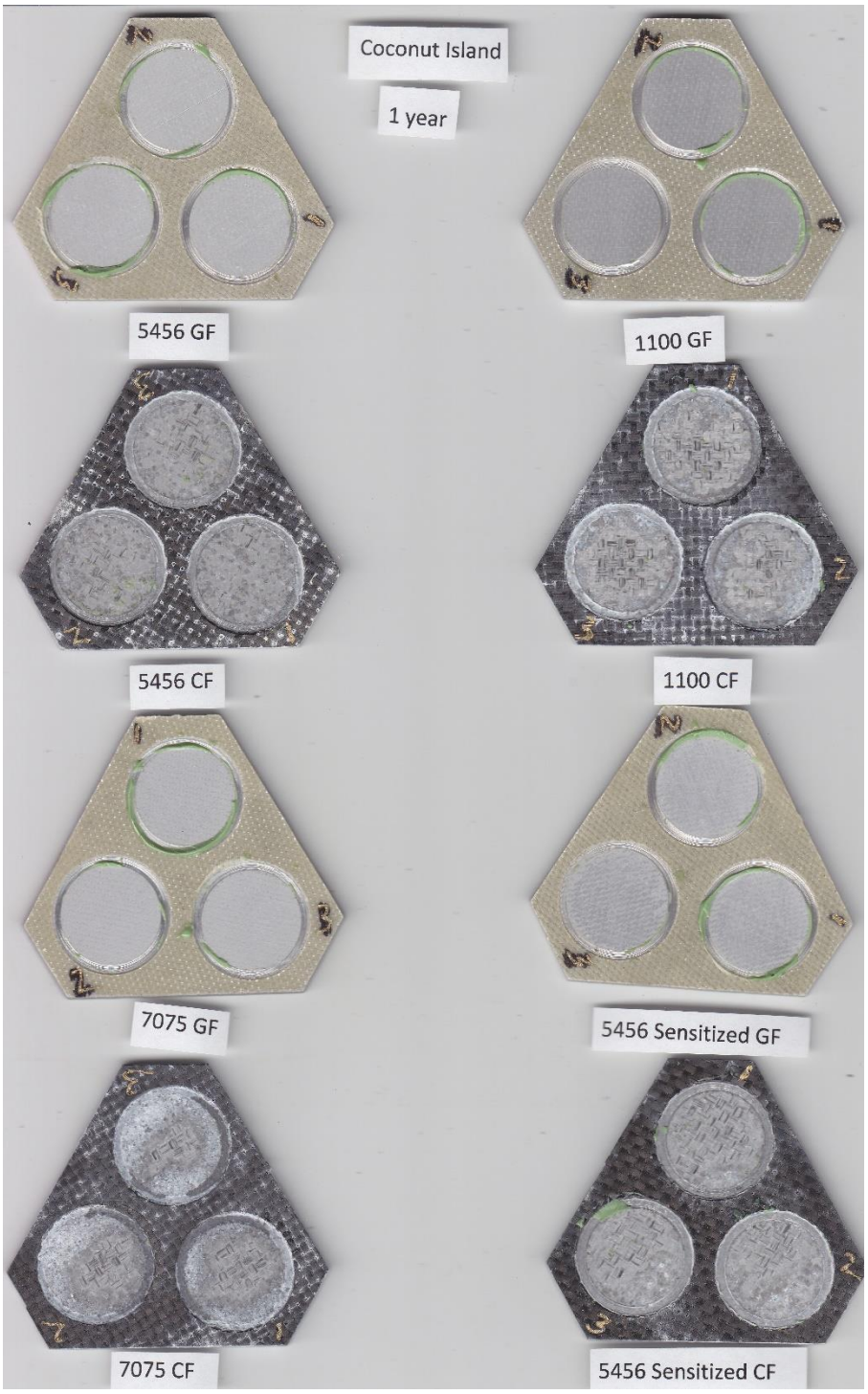

Figure 102: Coconut Island 12 Month Samples After Adhesion Testing

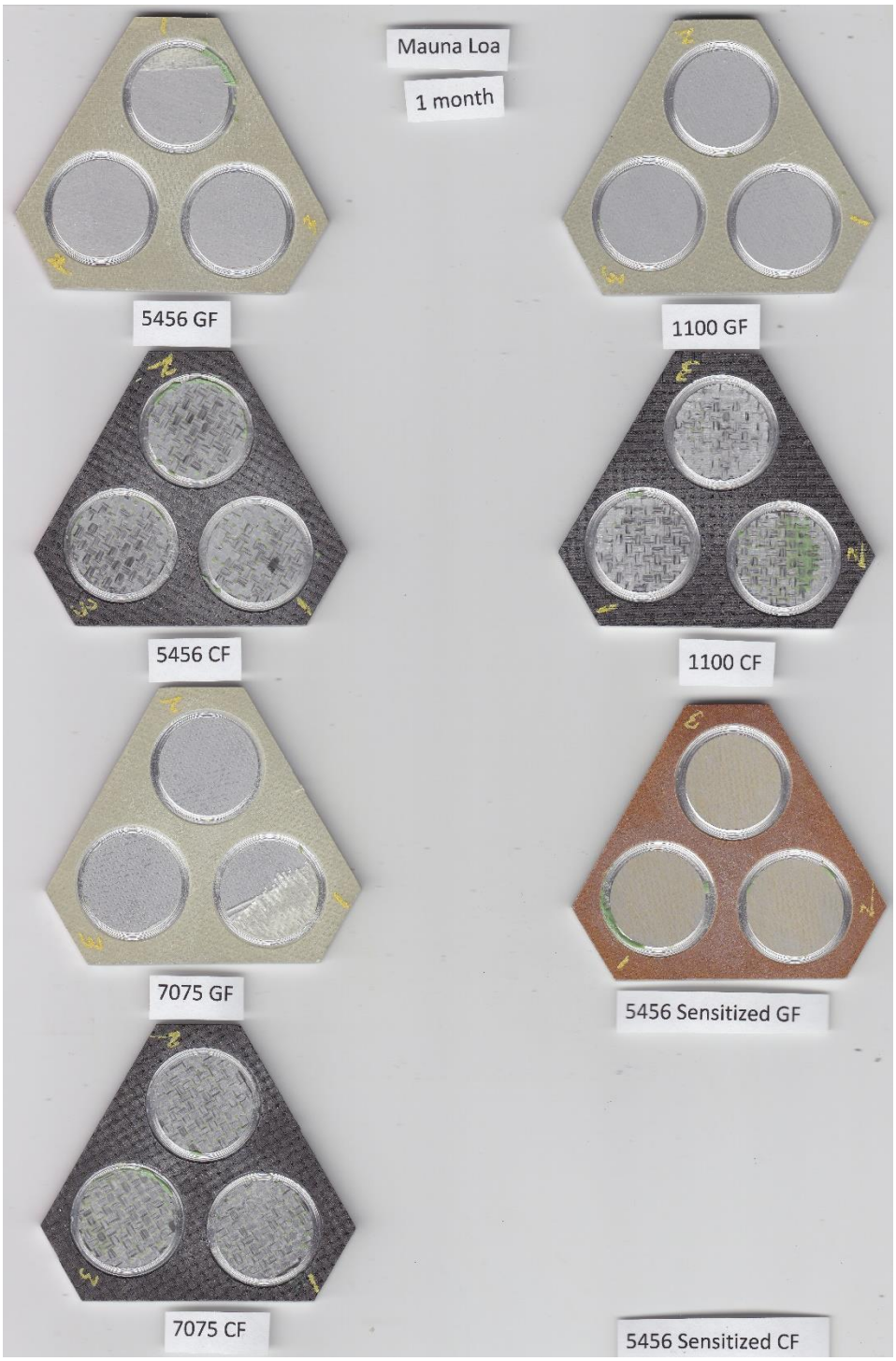

Figure 103: Mauna Loa 1 Month Samples After Adhesion Testing

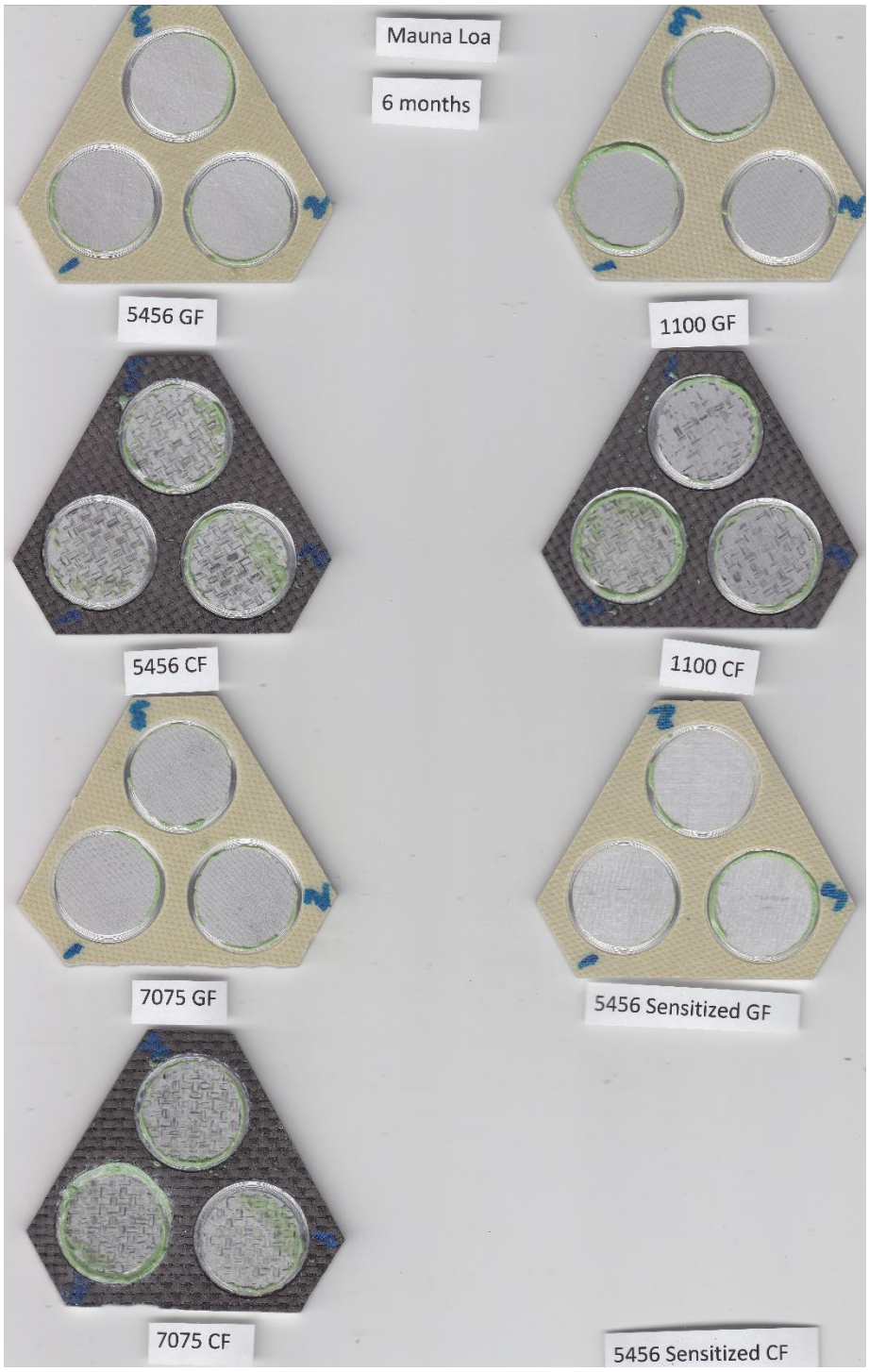

Figure 104: Mauna Loa 6 Month Samples After Adhesion Testing

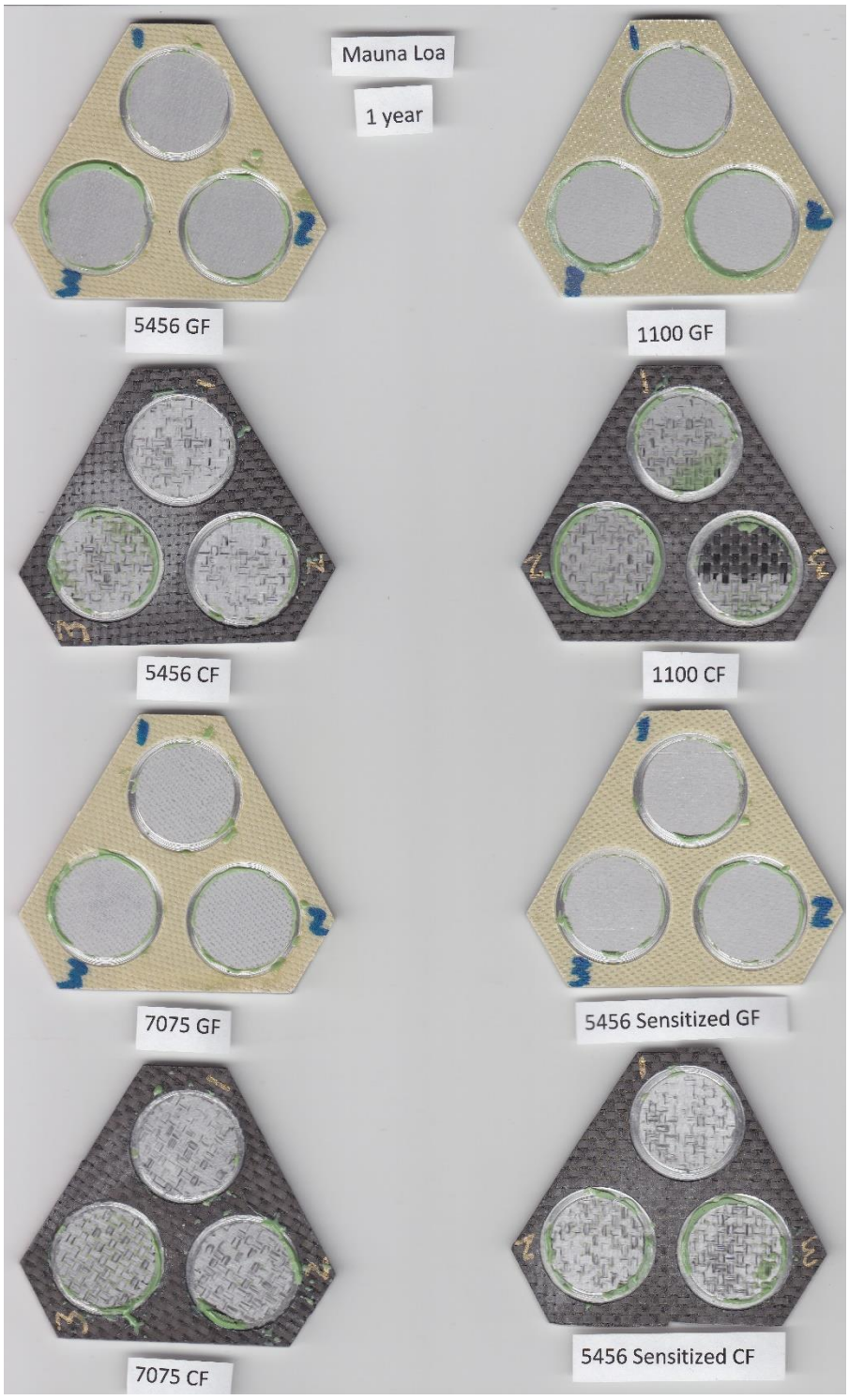

Figure 105: Mauna Loa 12 Month Samples After Adhesion Testing

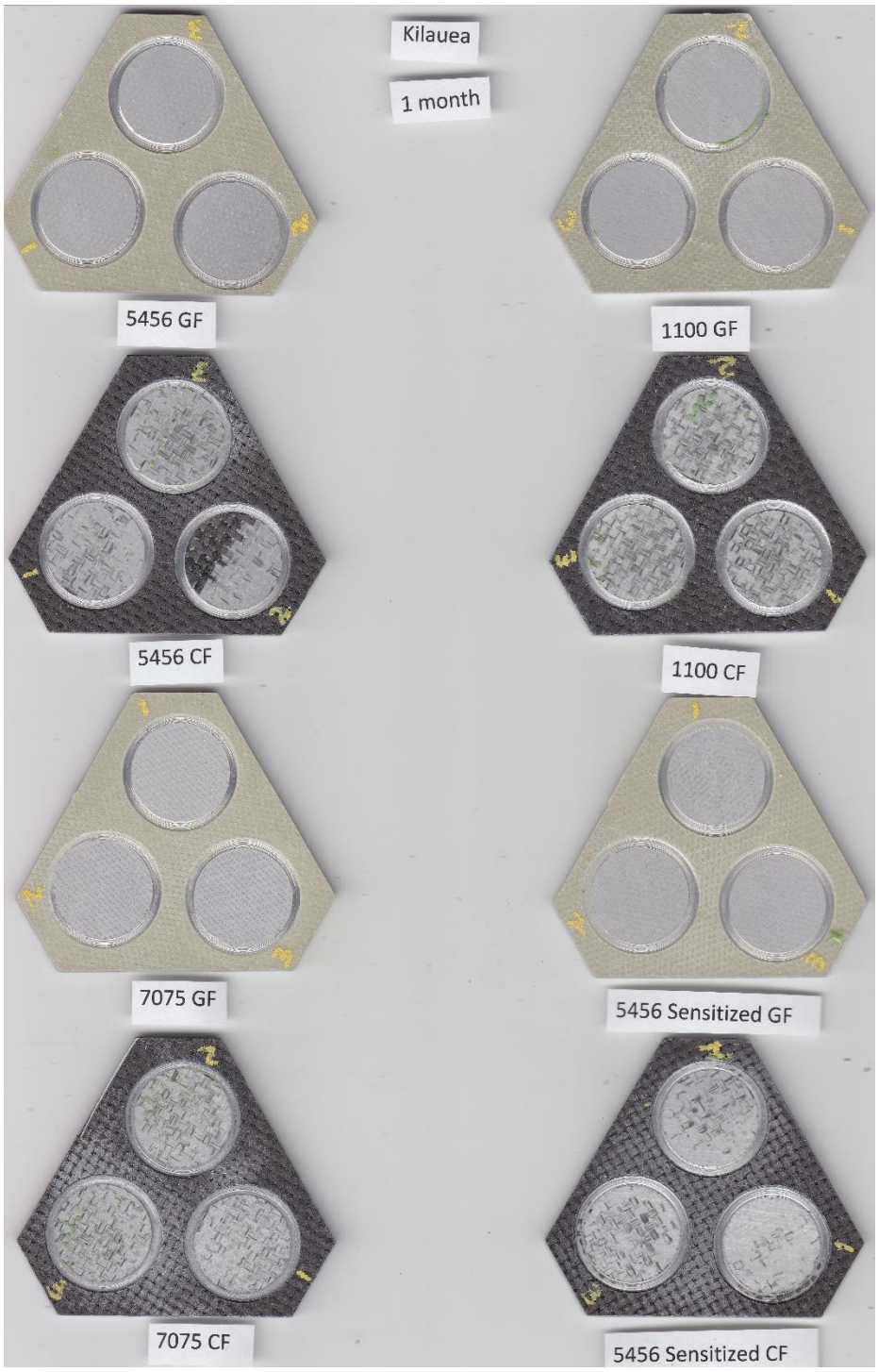

Figure 106: Kilauea Volcano 1 Month Samples After Adhesion Testing

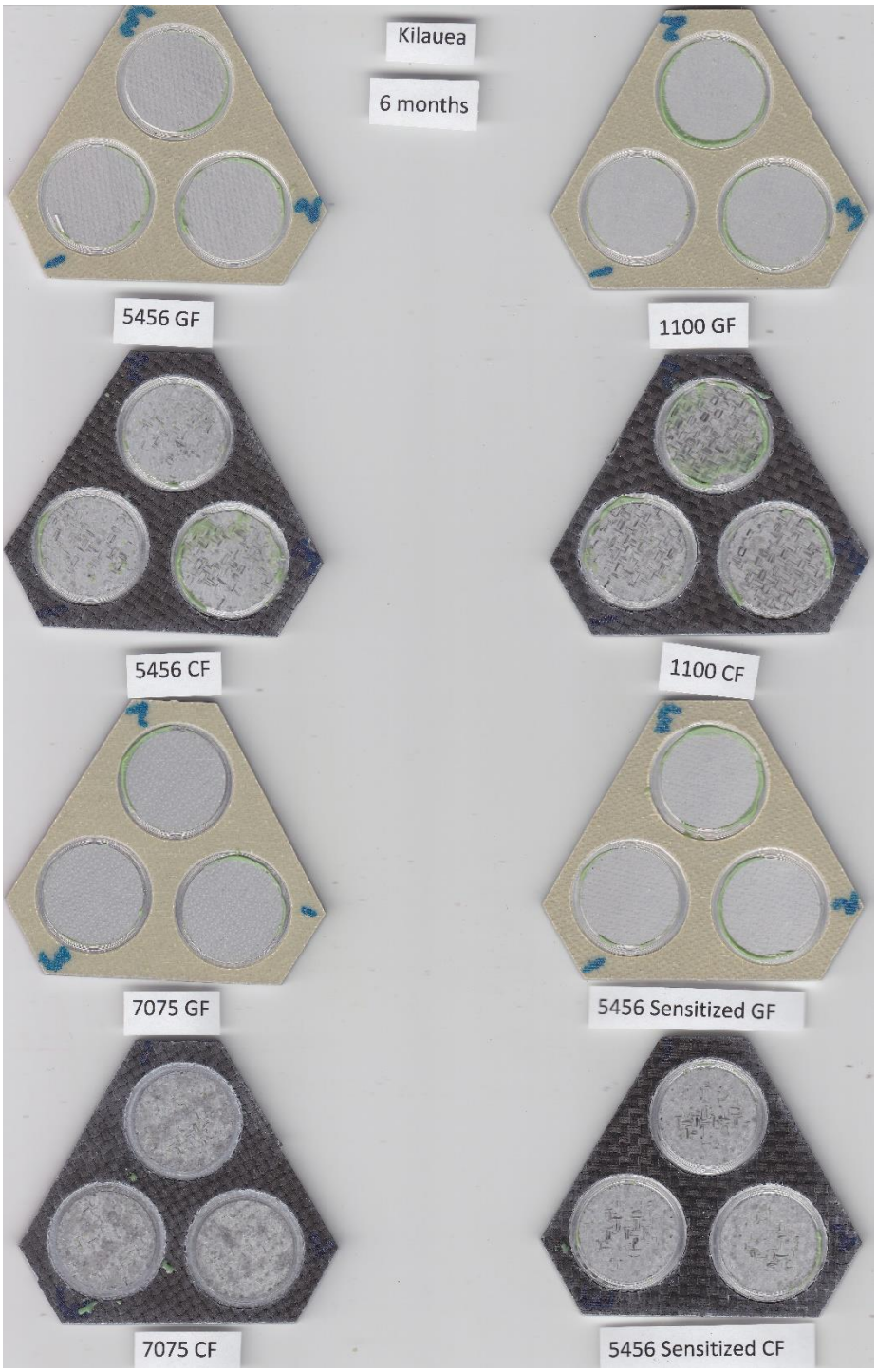

Figure 107: Kilauea Volcano 6 Month Samples After Adhesion Testing

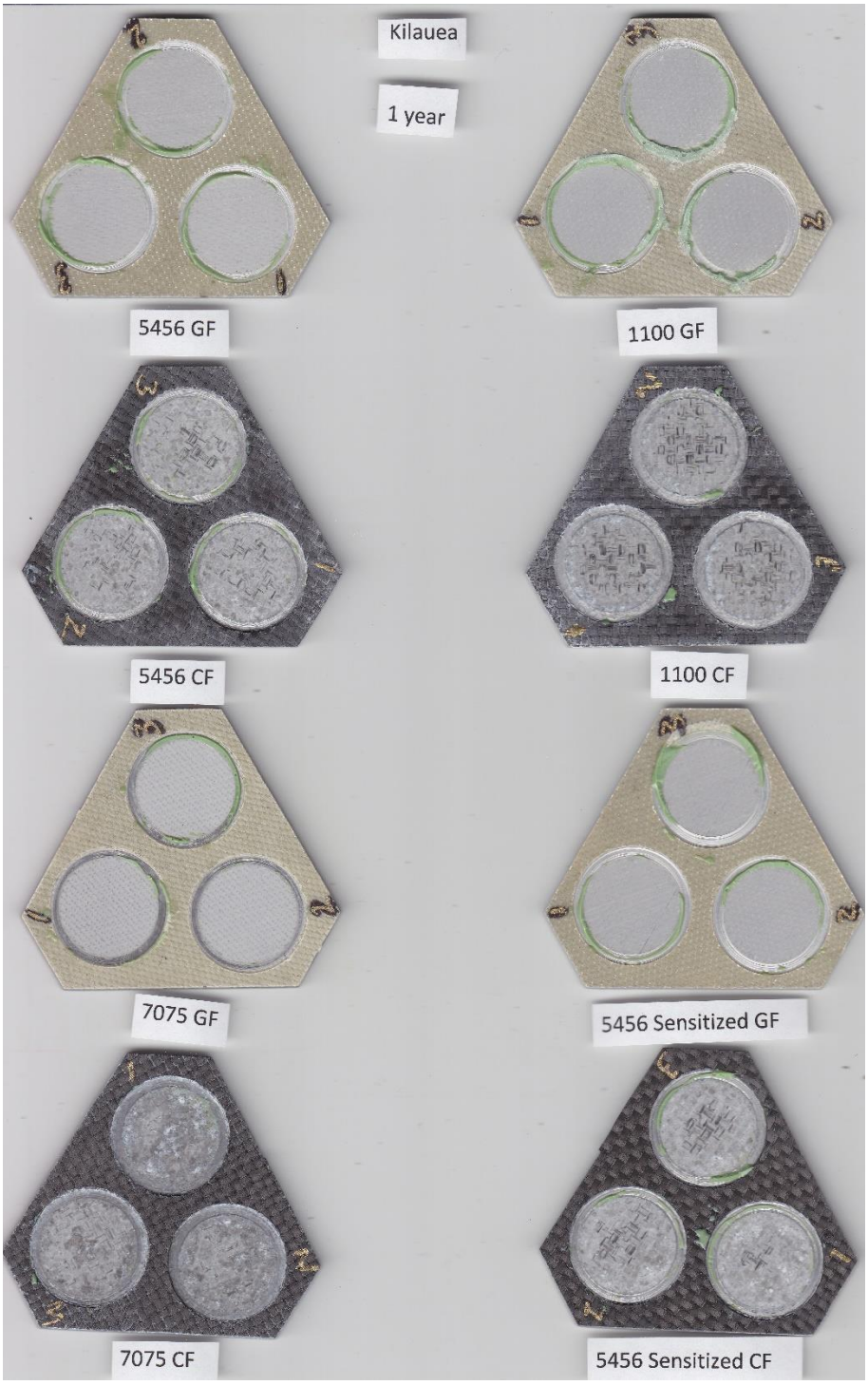

Figure 108: Kilauea Volcano 12 Month Samples After Adhesion Testing

References

[1] M. C. S. 2. C. P. D. Honnick, *photo #080626-N-6674H-048*, Navy, U.S..

[2] R. Schwarting, G. Ebel and J. Dorsch, "Manufacturing Techniques and Process Challenges with CG47 Class Ship Aluminum Superstructure Modernization and Repairs," American Society of Naval Engineers, 2011.

[3] L. H. Hihara, R. P. Alder and R. M. Latanision, Environmental Degradation of Advanced and Traditional Engineering Materials, Boca Raton: Taylor & Francis Group, 2014.

[4] J. R. Davis, Corrosion of Aluminum and Aluminum alloys, Materials Park: ASM International, 1999.

[5] D. R. Putnam, "Temporary Crack Repairs for Aluminum Structures on Surface Ships," NAVSEA Topic N151-052 (SIBR 2015.1), 2015.

[6] D. M. Jensen, "Corrosion of Aluminum Alloys - Polymer Matrix Composite Interfaces," Honolulu, 2015.

[7] P. K. Mallick, Fiber-Reinforced Composites: Materials, Manufacturing, and Design, New York: Marcel Dekker Inc., 1988.

[8] "Standard Test Method for Determining the Susceptibility to Intergranular Corrosion of 5XXX Series Aluminum Alloys by Mass Loss After Exposure to Nitric Acid (NAMLT Test)," ASTM Standard G67-13, 2013.

[9] B. E. Placzankis, "General Corrosion Resistance Comparisons of Medium- and High-Strength Aluminum Alloys for DOD Systems Using Laboratory-Based Accelerated Corrosion Methods," Army Research Laboratory, Aberdeen Proving Ground, 2009.

[10] K. K. Sankaran, R. Perez and K. V. Jata, "Effects of Pitting Corrosion on the Fatigue Behavior of Aluminum Alloy 7075-T6: Modeling and Experimental Studies," *Materials Science and Engineering*, vol. 297, no. 1, pp. 223-229, 2001.

[11] R. Ireland, L. Arronche and V. La Saponara, "Electrochemical investigation of galvanic corrosion between aluminum 7075 and glass fiber/epoxy composites modified with carbon nanotubes," *Composites Part B: Engineering*, vol. 43, no. 2, pp. 183-194, 2012.

[12] M. Ypma and B. Borgonje, "Influence of Moisture and Temperature on GLARE Material Properties and GLARE Structures," in *13th International Conference on Composite Materials*, Bejing, 2013.

[13] M. Ypma and B. Borgonje, "Long Term Behavior of GLARE," *Applied Composite Materials*, vol. 10, no. 4, pp. 243-255, 2003.

[14] F. Bellucci, "Galvanic Corrosion Between Nonmetallic Composites and Metals: 1 Effect of Metal and Temperature," *Corrosion*, vol. 47, no. 10, pp. 808-819, 1991.

[15] F. Bellucci, "Galvanic Corrosion Between Nonmetallic Composites and Metals: 2. Effect of Area Ratio and Environmental Degradation," *Corrosion*, vol. 48, no. 4, pp. 281-291, 1992.

[16] B. E. Placzankis, C. E. Miller and C. A. Matzdorf, "GM 9540P Cyclic Accelerated Corrosion Analysis of Nonchromate Conversion Coatings on Aluminum Alloys 2024, 2219, 5083, and

7075 Using DOD Paint Systems," Army Research Laboratory, Aberdeen Proving Ground, 2003.

[17] "Corrosion of Metals and Alloys - Removal of Corrosion from Corrosion Test Specimens," ISO Standard 8407, 1991.

[18] "MatWeb Material Property Data," 2016. [Online]. Available: http://www.matweb.com/index.aspx. [Accessed 3 October 2016].

[19] T. Giambelluca, Q. Chen, A. Frazier, J. Price, Y.-L. Chen, P.-S. Chu, J. Eischeid and D. Delparte, "Online Rainfall Atlas of Hawai'i," Bull. Amer. Metor. Soc. 94, 313-316, doi: 10.1175/BAMS-D-11-00228.1, 2013. [Online].

[20] M. Pourbaix, Atlas of Electrochemical Equilibria in Aqueous Solutions, Houston: National Association of Corrosion Engineers, 1974.

[21] R. Zhang, S. P. Knight, R. L. Holtz, R. Goswami, C. H. Davies and N. Birbilis, "A Survey of Sensitization in 5xxx Series Aluminum Alloys," *Corrosion*, vol. 72, no. 2, pp. 144-159, 2016.